Study on the Doping and Dedoping States of Poly(3,4-ethylenedioxythiophene) :Poly(styrenesulphonate)

LUO Yun

A Thesis Submitted in Partial Fulfilment

of the Requirements for the Degree of

Master of Philosophy

in

Physics

May 2004

Abstract

Poly(3,4-ethylenedioxythiophene): poly(styrene sulphonate) (PEDOT:PSS) is one of the most successful conducting polymers commercially available. It has been widely accepted and used as an effective hole injecting material in polymeric light emitting devices.

In this thesis, the doping and dedoping states of PEDOT:PSS were studied by X-ray photoemission spectroscopy (XPS) and conducting atomic force microscopy (CAFM). It was found that electrochemical dedoping could dedope PEDOT in PEDOT:PSS to a neutral state, and further dope it to an n-doped state with increasing dedoping potential. In this process, the Fermi level of PEDOT:PSS moved up from near the HOMO energy level, first to the mid of the band gap of PEDOT, then close to the LUMO energy level. Sulfur atoms acted as the main reduced center during dedoping and further n-doping. It is proposed that for PEDOT:PSS, the surface was dominated by PSS with a few PEDOT chains covered by PSS at different thickness, and that PEDOT formed a network structure beneath the surface. Either pH dedoping or electrochemical dedoping could not completely dedope the original PSS-doped PEDOT to its neutral state. However, electrochemical dedoping was more effective in dedoping when compared with pH dedoping. N-doped PEDOT had conductivity between neutral PEDOT and p-doped PEDOT.

论文摘要

在现今市场供给的范围内，poly (3,4-ethylenedioxythiophene):poly(styrene sulphonate) (PEDOT:PSS) 是最成功的导电高聚物之一。它在高分子发光二极管器件上被广泛用作高效的空穴注入材料。

本论文主要利用 X 射线光电子谱仪和导电原子力显微镜来研究 PEDOT:PSS 的掺杂态和去掺杂态。业已发现，随着去掺杂电压的提高，电化学方法可以将 PEDOT:PSS 去掺杂至中性态，进而将其变为电子型半导体。在这一过程中，PEDOT:PSS 的费米能级将从接近 HOMO 的位置上先移至 PEDOT 的能隙中央，再移至接近 LUMO 的位置。在去掺杂和电子掺杂的过程中，PEDOT 中的硫原子是主要的化学还原中心。据推断，PEDOT:PSS 薄膜表面为富 PSS 层，其中少量 PEDOT 为不同厚度的 PSS 所覆盖。在这层表面以下，PEDOT 形成网状交连结构。pH 去掺杂和电化学去掺杂都不能将 PEDOT 去掺杂到完全的中性态。相对来说，电化学去掺杂方法比 pH 去掺杂方法更为有效。电子掺杂型的 PEDOT 电导介于中性 PEDOT 和空穴掺杂型 PEDOT 的电导之间。

Acknowledgements

I would to like to express my sincere thanks to my supervisors, Professor W.M. Lau and Dr. K.W. Wong, for their kind guidance and advise throughout my study at the Chinese University of Hong Kong. My gratitude is extended to Professor K.Y. Wong, Professor D.H.C. Ong, and Professor J.B. Xu (Department of Electronic Engineer, CUHK) for their contributive suggestions.

My thanks are also given to the members of the Material Science and Technology Research Center (MSTRC) and the Laboratory of Surface Science and Technology, including Dr. J. Yu, Dr. X.J. Wang, H.L. Yip, L. Xi, R.F. Dou, M.K. Ho, X.Y. Deng, and Z. Zhi for their helpful support and incessant encouragement during the whole study period.

Finally, I want to thank my family for their encouragement during thesis writing.

Table of Contents

List of Figures

List of Tables

Chapter 1

Introduction

1.1 Conjugated Polymers

1.1.1 Overview

Polymers exist in a lot of substances in nature, including living organisms. Mankind has used natural polymers such as rubber, cotton and wool for a long time. In the beginning of the twentieth century the synthetic polymers were invented. [1] These synthetic polymers displayed a tremendous potential, mainly regarding their mechanical properties. Before 1977 polymers were only considered for purposes benefiting from their insulating properties. The emergence of the field of conjugated polymers came about in early seventies, when a researcher at the Tokyo Institute of Technology accidentally discovered a new way to synthesize trans-polyacetylene, producing free-standing silvery films instead of the usual dark powder. [2] In 1977, inspired by its metallic appearance, Heeger, MacDiarmid and Shirakawa, at the University of Pennsylvania, began to expose freestanding films of trans-polyacetylene to iodine and AsF_5, and found a substantial increase in conductivity of up to nine orders of magnitude. [3] Then, a new era in the field of polymers was born and has been developing very quickly ever since then.

1.1.2 Conducting Polymers

There are generally considered to be four main types of conducting polymers. [4] The first one – and the most important one commercially – are composites, in which the filling of an otherwise non-conducting polymer matrix with a powdered conductive medium such as metal or carbon gives rise to conductivity. These composite polymers are used as antistatic coatings, substitutes for solder and sundry, and in many other applications. The second group of polymers is called ionically conducting polymers, as they are organic polymers in which electric charge is carried by ions. Polyethylene oxide, in which lithium ions are mobile, is an example. These polymers are gaining importance in the battery industry. The third group of polymers is called *redox polymers*. Polymers in this group contain immobilized electroactive centers (or *redox* centers). Although they are not in direct contact with one another, they can exchange electrons by a "hopping" mechanism. The density of redox centers need to be great enough that the likelihood of electrons tunneling through the insulating barrier is sufficiently high. The fourth type, and the type to be discussed extensively in the present work, is electrically conducting polymers, or conjugated polymers (CPs). These polymers consist of alternating single and double bonds, creating an extended crosslinking-network. Electron movement or delocalization within this framework is the major source of conductivity. Structures for most common CPs are depicted in Fig. 1.1. The difference between redox polymers and CPs is not always clear-cut. Basically, conduction within one polymer chain of CPs is based on the conjugated nature of the polymer molecules and the resulting mobility of π-electrons, not on immobilized redox centers, which are the origins of conductivity in redox polymers.

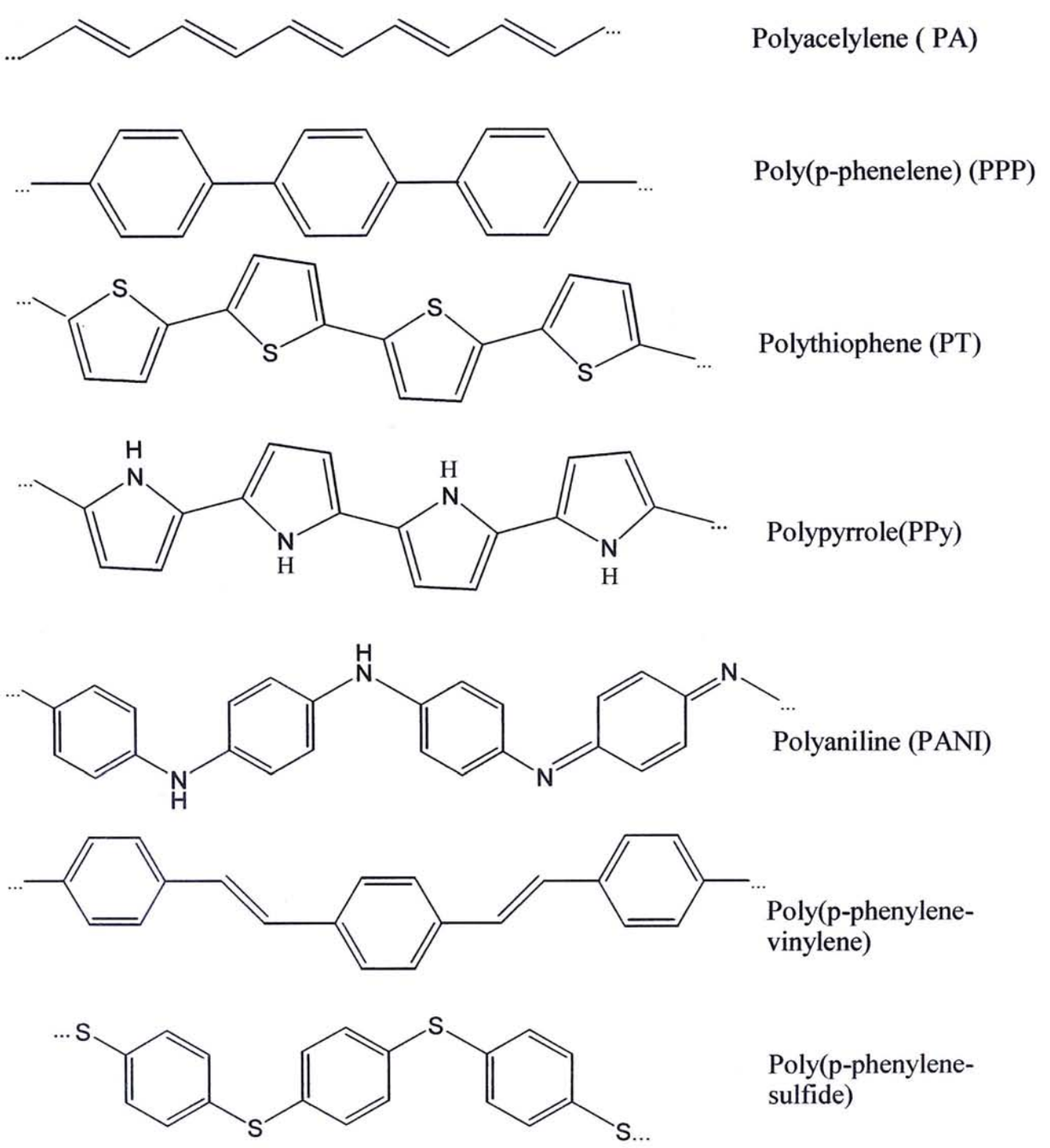

Fig. 1.1. Structures of common conducting polymers

With the discovery of electrical conductivity, electroactive polymers began a period of intense theoretical and experimental research on their physical and chemical properties. Polyacetylene (PA) was the first organic conducting polymer, synthesized in 1971 by Shirakawa and his co-workers, who accidentally used an excess of Ziegler-Natta catalyst in a synthetic process. [5] This was followed in 1977 by the discovery by Heeger, MacDiarmid and Shirakawa that polyacetylene doped with iodide demonstrated a much higher conductivity than with other dopants, with conductivities reaching as high as 106 S cm^{-1} under appropriate conditions. [6, 7] It was further found that polyacetylene could be obtained by both oxidative and reductive polymerization. Its conductivity depended on the dopant's properties and concentration. Following these discoveries, research in the field of conducting polymers began in earnest.

All CPs have in common conjugated systems, or in other words, organic systems of alternating single and double bonds. The surging interest in polyacetylene resulted in a thorough examination of its conjugated system and general properties. This in turn has resulted in a better understanding of conjugated conducting polymers in general. In 1979, Diaz and coworkers at IBM in San Jose reported that polypyrrole (PPy) could be obtained as a freestanding film by electrochemical oxidation of pyrrole in acetonitrile. [8] Polypyrrole had earlier been polymerized from aqueous sulfuric acid solutions by Dall'Olio et al. in 1969, but the poor mechanical and electrical properties of the material obtained discouraged further exploration of that synthetic method. [9] In 1982, Tourillon and Garnier prepared polythiophene (PT) by anodic oxidation of thiophene. [10] Since that time, many new conducting polymers have been synthesized and studied. Having started with simple molecules such as

acetylene, aniline and heterocycles such as pyrrole and thiophene, the field has expanded to include polymers made up of aromatic molecules such as benzene, phenol, polycyclic aromatic hydrocarbons such as naphthalene and anthracene, and even more exotic molecules.

Conductive organic polymers, which show significant conductivity, are potentially usable materials in many different areas. Good mechanical properties, high resistance to acids and bases and high conductivity are all important qualities in a polymer film. Their similarities to doped semiconductors in electrical conductivity have led many to label them synthetic metals. The conductivities of some of the more common CPs in comparison to other materials are listed in Table 1.1.

1.2 Electrochemical Doping of Conjugated Polymers

The report of Shirakawa et al. [3, 5, 12] showed that the electrical conductivity of polyacetylene could be increased through reaction with an oxidative agent or electron acceptor (p-doping) or a reducing agent or electron donor (n-doping) by several orders of magnitude. The electronic properties of conjugated polymers can be described by molecular orbital theory [13] leading to the structural characteristics of a linear π-electron system [14-16].

These conjugated polymers contain electronic states that can be reversibly emptied or filled with elecrochemical techniques resulting in metal-insulator transitions. This has an enormous potential for wide-ranging practical applications. As a result, electrochemistry of conjugated polymers is one of the hottest research fields in recent years.

Table 1.1 Conductivity of the most common polymers in the doped (D) and undoped (unD) forms, compared with other common materials [11]

Conducting Polymer	Conductivity/S cm-1	Commercial materials
	10^{6}	Copper
Polyacetylene (D)		
Poly(3-alkylthiophene)(D)		Platinum, graphite
Poly thiophene (D)		
Polyparaphenylene(D)	10^{2}	
Polypyrrole(D), polyaniline		
	1	
	10^{-2}	Germanium
Polycarbazole (D)		
Polyacetylene(unD)	10^{-6}	
	10^{-10}	
Polypyrrole(unD)		
Polyphenylene(unD)		
Polyaniline(unD)		
	10^{-14}	Diamond
	10^{-18}	Quartz

Electrochemistry is generally a powerful tool in the work with conjugated polymers. Besides the characterization, electro-polymerization by oxidation and reduction is also an important way of synthesis that can be applied for most of the important polymers [14,17-21].

1.2.1 Doping Conjugated Polymers

Chemically produced conjugated polymers are often insulators. Their metal-like properties, i.e. their high conductivity, arise only after appropriate "doping", concomitant with a change of the redox state of the polymer. The term "doping" is a terminology commonly used in inorganic semiconductors, through which a small quantity of dopant is added to a host material and this dopant can induce disproportional large changes in the electronic and electrical properties of that host material. The use of term "doping" implies certain similarity between the doping of organic and inorganic semiconductors in term of the effect exerted by the dopants. The underlying science governing the doping mechanism between inorganic and organic semiconductors is of fundamental difference. For inorganic semiconductors, e.g. silicon, dopants occupy positions within the lattice of the host material. This results in either electron-rich (e.g. phosphorus as dopant) or electron-deficient (e.g. boron as dopant). In contrast, doping of conjugated polymers [14,17,22,23] is essentially a charge transfer chemical reaction that results in a partially oxidized or reduced polymer. It can be done chemically with reducing (Donor D, n-doping) or oxidizing (Acceptor A, p-doping) agents or electrochemically. Oxidation in this context is referred to as p-doping (again in analogy to inorganic semiconductors), and the basic processes are shown in reactions (1) and (2) as examples for chemical and electrochemical doping, respectively.

p-doping: $(\pi\text{-polymer}) + A \rightarrow (\pi\text{-polymer})^{+}A^{-}$ (1)

$$(\pi\text{-polymer}) + [Li^{+}(BF_4^{-})]_{solvent} \rightarrow [(\pi\text{-polymer})^{x+}(BF_4^{-})_x] + xLi^{+} + xe- \quad (2)$$

if $Li^{+}(BF_4^{-})$ is the electrolyte used.

As can be seen in both cases, a compensation of the generated charge is needed resulting in a "poly-salt". Similarly n-doping results in partial reduction of the polymer chain, as shown in reactions (3) for chemical doping and (4) for electrochemical doping.

n-doping: $(\pi\text{-polymer}) + D \rightarrow (\pi\text{-polymer})^{-}D^{+}$ (3)

$$(\pi\text{-polymer}) + xe- + [Li+(BF_4^{-})]_{solv} \rightarrow [(\pi\text{-polymer})^{x-}(Li^{+})_x] + x(BF_4^{-}) \quad (4)$$

The main advantage of electrochemical doping over the chemical way lies in the control of the doping level [23]. This can easily be done electrochemically with highly reproducible results, whereas chemical doping attempting to reach intermediate doping levels often results in inhomogeneous doping.

1.2.2 Doping Level

The doping level is a measure of the extent of the polymer having been oxidized or reduced. The electrically conducting form is obtained when the polymer is doped. For example, polyacetylene exhibits a conductivity of 10^{-9} $\Omega^{-1}cm^{-1}$ in its undoped form while achieving conductivities of 10^{3} $\Omega^{-1}cm^{-1}$ and higher in the doped form. The electrical conductivity is strongly dependent upon the polymer's doping

level. Polymers may be doped either chemically or electrochemically. The doping level is normally higher for electrochemically doped polymers than for chemically doped polymers. With chemical doping, electron acceptors (*p*-doping) or electron donors (*n*-doping) need to be added to the solution in order to make the doping reaction take place. Some examples are oxygen, iodine and arsenic pentafluoride. [24] A polymer can be doped electrochemically by simply applying an appropriate potential across the film in the presence of counter ions.

More specifically, the doping level or degree of doping expresses the ratio of the number of charges in the polymer to the number of monomer units. It is an important characteristic describing a polymer film. The stoichiometry of the polymer formation may be expressed as follows:

$$(n+2)RH_2 - (2n+2)e^- \rightarrow HR\text{–}R_n\text{–}RH + (2n+2)H^+ \qquad (R\ 1)$$

When n is sufficiently large, a charge of 2 faradays per mole of monomer is required for bond formation (for a linear polymer). An extra amount is needed for doping/oxidizing the polymer to the doped form.

$$HR\text{–}R_n\text{–}RH + (n+2)y\ A \rightarrow (HR\text{–}R_n\text{–}RH)^{+(n+2)y}A^-_{(n+2)y} \qquad (R\ 2)$$

The variable y denotes the doping level, which is typically between 0.1 and 0.4. Its inverse is then logically the number of monomer units neutralized by the doped ion.

Doping level characterizes the electrical quality of the conducting polymer, especially in terms of charge storage. The subscript n refers to the length of the polymer, which cannot be measured exactly. It is likely that there is a wide distribution of chain lengths. Tritium studies have been performed with the polymer poly-3, 4-dimethylpyrrole, demonstrating an n value close to 750, but for the most part, chain lengths remain unknown. [25] Methods such as ultraviolet photoelectron

spectroscopy and electron energy loss spectroscopy can be employed to estimate the lower limits of chain length. [26,27]

1.3 Charges in Conjugated Polymers

1.3.1 Electronic and Geometric Configurations

In conjugated polymers, two of the three p-orbitals of carbon are in the three-sp2 hybrid orbitals [13]. Of these, two are used for the σ bonds of the polymer backbone. The remaining third p-orbital, the p_z-orbital, gives rise to an extended π-system along the chain, which gives conjugated polymers their unique properties [28-30]. The bond formation is depicted in Fig. 1.2 using trans-polyacetylene as an example. Principally, this should give a metallic material with a half-filled conduction band if all bonds were of equal length. But due to the Peierls distortion [31] dimerization occurs that breaks the symmetry of the polymer chain. In this dimerized form the π-electrons are concentrated between alternate pairs of carbon atoms, which is consistent with the observation of alternation of double and single or shorter and longer bonds along the chain. Extension of the π system (through overlapping of p_z-orbitals) results in a filled π-orbital (HOMO, valence band, bonding orbital) and an empty π* orbital (LUMO, conduction band, antibonding orbital) with a certain energy gap between, the so called π-π* bandgap, which is characteristic for semiconducting materials and lies in the range of 1 to 4 eV for conjugated polymers.

1.3.2 Charge Carriers

Solitons

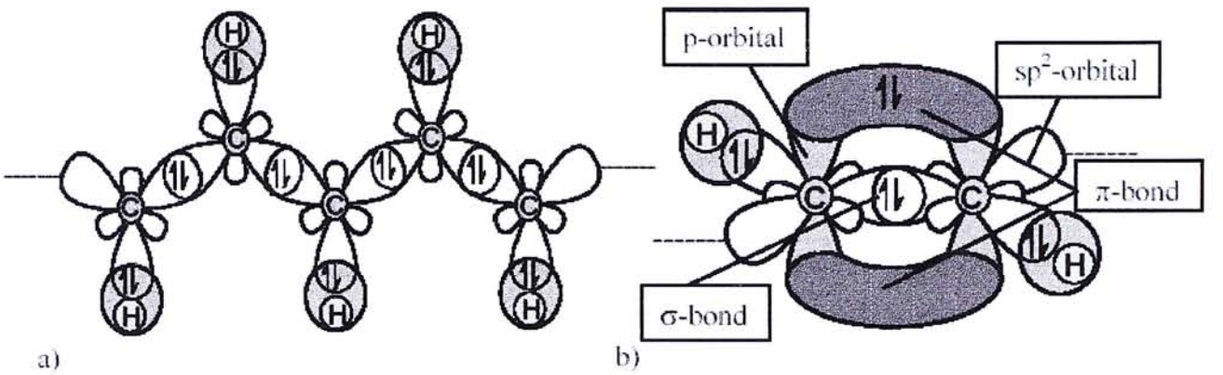

Fig. 1.2 a) Formation of bonds in polyacetylene by overlapping of sp^2- (carbon) and 1s-(hydrogen) obitals; b) Formation of π–bonds through overlap from the side of the P_z-orbital

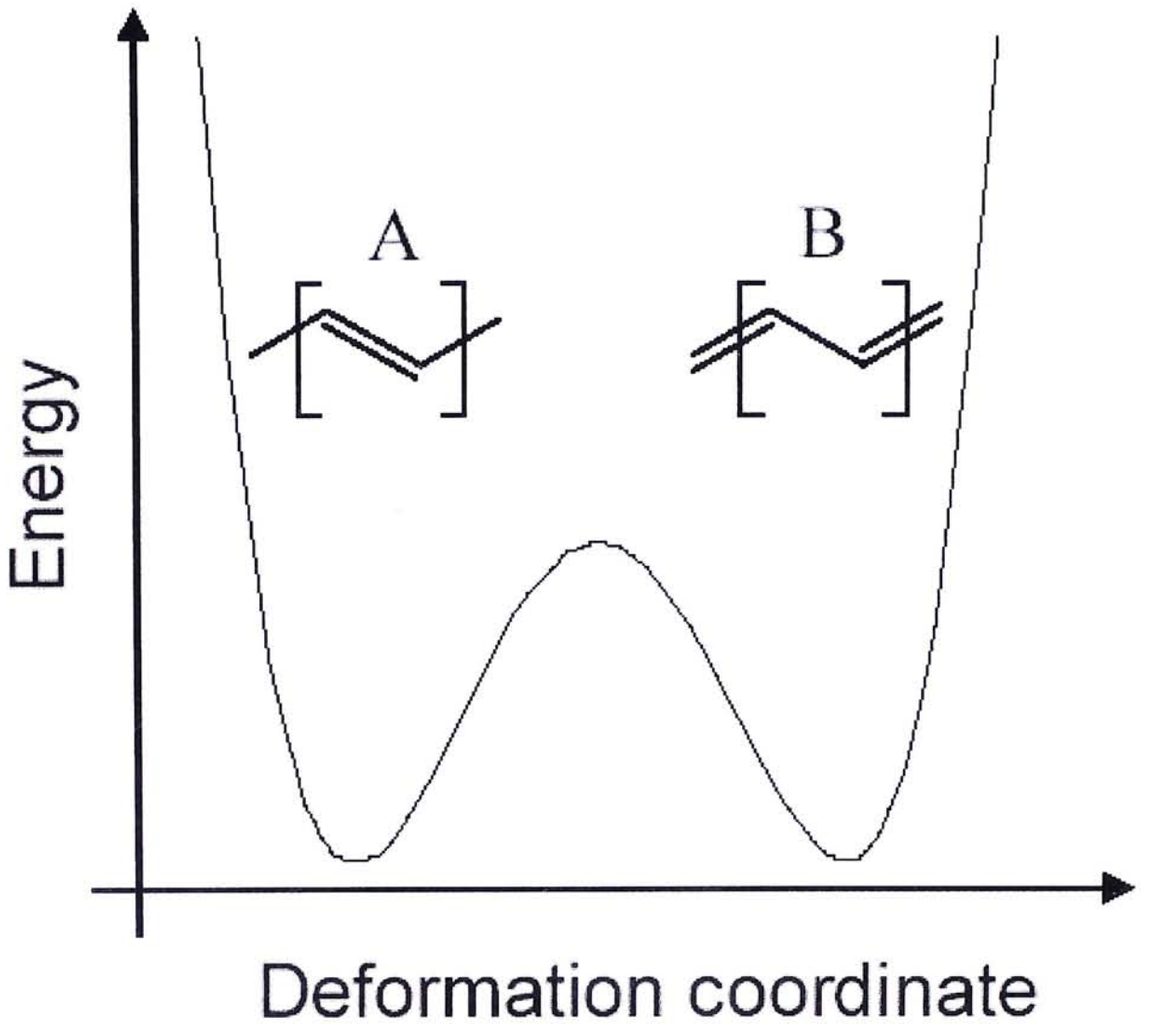

Fig. 1.3 Potential energy curve for trans-polyacetyene showing the two equivalent structures

Trans-polyacetylene is a polymer with a degenerate ground state since the double and single bonds can be interchanged without changing the ground state energy. Therefore the ground state has two configurations A and B with the same energy as shown in Fig. 1.3 [15,16,32].

If both of the energetically equivalent configurations coexist on the same chain a structural defect will occur at their interface. This defect is called a (neutral) soliton; it consists of a single unpaired electron that can extend over approximately ten carbon atoms [15,16,33]. One new localized electronic state is formed in the middle of the π-π^* gap, which can accommodate up to two electrons. Doping adds or removes an electron to or from this state during n- or p-doping leading to a negatively or positively charged soliton, which can also be called spinless anion or cation. A band diagram for neutral, positive and negative soliton is shown in Fig. 1.4. Associated with these three types of solitons new optical transitions depending on their symmetry allowance can be observed in optical absorption spectra, which are indicated with dotted arrows in Fig. 1.4. Only transitions from levels with an odd parity to levels with an even parity in the wave function or vice versa are allowed. The parity of the wave function is alternating with every energetic level.

Polarons and Bipolarons

Most other conjugated polymers have two energetically non-equivalent bond alternation structures, which means they have a non-degenerate ground state [34-37]. For example in poly(*p*-phenylenevinylene) (structure is shown in Fig. 1.5) the quinoid structure (B) is less stabilized and therefore higher in energy than the benzenoid form (A). Fig. 1.5 shows the energy diagram for these two structures.

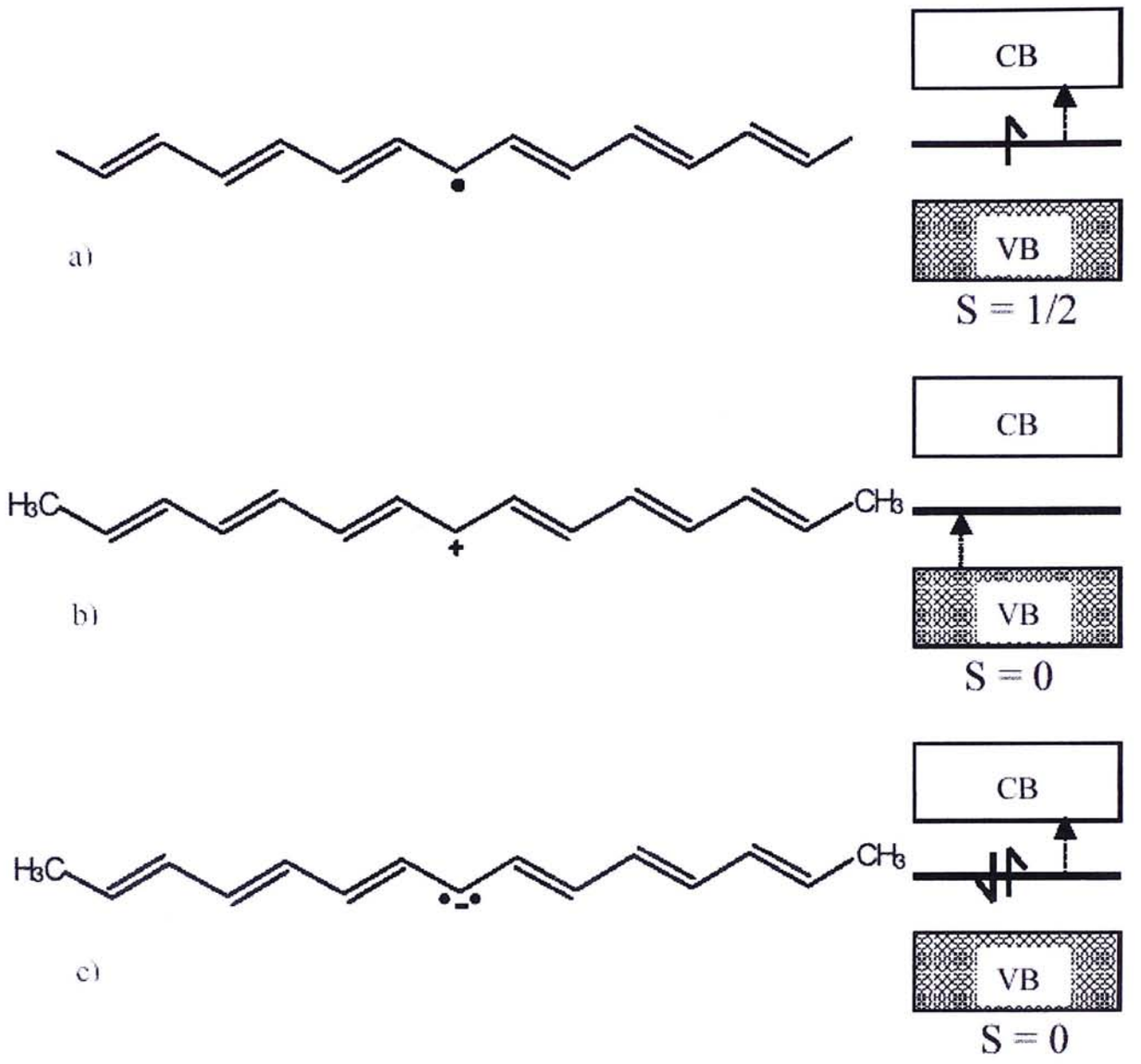

Fig. 1.4 Soliton structures in polyacetylene and corresponding electronic states in the band gap; a) a neutral soliton, b) a positive soliton, c) a negative soliton; dotted arrows indicate optical transitions to and from the mid-gap state.

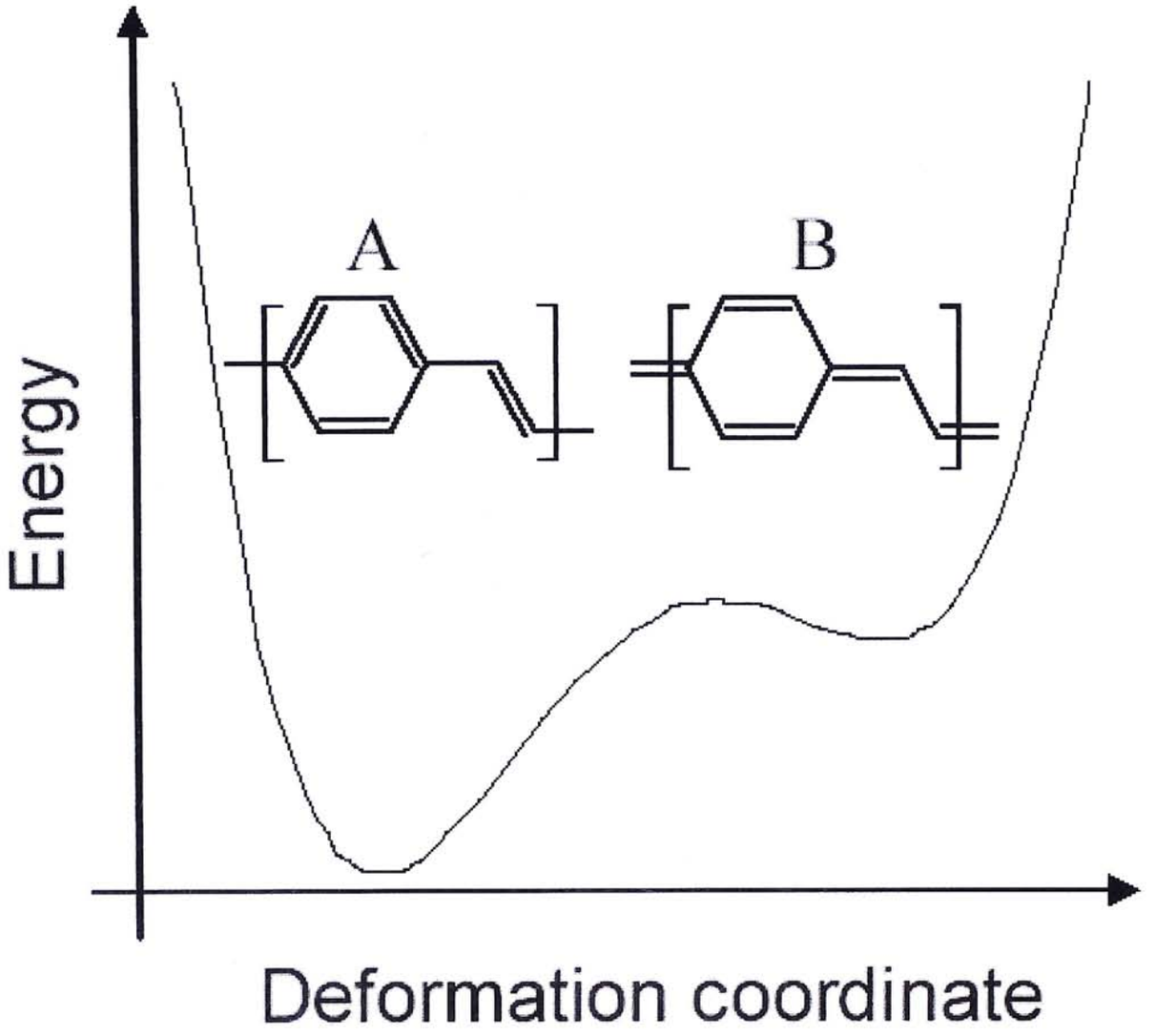

Fig. 1.5 Potential energy curve for poly(p-phenylenevinylene) with its energetically non-equivalent structures, benzenoid(A) and quinoid (B)

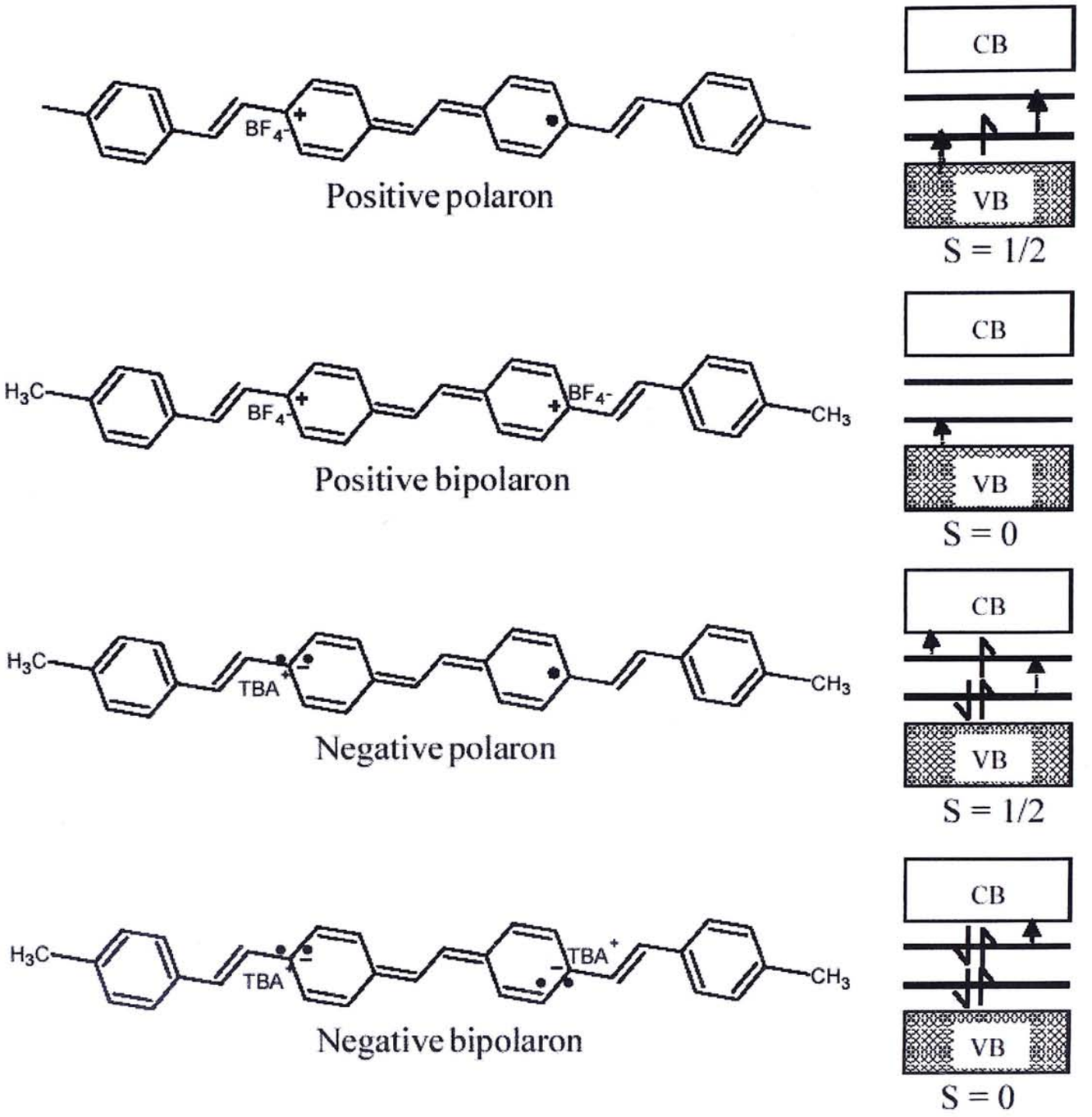

Fig 1.6 Polaron and bipolaron structure in poly(p-phenylenevinylene) with their corresponding electronic states in the band gap; only positive and negative charge carry a spin (S); dotted arrows indicate optical transitions to and from the mid-gap state.

A defect region will be created in the presence of charge carriers between uncharged benzenoid parts on the conjugated polymer. Upon p- or n-doping charge carriers called polarons (radical cation or anion) and bipolarons (spinless dication or dianion) are formed and two new electronic states are created in the π-π^* band gap. A band scheme of the above described is given in Fig. 1.6. The dotted arrows indicate new possible optical transitions, depending whether they are allowed by symmetry or not. Only transitions from levels with an odd parity to levels with an even parity in the wave function or vice versa are allowed. The parity of the wave function is alternating with every energetic level.

Calculations show that the removal of an electron (p-doping) leads to the formation of a positive polaron (radical cation) whose associated quinoid geometry relaxation extends over three phenyl rings [36]. For removing a second electron from the polymer chain when doping proceeds, two possibilities are given. The first possibility is that a second polaron will be created anywhere along the chain leading to two polarons. The second possibility is that the second electron is removed from the already existing polaron giving rise to a bipolaron. For both processes the formation energies are predicted to be roughly the same, but the ionization energy for bipolaron formation should be substantially lower. Therefore one bipolaron is thought to be thermodynamically more stable than two coexisting polarons [32], despite the coulombic repulsion, which is screened to a large extent by the counter ions near the charge carrier introduced upon chemical or electrochemical doping.

However, experimental findings attributed to bipolarons can in the same way be explained by using the concept of interchain polaron pair formation without any creation of bipolarons [37,38]. These are formed due to Coulomb interactions between a positive and a negative polaron on two neighboring chains also leading to

no macroscopically detectable spin. Moreover, there has been no direct experimental proof for bipolarons yet. The question which model better reflects the reality is not solved and the discussion is still controversial.

1.4 Effects of Localization and Structural Disorder on Conductivity

Despite the seemingly good comprehension of transport related topics within conjugated polymers, no consistent theory of conduction yet exists that accurately predicts the current densities over the hole conductivity range, i.e., from insulator to metal. Instead, a dual conduction model that emanates from different possible arrangements of disordered polymer chains has been adopted. According to this, disorder is either homogeneously, [39] or heterogeneously [40] distributed throughout the sample, depending on the doping concentration. When lightly or moderately doped, the homogeneous model applies and the interesting properties of conduction are controlled by Anderson localization in the bulk, while at higher doping concentrations the heterogeneous model more accurately describes the current transport process.

1.5 Cyclic Voltammetric Behavior of Conjugated Polymers

Under assumption of the ideal case with fast electron transfer across the polymer and a reasonable large concentration of mobile ions inside the polymer, one could anticipate from cyclic voltammetry of redoxactive films completely symmetrical and mirror-image cathodic and anodic waves. [14, 23] The peak

potentials and current levels are identical and the current for this case is described through equations (a) to (c) [41-43]

$$i = \frac{n^2 F^2 A \Gamma_T \nu \exp\theta}{RT(1+\exp\theta)^2} \qquad \text{(a)}$$

with $$\theta = \frac{nF}{RT} \bullet (E - E^0) \qquad \text{(b)}$$

and $$\Gamma_T = \Gamma_O + \Gamma_R . \qquad \text{(c)}$$

Equation (c) corresponds to the total surface Γ_T covered with reduced (Γ_R) and oxidized (Γ_O) sites, n is the number of electrons taking part in the reaction, F is the Faraday constant, A is the electrode area, v is the scan rate, θ is the potential for the investigated reaction (see equation (b)), R is the gas constant and T is the temperature.

In reality, the waves are shifted in relation to each other and become increasingly asymmetrical [44-46]. This can be seen from Fig. 1.7, where a cyclic voltammogram of PTPTB is used as a simple example.

The first explanation for these phenomena was made in terms of the simple theory for redox polymers as a kinetic effect of slow heterogeneous charge transfer, in which the interactions between the charged oligomeric segments were assumed to be negligible. The thermodynamic redox potential was calculated as the mean value between the peak potentials of the cathodic and the anodic wave [14, and references in there]. From the discrepancies of this theory it was concluded that the neutral polymer should have a conjugation length of 5 to 10 monomeric units. Quantum mechanical calculations also suggested that the onset potential reflects only the initial ionization of conjugated polymers while further ionization should lead to structural changes [14,47].

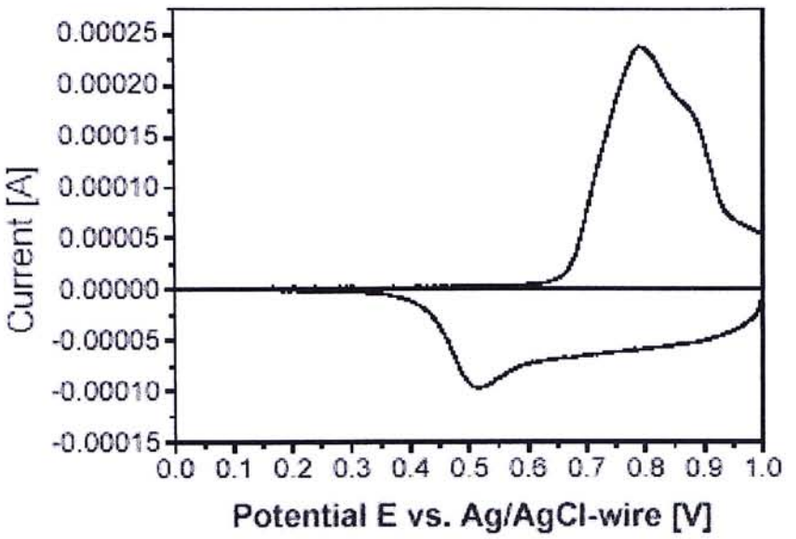

Fig. 1.7 Cyclic voltammogram of PTPTB dropcast onto a Pt electrode in CH_3CN/0.1 M $TBAPF_6$

Based on this first assumption other concepts were developed to refine agreement with the experimental results, taking also structural changes in account. The fact that the peak separation is not essentially a function of the potential sweep rate suggests a chemical reaction following charge transfer. Upon oxidation, the molecules stabilize themselves from the twisted benzenoid to the partially planar quinoid form in the case of aromatic polymers. Confirmation of this theory was found through work with the corresponding oligomers [23, and references in there]. In solution, electrochemistry on oligomers gives reversible reactions, whereas when deposited as a film and the free rotation is hindered in the bulk, electrochemical irreversibility appears.

For the explanation of the constant current region, the question arises to what extent one can or must distinguish between faradic and capacitate processes. In a first assumption only the anodic ´peak-shaped´ wave was considered to be a faradic process and the broad anodic tail was considered to be just an effect of the double layer capacity [14,48,49]. However, the results of the oligomer experiments mentioned above also can give a plausible explanation for this phenomenon [23], which does not take capacitative effects into account.

1.6 PEDOT: PSS Systems

Researchers are constantly searching for polymers with better qualities – longer lifetimes, higher conductivities, lower bandgaps, and so on. Polyacetylene, while reaching conductivities as high as 10^5 $S \cdot cm^{-1}$ under proper conditions, is not stable enough for technical applications. [50] Polypyrrole, polythiophene and their derivatives demonstrate conductivities which remain stable over years at temperatures exceeding 25° C. [51] Unfortunately, polymer conductivities often need to remain

unaffected at temperatures exceeding 120° C for over 1000 hours in a standard atmosphere to be used in many applications.

When comparing doped PPy and PT with positively charged PA, the question arises why they have such better stability. It has been postulated that it stems from the stabilizing effect of nitrogen and sulfur on the free charges. [50] Therefore, it seems that the addition of more, similar stabilizing substituents should increase the resulting polymer's stability and perhaps even its conductivity by increasing chain order. Out of this thinking came the first exploratory polymerizations by Bayer and AGFA of PEDOT (see Fig. 1.9), with the intent of applying it to the fields of antistatic coatings and photographic films.

PEDOT's properties are far superior to those of other conducting polymers such as Ppy and PANI. [52] It has high visible light transmission/blue (undoped), absorption beginning at around 1.5 eV → transparent/colorless (doped), absorption maximum appears at 0.6 eV, while maintaining comparable conductivity (~200 $S \cdot cm^{-1}$). The bandgap of 1.6 – 1.7 eV is one of the narrowest band gaps ever measured for a thiophene system, 0.5 eV lower than that of polythiophene. [53] The low bandgap – considered to be due to the electron donating oxygen atoms – also enables *n*-doping by electrochemical methods. PEDOT is a stable doped conjugated polymer, both chemically and thermally, evidencing no change in film conductivity at 110 ° C in air. [52]

The so-called BAYTRON P synthesis, developed by Baytron AG, is now the most practically useful, polymerization method for EDOT. [54,55] This method utilizes the polymerization of EDOT in an aqueous polyelectrolyte (most commonly

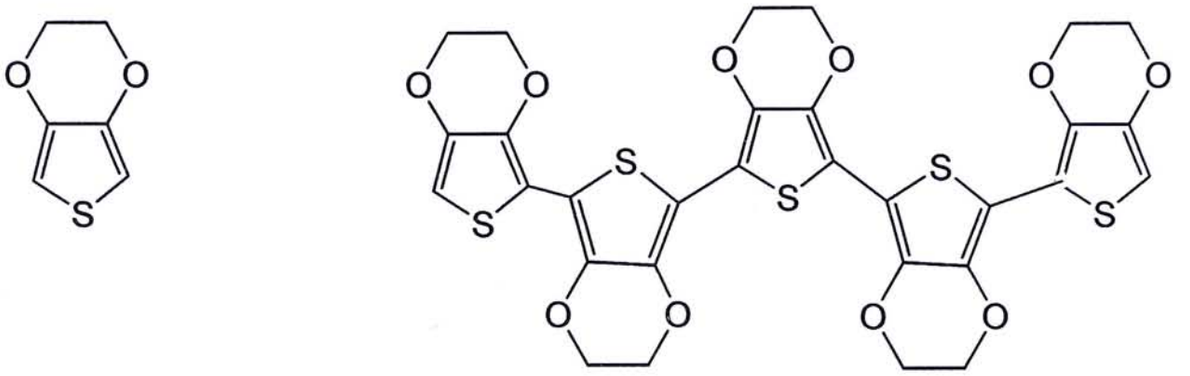

3,4 ethylenedioxythiophene
(EDOT)

poly (3, 4-theylenedioxythiophene)
(PEDOT)

Fig. 1.8 EDOT and PEDOT structures; note how the ethylenedioxy substituents' filling of the 3 and 4 positions prevents polymerization at those positions and increases the conjugation of the polymer chain.

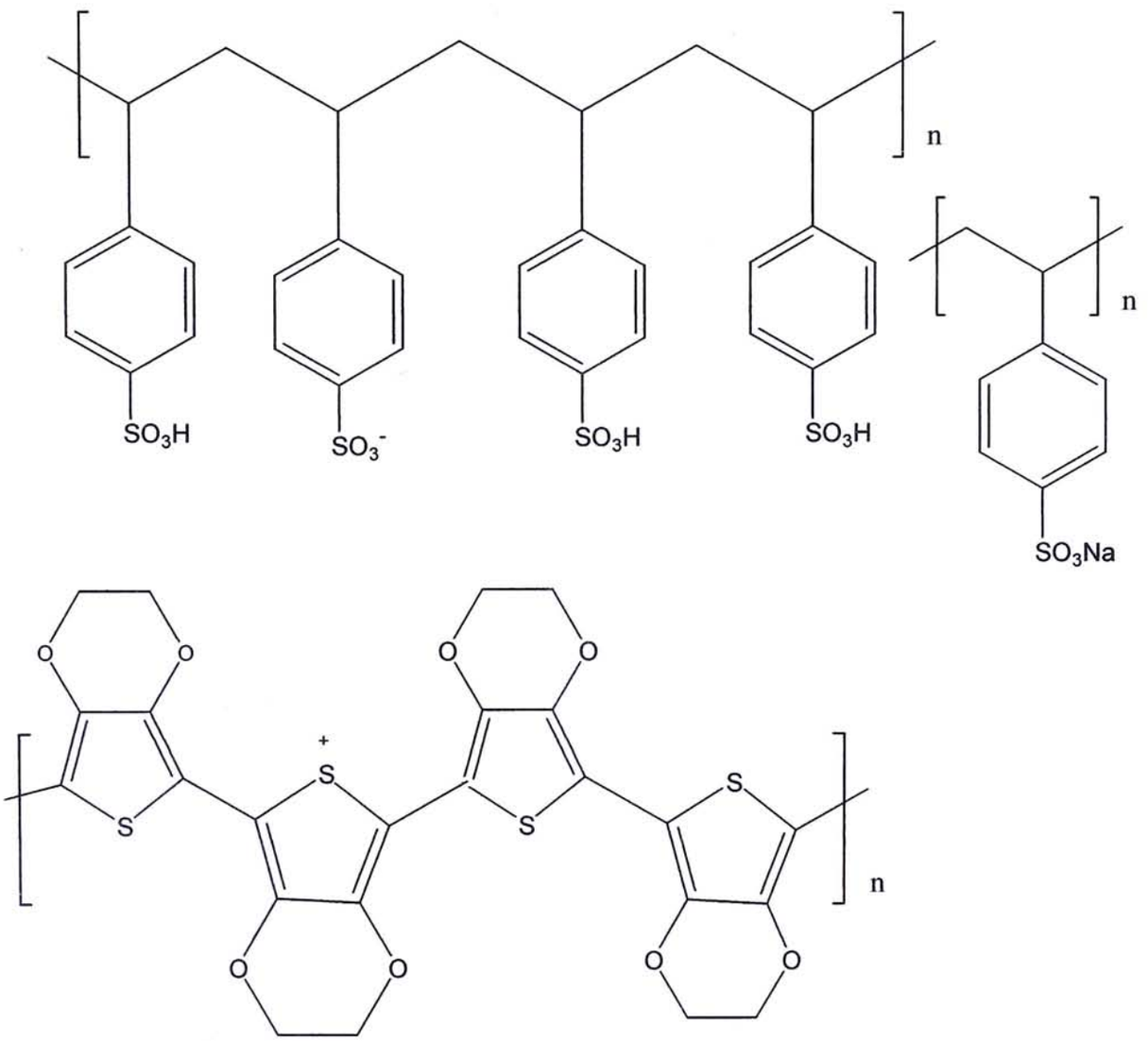

Fig. 1.9 Chemical structures of the PEDOT:PSS blend and PSS^- Na^+ (right) (Baytron P)

PSS) solution using $Na_2S_2O_8$ as the oxidizing agent. Carrying this reaction out at room temperature results in a dark blue, aqueous PEDOT/PSS dispersion, which is commercially available from Bayer AG under its trade name BAYTRON P (Fig. 1.10). There are several distinct chemical species present in this complex, the most obvious being PSSH and PEDOT. But there has also been some sodium contamination detected in these systems, in the form of PSS^-Na^+. The doping of PEDOT results in $PEDOT^+$ charged balanced by the PSS^- species. Since the quasi-particles induced by the doping in PEDOT are delocalized over several monomer units there is a spread in PEDOT species from completely neutral to completely doped state. The positive charge on a particular PEDOT ring depends in part on the distance from the PSS^- counter ion.

The obtained surface morphology of spin- or drop-coated PEDOT-PSS films is a phase-segregated system. It can be described as having a grain-like structure, in which neutral parts of the template, PSSH and PSS^-Na^+, forms the grain boundary layer, having a thickness of about 30-40 Å [56].

1.7 Motivation

This thesis work aims at clarifying the electrochemical doping and dedoping states of poly (3,4 -ethylenedioxythiophene) (PEDOT) by using X-ray photoemission spectroscopy (XPS), and conducting atomic force microscopy (CAFM). PEDOT is commonly considered as a very stable conducting polymer, widely used in electrochromic displays, antistatic transparent films, as electrodes for solid-electrolyte capacitors, and as transparent hole injection layer in polymer light emitting diodes. However, the mechanism of doping and dedoping of PEDOT is still obscure. Cyclic voltammetry is a common method for the study of the redox process and different

doped states of conducting polymers. Although cyclic voltammetry is commonly used, it cannot fully reveal the electronic structure, the core levels, and valence region, especially for conducting polymer in solid form. Other spectroscopic characterizations are lacking in the study of the doping states of PEDOT. In the present work, XPS was used as a "fingerprinting" method in analyzing the chemical composition and chemical states of PEDOT. In addition, CAFM was used to study the localized morphology of PEDOT, and nano-scale I-V measurement was used to investigate the electronic properties of PEDOT film before and after electrochemical dedoping.

References:

[1] Morawetz, H., *Polymers. The origins and growth of a science*, John Wiley & Sons, New York, 1985

[2] T. Ito, H. Shirakawa, and S. Ikeda, *Journal of Polymer Science- Polymer Chemistry* **12** (1974), 11

[3] C. K. Chiang, C. R. Fincher, Y. W. Park, A. J. Heeger, H. Shirakawa, E. J. Louis, S. C. Gau, and A. G. MacDiarmid, *Phy. Rev. Let.* **39** (1977), 1098

[4] Wise, D.L. Wnek, G.E. Trantolo, D.J. Cooper, T.M. Gresser, J.D. (Eds.). *Electrical and Optical Polymer Systems.* Marcel Dekker, NY. 1997, p.167.

[5] Shirakawa, H; Louis, E.J.; MacDiarmid, A.G.; Chiang, C.K; Heeger, A.J. *Journal of the Chemical Society, Chemical Communications,* 1977, 578.

[6] Chiang, C.K.; Fincher, C.R.; Park, Y.W.; Heeger, A.J.; Shirakawa, H.; Louis, E.J.; Gau, S.C.; MacDiarmid, A.G. *Phys. Rev. Let.* **39** (1977), 1098.

[7] Schimmel, T.; Schwoerer, M; Naarmann, H. *Synth. Met.* **1** (1990), 1-3.

[8] Diaz, A.F.; Kanazawa, K.K.; Gardini, G.P. *J. Chem. Soc. Chem. Commun.*, 1979, 635.

[9] Dall'Olio, A.; Dascola, Y.; Dardini, G.P. *C. R. Acad. Sci.*, **267** (1969), 4336.

[10] Tourillon, G.; Garnier, F. *J. Electroanal. Chem.*, **135** (1982), 173.

[11] Kanatzidis, M.G. *Chem. Eng. News.,* ec. **3** (1980).

[12] C.K. Chiang, M.A. Druy, S.C. Gau, A.J. Heeger, E.J. Louis, A.G. MacDiarmid, y.W. Park, H. Shirakawa, *J. Am . Soc. Chem* **100** (1978), 13

[13] G.M. Barrow, *Physical Chemistry* (WCB/McGraw-Hill Boston, Burr Ridge, Dubuque, Madison, New York, San Francisco, St. Louis, 1996) 6th ed., Chap. 10, 11

[14] J. Heinze in *Topics in Current Chemistry* Vol. 152 (Springer Verlag Berlin Heidelberg, 1990), 1

[15] M.J. Rice, *Phys. Lett.* A **71** (1979), 152

[16] W.P.Su.J.R.Schrieffer, A.J. Heeger, W.P. Su, J.R. Schrieff , *Phys. Rev. Lett.* **42** (1979), 1698

[17] G.P. Evans in *Advances in Electrochemical Science and Engineering,* 2 Volumes, Ed. H. Gerischer and C.W. Tobias (VCH-Wiley, Weinheim, 1990), 1-74

[18] J. Roncali, *Chem. Rev.* **92** (1992), 711

[19] P. Damlin, C. Kvarnström, A. Ivaska, *Electrochim. Acta* **44** (1999), 4087

[20] A.F.Diaz, J.Bargon in *Handbook of Conducting Polymers*, Vol. 1, Ed. T.A. Skotheim, (Marcel Dekker Inc., New York 1986), Chap. 3, 81

[21] G. Zotti in *Handbook of Organic Conductive Molecules and Polymers*, Vol. 2, Ed. H.S. Nalwa (John Wiley & Sons, New York, 1997), Chap. 4, 137

[22] A. J. Heeger, J.Phys.Chem.B **105** (2001), 8475

[23] K. Doblhofer, K. Rajeshwar in *Handbook of Conducting Polymers*, Ed. T.A. Skotheim, R.L.Elsenbaumer, J.R. Reynolds (Marcel Dekker Inc., New York 1998), Chap. 20, 531

[24] A.G. MacDiarmid, *The polyanilines: anovel class of conducting polymers, Conjugated polymers and related materials*, Oxford University Press, 1993

[25] Ford, W.K.; Duke, C.B.; Salanek, W.R. *J. Chem. Phys.,* **77** (1982), 5030

[26] Ritsko, J.J.; Fink, J.; Crecelius, G. *Solid State Commun.,* **46** (1983), 477

[27] Bobacka, J; Ivaska, A; Grzeszczuk, M. *Synthetic Metals,* **44** (1991), 9

[28] J.L. Bredas in *Handbook of Conducting Polymers*, Vol. 2, Ed. T.A. Skotheim, (Marcel Dekker Inc., New York 1986), Chap. 25, 859

[29] J. Tanaka, M. Tanaka in *ducting Polymers*, Vol. 2, Ed. T.A. *Handbook of Con* Skotheim, (Marcel Dekker Inc., New York 1986), Chap. 35, 1269

[30] M. Zagorska, A. Pron, S. Lefranters, Vol. 3, Ed. H.S. Nalwa in *Handbook of Organic Conductive Molecules and Polym* (John Wiley & Sons, New York, 1997), Chap. 4,183

[31] R.E. Peierls, *Quantum theory of solids* (Oxford University Press, London, 1955)

[32] J.L. Bredas, G.B. Street, *Acc. Chem. Res.* **18** (1985), 309

[33] R. Chance, D.S. Boudreaux, J.L. Bredas, R. Silbey in *Handbook of Conducting Polymers*, Vol. 2, Ed. T.A. Skotheim, (Marcel Dekker Inc., New York 1986), Chap. 24, 825

[34] J.L. Bredas, R.R. Chance, R.Silbey, *Phys. Rev. B* **26** (1982), 5843

[35] J.L. Bredas, B. Themans, J.G. Fripiat, J.M. Andre, R.R.Chance, *Phys. Rev. B* **29** (1984) , 6761

[36] J.L. Bredas, D. Beljonne, Z. Shuai, J.M. Toussaint, *Synth. Met.* **41-43**(1991), 3743

[37] E.L. Frankevich, A.A. Lymrev, I. Sokolik, F.E. Karasz, S. Blumstengl, R.H. Baughman, H.H. Horhold, *Phys. Rev. B* **46**(1992), 9320

[38] E. Conwell in *Primary Photoexcitations in Conjugated Polymers: Moleculat Exciton versus Semicondu tor Band Model*, Ed. N.S. Sariciftci (World Scientific Publishing, Singapore, New Jersey, London, Hong Kong, 1997), Chap. 16, 489,

[39] M. Ahlskog, M. Reghu, A. J. Heeger, T. Noguchi, and T. Ohnishi, *Phys. Rev. B* **55** (1997), 6777.

[40] A. J. Epstein, J. Joo, R. S. Kohlman, G. Du, A. G. MacDiarmid, E. J. Oh, Y. Min, J. Tsukamoto, H. Kaneko, J. P. Pouget, Synthetic Metals **65** (1994), 141

[41] H. Angerstein-Kozlowska, J. Klinger, B.E. Conway, *J. Electroanal. Chem.* **75** (1977), 45-61

[42] R.F. Lane, A.T. Hubbard, *J. Phys. Chem.* **77** (1978), 1401

[43] E. Laviron, *J. Electroanal. Chem.* **100** (1979), 263

[44] A.T. Hubbard, *J. Electroanal. Chem.* **22** (1974), 165

[45] E. Laviron, *J. Electroanal. Chem.* **52** (1974), 355-395

[46] H. Angerstein-Kozlowska, B.E. Conway, J. Klinger, *J. Electroanal. Chem.* **87** (1978), 301-321

[47] J.L. B redas, R. Silbey, D.S. Boudreaux, R.R. Chance, *J. Am. Chem. Soc.* **105** (1983), 6555

[48] R.A. Bull, F.F. Fan, A. J. Bard, *J. Electrochem. Soc.* **129** (1982), 1009

[49] S.W. Feldberg, *J. Am. Chem. Soc.* **106** (1984), 4671

[50] Heywang, G.; Jonas, F. *Advanced Materials,* **4(2)** (1992), 116

[51] Münstedt, H. *Polymer,* **29** (1988), 296

[52] Pei, Q.; Zuccarello, G.; Ahlskog, M.; Inganas, O. *Polymer*, **35** (1994), 1347

[53] Dietrich, M.; Heinze, J.; Heywang, G.; Jonas, F. *Journal of Electroanalytical Chemistry,* **369** (1994), 87

[54] a) Bayer AG, *Eur. Patent* 440 957, 1991. b) Agfa Gevaert, *Eur. Patent* 564 911, 1993. c) F. Jonas, W. Krafft, B. Muys, *Macromol. Symp.* **100** (1995), 169

[55] a) Bayer AG, *Eur. Patent* 553 671, 1993. b) Bayer AG, *Eur. Patent* 686 662, 1995. c) Bayer AG, *US Patent* 5 792 558, 1996 d) F. Jonas, G. Heywang,

Electrochim. Acta **39** (1994), 1345 e) J. Hupe, G. D. Wolf, *Galvanotechnik* **86** (1995), 3404 f) F. Jonas, J. T. Morrison, *Synth. Met.* **85** (1997), 1397. g) K. Lerch, F. Jonas, M. Linke, *J. Chim. Phys.* **95** (1997), 1506 h) F. Jonas, K. Lerch, Kunststoffe **87** (1997), 1401

[56] G. Greczynski, T. Kugler, M. Keil, W. Osikowicz, M. Fahlman, and W. R.Salaneck, *Jour. Elec. Spec. & Rel. Phenom.* **121** (2001), 1-17

Chapter 2

Instrumentation

2.1 X-ray Photoelectron Spectroscopy

2.1.1 Introduction

From the early pioneering work of Kai Siegbahn (Nobel prize winner, 1981) and his colleagues at Uppsala, Sweden, through intensive and exciting years of instrumental, interpretational and applicational development over the last decade, X-ray photoelectron spectroscopy (XPS) has matured into one of the most powerful and valuable methods of surface analysis currently available. The universal applicability, high throughput, ease of interpretation and wealth of information provided by this technique, place XPS above most other methods of surface analysis in a large number of areas of application, such as polymers, organics, biological specimens, fibers, films, powders and particles. XPS is one of the few techniques, which would possess the following attributes: quantitative molecular speciation (including sensitivity to conformation etc.), sampling depth variability from 0.2 to 10nm, real time analysis (fast measurements). Thus it is a strong technique in polymer surface analysis. [1]

2.1.2 Basic Principles and Theory

In XPS, the X-ray causes photoionization of atoms in the specimen and the response of the specimen (the photoemission) is observed by measuring the energy spectrum of the emitted photoelectrons.

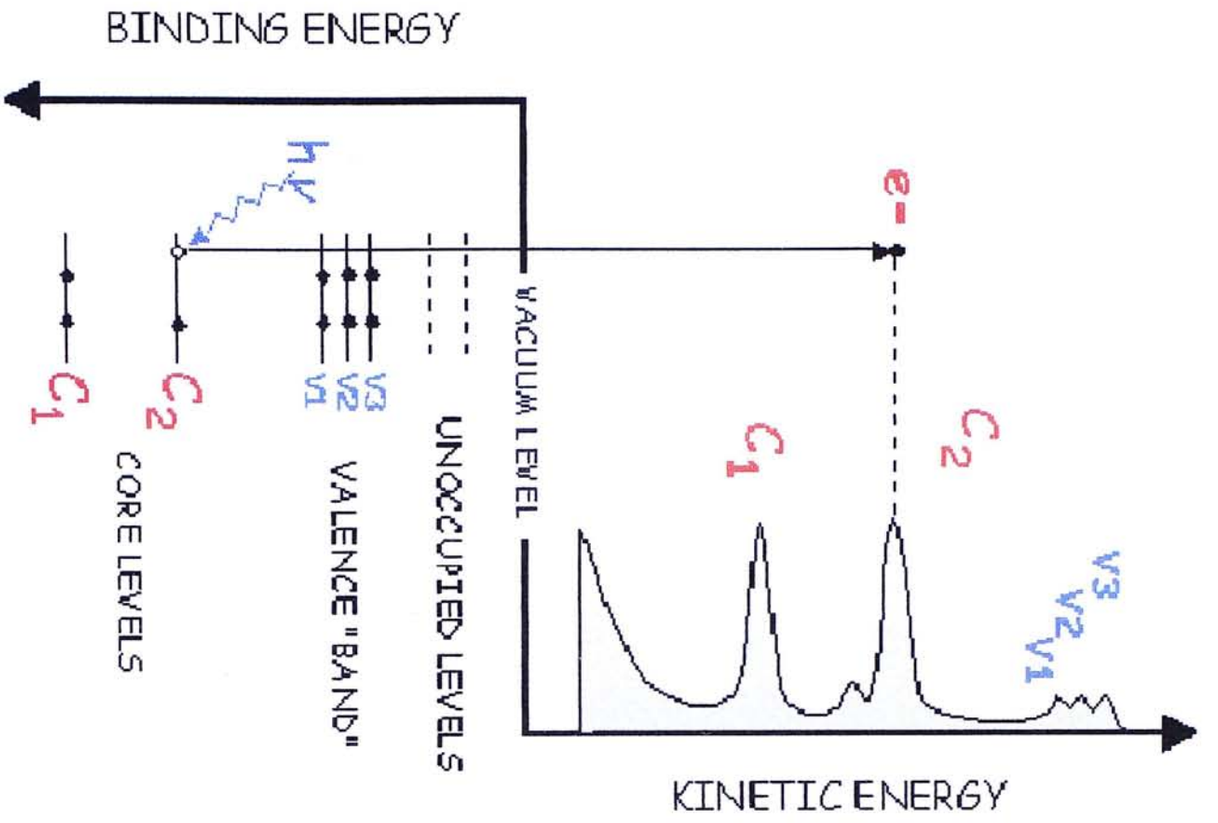

Fig 2.1 Simplified picture of how a spectrum is obtained through the ionization of the various electron levels

Each atom present in the surface (except hydrogen and helium) possesses core level electrons not directly involved in the bonding. The so-called binding energy (E_b) of each core level electron (conceptually, but not strictly, equivalent to the ionization energy of that electron) is characteristic of the individual atom to which is bounded. Information on the binding energies of electrons within a sample allows qualitative elemental analysis. In the basic XPS experiment, the sample surface is irradiated by a source of low-energy X-rays under ultra-high vacuum (UHV) conditions. Photoemission then takes place in the sample surface, the resultant photoelectrons having a kinetic energy (E_k), which is related to the X-ray energy ($h\nu$) and E_b by Einstein relation (Einstein, 1905):

$$E_k = h\nu - E_b$$

If the photoelectrons have sufficient kinetic energy they are able to escape from the surface by overcoming the specimen work function, and photoemission is said to occur. The entire process is referred to as the photoelectric effect.

During an experiment, a sample is inserted into the spectrometer and is irradiated with photons. The ejected electrons are collected and detected by a system consisting of electromagnetic lenses, a hemispherical analyzer and for some, an electron multiplier, typically a multi-channel plate setup. Such a system can be adjusted to collect and analyze electrons from different energy regions (basically works as a band pass filter). Each element gives rise to its own specific photoemission peak pattern: a spectrum. This is because each filled electron orbital gives rise to a peak at a specific energy (depending on the photon energy). Fig. 2.1 shows an example of a photoelectron spectroscopy spectra and how the different electron energies/orbitals give rise to specific peaks.

2.1.3 Qualitative Analysis Using XPS

A number of sharp peaks with varying intensities are observed in an XPS spectrum. The intensity of each peak is proportional to the probability of photoemission from different core levels. As the binding energy is unique for each core level, if the binding energy range of a peak is located, the core levels appeared in the sample of interest can be identified. Characteristic binding energies for different elements for reference can be found in the relevant XPS literature and database. [2] Therefore, XPS can give an elemental analysis of the sample.

2.1.4 Angular Effect on XPS

The XPS spectra can be strongly influenced by the particular geometry employed in the measurement, i.e. the relative orientation of the X-ray source, the sample and the detector and their relationship is shown in Fig. 2.2.

If λ is the inelastic mean free path of the specimen of interest, then 95% of the signal intensity is derived from a distance 3λ within the solid. However, the vertical depth is given by

$$d = 3\lambda \sin\alpha$$

and d_{max} is 3λ when $\alpha=90°$. [3] α is often called the take off angle. As a result, at a small take off angle, XPS will probe a shallow depth.

2.1.5 Chemical Shift

The binding energy of an electron is sensitive to the electronic charge associated with the parent atoms. When the parent atom is bonded to non-equivalent atoms, the charge distribution on the parent atom will differ from its pure state(s).

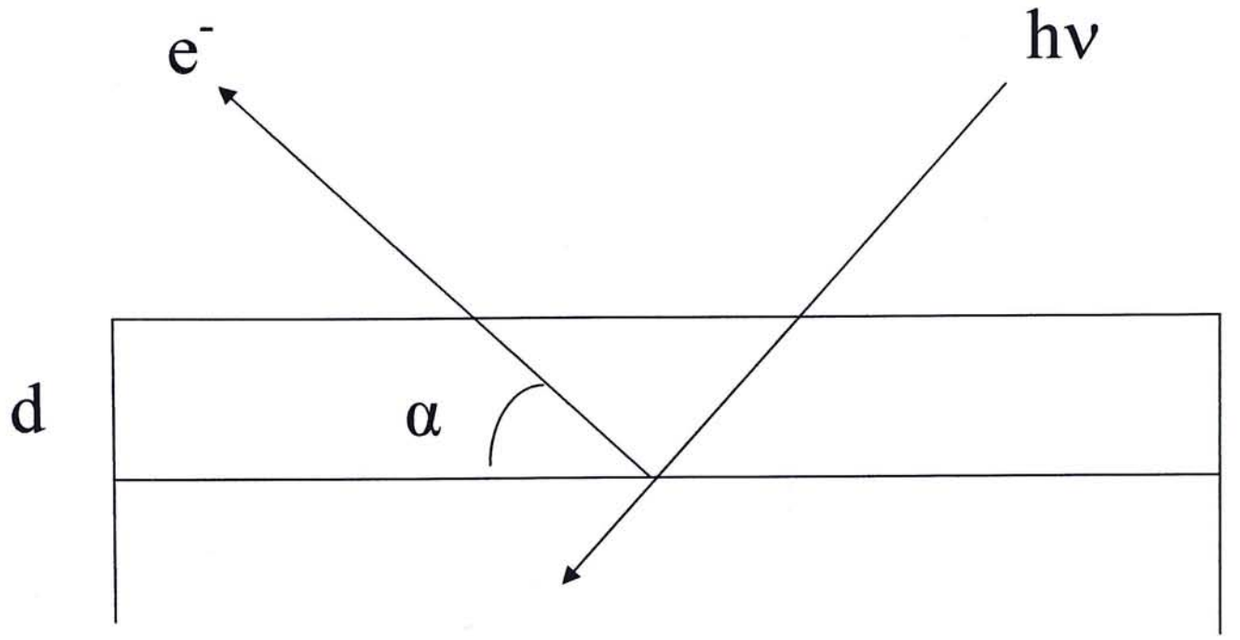

Fig. 2.2 Surface sensitivity enhancement by variation of the electron take off angle

Hence, the binding energy of the electron will change. This kind of change of binding energy due to different chemical environment is called chemical shift.

Qualitatively, when an atom is bonded to an atom with a higher electronegativity, the electronic charge density on the atom will decrease and shift the electron to a high binding energy since the electron experiences a stronger nuclear attractive force. On the other hand, when an atom is bonded with an atom with a lower electronegativity, the electron charge density on the atom will increase and shift the electron to a lower binding energy. Using the above principles as a rule of thumb, the chemical states of the element can be estimated from the XPS analysis.

2.1.6 Valence Band Investigation

Valence levels are those occupied by electrons of low binding energy (say 0-20eV), which are involved in delocalized, or bonding orbitals. The spectrum in this region consisted of many closely packed energy level giving rise to a band structure. Therefore, isolated peaks usually are not clearly differentiated in the valence band spectrum. Generally speaking, the cross-sections for X-ray induced photoelectron emission from valence levels are much lower than those from core levels. However, valence band spectra can act as fingerprints for electronic materials and polymers, providing electronic structure information that cannot be obtained from common core level analysis.

2.1.7 Quantitative Analysis Using XPS

The complete XPS spectrum of a material contains peaks that can be associated with the various elements (except H and He) present in the outer 10 nm of that material. The area under these peaks is related to the amount of each element

present. So, by measuring the peak areas and correcting them for the appropriate instrumental factors, the percentage of each element detected can be determined. The equation that is commonly used for these calculations is:

$$I_{ij} = KT(KE)L_{ij}(\gamma)\sigma ij \int n_i(z)e^{-z/\lambda(KE)\sin\theta}dz \qquad (1),$$

where I_{ij} is the area of peak j from element i, K is an instrumental constant, T(KE) is the transmission function of the analyzer, $L_{ij}(\gamma)$ is the angular asymmetry factor for orbital j of element i, σ_{ij} is the photoionizaton cross-section of peak j from element i, $n_i(z)$ is the concentration of element i at a distance z below the surface, $\lambda(KE)$ is the inelastic mean free path length, and θ is the take off angle of photoelectrons. This equation assumes that the sample is amorphous.

In general, a fractional atomic concentration, C_A, of element A in a matrix is often given by:

$$C_A = \frac{I_A / S_A}{\sum_n (I_n / S_n)}, \qquad (2)$$

where I_n is the measured peak intensity for element n and S_n is the relative atomic sensitivity factor for that peak.

2.1.8 Instrumental Setup for XPS

The XPS system used in this study was the PHI Quantum 2000 Scanning ESCA Microprobe (Fig. 2.3). It is a laboratory-based spectrometer with automated operation and large productivity. The system includes the following components: a monochromatized Al K_α source, a hemispherical energy analyzer, an electron gun for sample charge neutralization, an argon ion

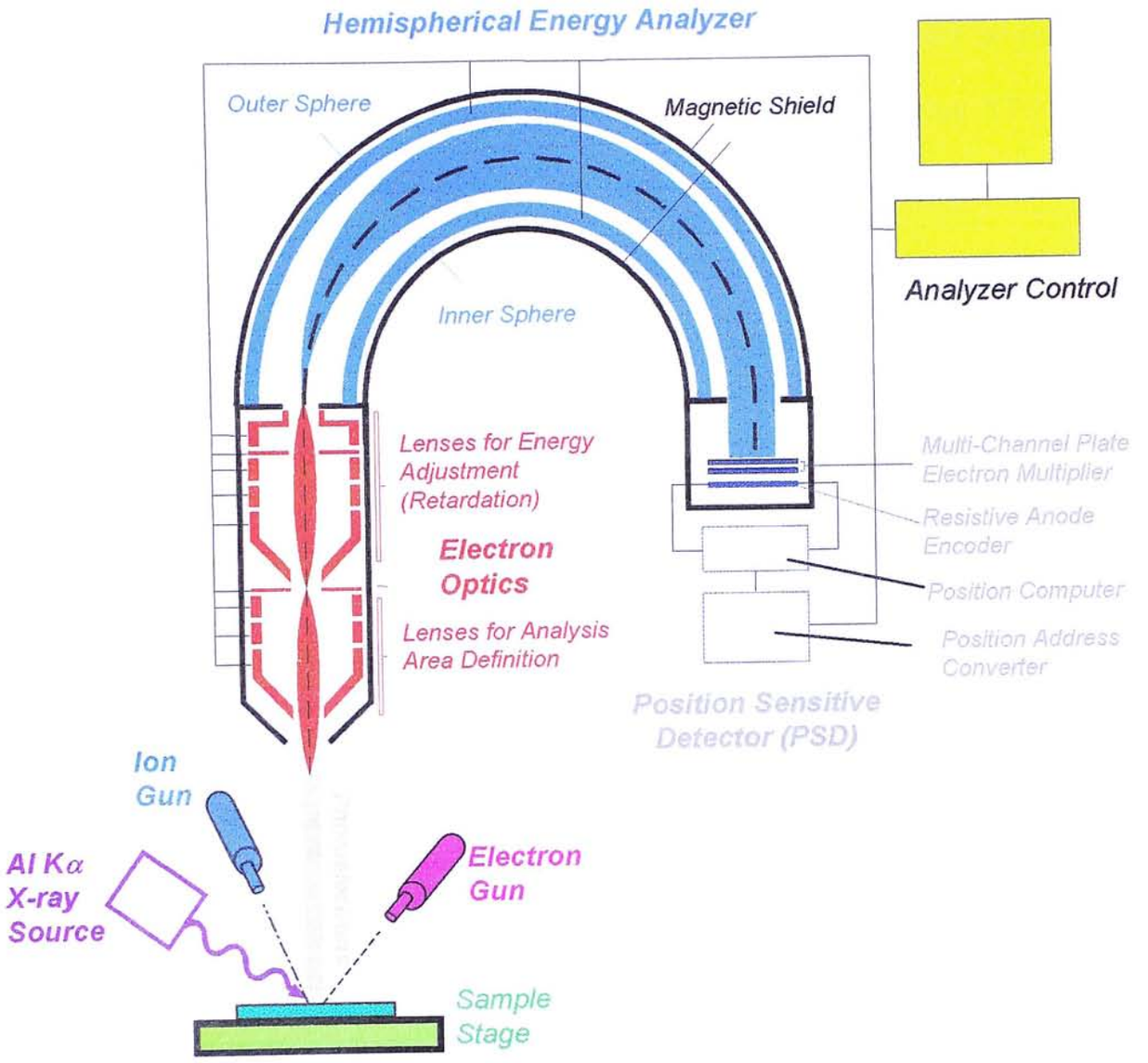

Fig 2.3 Diagram of the operation system in XPS

gun for both sample charge neutralization and sample sputtering, and a sample stage which can be tilted to 180°. All these components were installed in an ultra high vacuum (UHV) chamber at a common pressure of 1 x 10^{-9} Torr. Au $4f_{7/2}$ line of a

sputtered cleaned gold foil at 84.00 eV is used for the calibration of the binding energy scale. In all the experiments, the take off angle was 90°, thus a probing depth of ~ 55Å was achieved. The charging effect possibly induced during XPS analysis was examined by performing acquisitions with two different X-ray powers from a maximum of 25W to a minimum of 2.5W. If the peak position of the signal remains the same in both circumstances, there should be no charging effect on the sample examined.

2.2 Scanning Probe Microscopy

2.2.1 General Introduction

In 1981, Binnig and Rohrer [4], and their colleagues at the Zurich Research Laboratory of the International Business Machines (IBM) developed a new kind of surface analytical instrument – scanning tunneling microscopy (STM). The emergence of STM made it possible to observe the arrangement of individual atoms on conducting material surfaces, and physical and chemical properties related to the behavior of surface electrons in real space. This successful achievement brought rapid advances in STM technology and led to the many other novel scanning probe microscopy, such as atomic force microscopy (AFM), lateral force microscopy (LFM), magnetic force microscopy (MFM), ballistic-electron-emission microscopy (BEEM), scanning ion-conductance microscopy (SICM), near-field scanning optical microscopy (NSOM), scanning thermal microscopy, and scanning tunneling potentiometry (STP). These microscopes take advantage of the remarkable ability to control the spatial position of the tip relative to the sample. This provides new information about the physical properties of surfaces on an atomic or nanometer scale.

2.2.2 Atomic Force Microscopy and Conducting Atomic Force Microscopy

The tunneling phenomenon utilized by the STM requires the instrument be used only for conductors or semiconductors. For non-conducting materials, its surface must be covered with a thin conducting film, which often lowers the resolution and thus limits the usefulness of the STM. It was chiefly this limitation that prompted the development of atomic force microscopy (AFM) in 1986 [4-6], which can be applied to image both conductors and non-conductors in air, liquid, and vacuum.

The operational principle of AFM is explained in Fig. 2.4. The cantilever, which is extremely sensitive to weak forces, is fixed at one end; the other end has a sharp tip which gently contacts the surface of a sample. When the sample is being scanned in x-y direction, because of the ultra-small force, which can be inter-atomic, frictional, magnetic and electrostatic forces, existing between the tip atoms and the surface atoms of the sample, the cantilever will move up and down in the direction vertical to the surface of the sample, corresponding to the contours of the interaction force between the tip and the surface atoms of the sample. The topographic images can be obtained either by recording the deflection of the cantilever at each point (variable deflection mode) or by keeping the force constant using an integral feedback loop and recoding the z-movement of the sample (constant force mode). While the STM yields images related to surface electronic states near the Fermi level, AFM

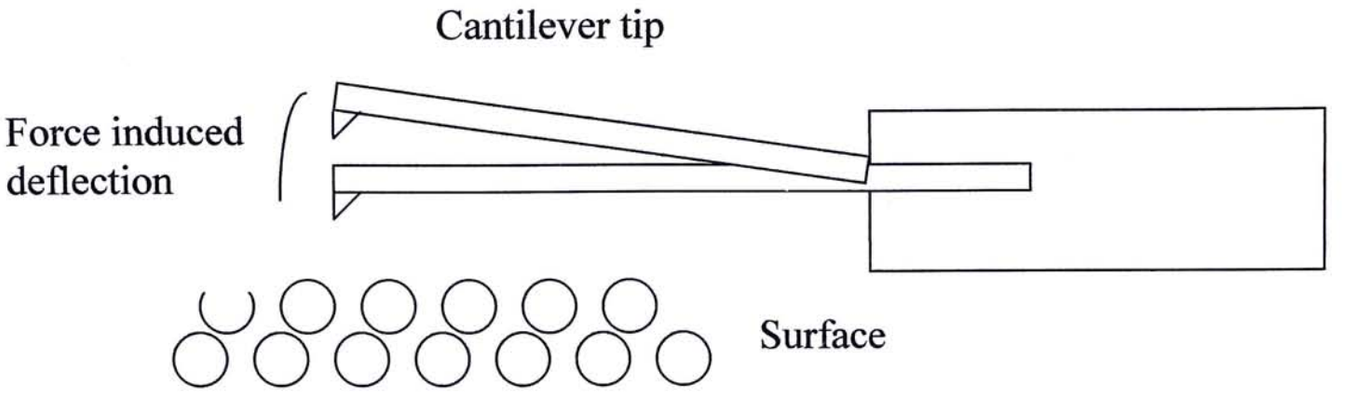

Fig. 2.4 schematic diagram of AFM operation

images are related to surface electronic energies up to the Fermi level. The AFM tip may be kept in direct contact with the surface (contact mode) or it may be vibrated above the surface (non-contact mode).

A comparatively newly developed area is the use of AFM with conducting tips to measure the local electrical properties of materials. In contrast to scanning tunneling microscopy (STM), conducting AFM technique can measure electrical properties on insulating surfaces and equally importantly the tip-sample distance is controlled independently of the measured current.

Tips used for conducting AFM should be mechanically robust to survive the forces applied when scanning and the additional forces to form an electrical contact by penetrating or displacing contaminant or passivation layers. And tips should also be chemically inert to avoid passivation by oxidation or electrochemically induced reactions that could interfere with their conductivity. In addition, they should be sharp enough to provide a good resolution of scan images. [7,8] Tips coated with Au, Ag, or Pt, used for conducting AFM at present are of highly conductivity, but susceptible to wear. [8, 9] Coatings of boron-doped diamond [10] provide excellent mechanical stability and promising electrical properties, but contamination of the tip can compromise its conductivity. [7, 9] Conducting diamond tips have been used successfully for AFM application such as high-resolution scanning resistance profiling on the nanoscale [11, 12], local electrical characterization of semi-conducting films [13] or organics [14].

2.2.3 Instrumental Setup for Conducting AFM

The AFM systems used here is a commercially available UHV STM/AFM (Omicron UHV VT AFM). All the experiments were done at room temperature and at a base pressure of 5×10^{-9} Torr. Local I-V measurements were done in such a way: when recording the I-V curves, the actual scan was stopped, the tip was moved to the desired position, and after a delay of 2.5 ms the feedback loop was switched off and a voltage ramp was applied. With completion of the procedure, the interrupted scan was continued. The measurement range of the tunneling current was $\pm$ 50 nA, to safely avoid over-modulation at the ends of the I-V measurements. The positive bias means the voltage from tip to the sample is positive, and the samples were always grounded during all experiments. For conducting AFM measurement, triangular SiN cantilevers with spring constants of 0.15 N/m were used in contact mode for simultaneous topography and current measurements. The tips were precoated a Cr layer and then an Au film by the manufacturer.

2.3 Cyclic Voltammetry

Cyclic voltammetry was used both to polymerize the monomers and to characterize electrochemically the resultant polymers. The method basically involves measurements over the resultant current produced by an applied triangular potential waveform. The potential is cycled within a given potential range at a constant rate and the current is measured as a function of the potential. The rate can vary from less than 1 mV/s to several hundred V/s.

When a high enough potential is applied at an electrode surface to cause oxidation or reduction of species in solution, a sharp current change occurs due to the depletion of said species in the vicinity of the electrode surface. A concentration

gradient appears in the solution in question. The current i is proportional to the gradient slope imposed:

$$i \propto \frac{dc}{dx}.$$

The slope decreases with time, as the ion must diffuse to the electrode surface from farther and farther away. The current thus decreases as well (if the potential remains constant).

In the case of cyclic voltammetry, however, the potential does not stay constant. It rises at a constant rate until it reaches a chosen maximum, and then decreases again at the same rate. The current does not reach a maximum immediately after imposition of the potential, as the potential is not immediately great enough to give rise to any reaction. The current starts to rise as the potential enters the area where oxidation or reduction can occur. It then continues to rise rapidly as the surface concentration of the species becomes smaller and smaller (the concentration gradient increases). The peak current consists of two components. In addition to the diffusion-controlled current discussed above, there is also a contribution from the initial current surge required to adjust the surface concentration of the reactant to its equilibrium concentration as given by the Nernst equation. The current then decays rapidly as the diffusion layer begins to extend further and further away from the electrode surface (gradient slope decreases and therefore, so does the current). The same progression is seen on the negative scan as well, but in the opposite direction. From the anodic and cathodic peak currents and potentials, important parameters characterizing chemical materials can be calculated, such as rate constants for oxidation/reduction processes and the doping/dedoping within a polymer film. Cyclic voltammetry is often used to study reaction mechanisms and detect reaction intermediates.

Here a homemade cyclic voltammeter is used to utilize the cyclic voltammogram measurements. Control programme was written based on National Instruments Labview 6.1 to control a Keithley 236 source measurement unit and to perform the CV measurements. The work place for CV solution measurements was set up to control the electrochemical reaction at a fixed distance between the cathode and anode, as has been illustrated in Fig. 2.5.

2.4 Kelvin Probe

Kelvin probe is a vibrating capacitor technique used to measure the work function of metals and semiconductors. In this study, the Kelvin probe being used is a UHV compatible McAllister KP-6000 system. It consists of a vibrating reference electrode in plane-parallel orientation to the sample, forming a vibrating capacitor, thus it is able to measure the change in work function of metals, semiconductors and liquids. The Kelvin method has extremely high surface sensitivity (<0.1 meV, typically corresponding to $10^{-3}$of an adsorbate layer) and is completely non-damaging, even to the most sensitive adsorbates. The sample and probe are connected via a voltage source called the "backing potential" (V_b). When V_b is set to zero, a contact potential difference (V_{cpd}) equal to the difference in the probe work function and sample work function appears across the probe/sample surfaces. The change in work functions is measurable by $\Delta wf = e\Delta V_{cpd}$ where e is the electronic charge. At the unique point where $V_b = -V_{cpd}$ the circuit is balanced, and the electric field between the surfaces vanishes and results in a null output signal. This null condition can be detected with high precision, thereby directly measuring the change in work functions. In our experiment, the work function of the probe is calibrated with a UV ozone etched gold sample with a work function of 5.4 eV.

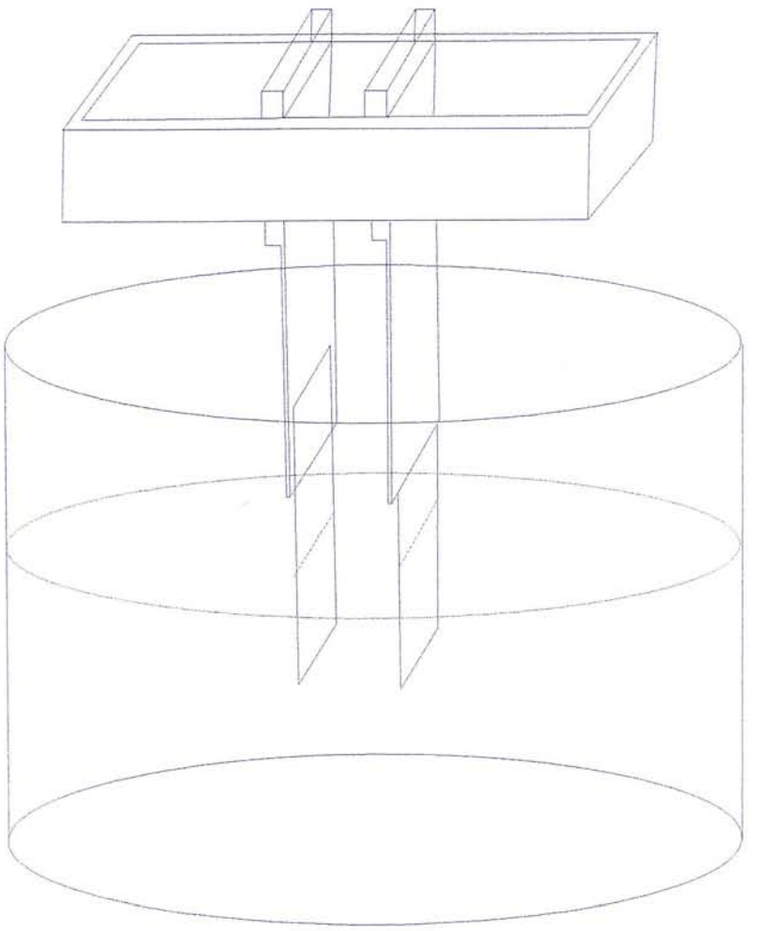

Fig. 2.5 The homemade work place for CV solution measurements where electrochemical reaction is controlled at a fixed distance between the cathode and anode

2.5 α-Step Profilometer

The thickness of thin films prepared in our experiments was measured by the Tensor Alpha Step 500 profilometer. It uses a diamond tip to scan the sample surface to get information about the surface topography. The tip has a finite surface area which interacts with the sample being scanned. When the tip scans across the surface of the sample, an inductive sensor registers the vertical motion of the tip. The signal generated by the motion of the tip is used to create a two-dimensional profile of the surface. The measuring range of thickness for the profilometer is from 10 Å to 0.3mm with vertical resolution of 1 Å. For the thickness measurement of the polymer film samples, the film was first slightly scratched by a cutter to produce a groove, and then the tip was scanned across the groove to give the thickness information.

References

[1] D. Briggs, *Surface Analysis of Polymers by XPS and Statics SIMS* (Siacon Consultats Ltd, 1998)

[2] C. D. Wagner, W. M. Briggs, L. E. Davis, J. F. Moulder and G. E. Muilenburg, *hand book of X-ray photoemission spectroscopy* (Perkin-Elmer Corporation, eden Praire, 1979)

[3] D. Briggs and M. P. Seah, *Practical Surface Analysis*, 2nd edition (Wiley, Chichester, 1996), Vol. 2.

[4] G. Binnig, C.F. Quate, C.Gerber, *Phys. Rev. Lett.* **56** (1986), 930

[5] N.A. Burnhm, R.J. Colton (des.), *Force Microscopy, in Scanning Tunneling Microscopy and Spectroscopy* (VCH, Weinheim 1993)

[6] D. Sarid, *Scanning Force Microscopy* (Oxford Univ. Press, Oxford 1990)

[7] S. J. O' Shea, R. M. Atta, and M. E. Welland, *Rev. Sci. Instrum.* , **66** (1995), 2508

[8] R. E. Thomson and J. Moreland, *J. Vac. Sci. Technol. B*, **13** (1995), 1123

[9] M. A. Lantz, S. J. O'Shea, and M. E. Welland, *Rev. Sci. Instrum.*, **69** (1998), 1757

[10] Ph. Niedermann, N. Blanc, R. Christoph, and J. Burger, *J. Vac. Sci. Thehnol. A* **14** (1996), 1233

[11] J. N. Nxumalo, D. T. Shimizu, and D. J. Thomson, *J. Vac. Sci. Technol. B*, 386 (1996)

[12] P. De wolf, T. Clarysse, W. Vandervorst, L. Hellemans, P. Niedermann, and W. Hanni, *J. Vac. Sci. Thchnol. B*, **16** (1998), 355

[13] C. Ballif, M. Regula, F. Levy, F. Burmei, P. Niedermann, T. Matthes, P. Liederer, W. Gutmannsbauer, and R. Bucher, *J. Vac. Sci. Technol. A*, **16** (1998), 1239

[14] M. J. Loiacono, E. L. Granstrom, and C. D. Frisbie, *J. Phys. Chem. B*, **102** (1999), 1679

Chapter 3

Cyclic Voltammetric Characterization of PEDOT:PSS

3.1 Film Preparations

The polymer (PEDOT: PSS) films were dropped and spin-cast from as received PEDOT:PSS solution (as has been described in Section 1.4 of Chapter 1) onto the clean Au/glass which was used as a clean working electrode. The detailed steps for film preparations are listed below.

1. Glass substrate preparations (which is similar as common clean method for ITO) [1]
    1) The pieces of glasses were cleaned in acetone in the ultrasonic bath for 5 min.
    2) Swabbed in deionized (DI) water.
    3) Cleaned in propyl alcohol in the ultrasonic bath for 20 min.
    4) Swabbed in DI water.
    5) Cleaned in DI water in the ultrasonic bath for 5 min.
    6) Swabbed in DI water.
    7) Cleaned in acetone for 20 min in the ultrasonic bath.
    8) Swabbed in DI water.
    9) Cleaned in ethanol in the ultrasonic bath for 20 min
    10) Dried with N_2 flux.

11) UV/O_3 treated at an O_2 flow rate of 500cc/min for 15min.

2. Preparation of the working electrode

12) Au was sputtered onto the cleaned glass surface through Ar^+ sputtering using the POLARON SC502 SPUTTER COATER.

13) Au/glass was flame annealed using a butane flame, the temperature of which is about 1200 K, so as to make the Au film smoother.

14) Au/glass was UV/O_3 treated for 15 min at an O_2 flow rate of 500 cc/min.

3. PEDOT: PSS film formation

15) The as received PEDOT: PSS solution was spin cast onto Au/glass surface at a spin speed of 2000 rpm using the CHEMAT TECHNOLOGY Spin-coater (KW-4A).

16) The PEDOT: PSS/Au/glass film was put into vacuum where pressure was about 5 Torr for more than 10 hours so as to get a dry PEDOT: PSS film.

3.2 Electrochemistry

All electrochemical experiments were carried out at room temperature in a homemade setup as illustrated in Fig. 2.5. The supporting electrolyte was tetrabutylammoniumhexaflurophophate ($TBAPF_6$) 98% (Aldrich) in acetonitrile anhydrous (Aldrich) at a concentration of 0.2 M. For cyclic voltammetry (CV) the working electrode was PEDOT:PSS/Au/glass while the counter electrode was Au/glass. CV was done on the polymer films with a potential sweep rate of 50mV/s between two limited potential values. The current that passed through the electrochemical cell was measured between the working electrode and the counter

electrode. The potential values here referred to the Au counter electrode, as a reference electrode cannot be used in the homemade CV measurements. Thus the potential value here was a bit larger than that between working electrode and the "reference electrode" (if there can be one in present experiments) due to the non-compensation of the potential ullage in the electrolyte solution.

3.3 Results and Discussion

Kvarnstrom et al. found that a small peak occured with a maximum at –1750 mV in the redox response of the PEDOT film in a monomer free solution during n-doping. [2] Ahonen, et al, also found that in voltammetry of PEDOT films, the cathodic branch exhibits increasing cathodic currents during downward sweep after a small shoulder at ca. –2.2 V and a single anodic peak at –2.05 V on the return sweep. In addition, whenever the potential sweep was extended to the opposite side of the voltammogram, sharp prepeaks on the cathodic branch could be seen at ca. –1.8 V. [3]

The cyclic voltammetric response of a PEDOT: PSS film in a 0.2 M $TBAPF_6$-acetonetrile solution at a scan rate of 50 mV/s can be seen in Fig. 3.1. The potential range between –2.0V and +0.2V was cycled for n-doping. The illustrated plot shows the first scan.

The redox response during n-doping is essentially the same as those reported in references [2, 3]. At the beginning of the forward scan, the current increased gradually with the increasing negative potential and PEDOT was dedoped from its p-doped state (p-doped by PSS^-). A small peak occurred with a maximum at –1.75 V, at more negative potentials the current increases and during the reverse scan a re-oxidation (dedoped from n-type PEDOT) from the process can be seen immediately after the scan direction is reversed. Generally this kind of voltammetric behavior has

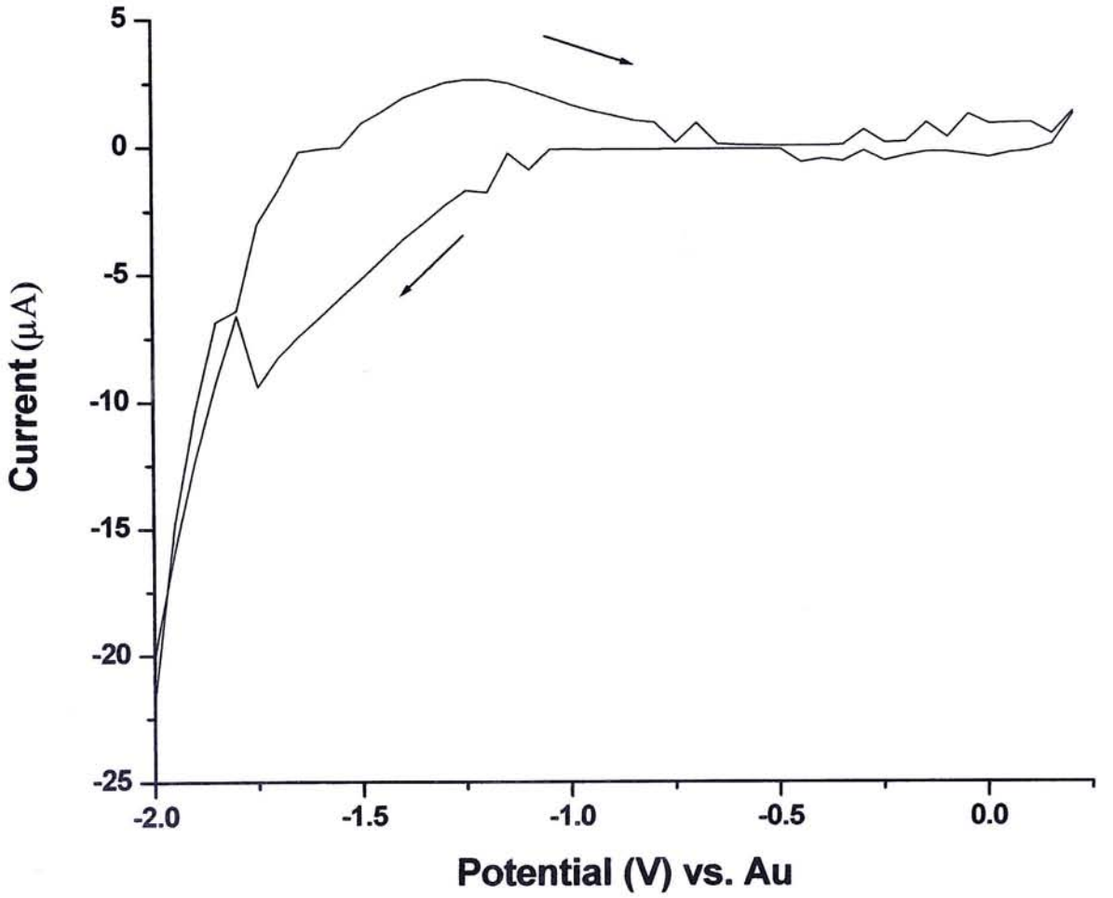

Fig. 3.1 A cyclic voltammogram of a PEDOT: PSS film on an Au electrode in 0.2 M $TBAPF_6$-acetonetrile solution at a scan rate of 50mV/s (n-doping process)

been attributed to n-doping with polythiophene derivatives. [4, 5, 6]

The CV measurement here shows that as received PEDOT: PSS (PEDOT p-doped by PSS^-) had similar CV characteristics as common electrochemically synthesized PEDOT. In the next sections, X-ray photoemission spectroscopy (XPS) and conducting AFM were used to study PEDOT:PSS system electrochemically dedoped and n-doped at different potentials so as to further characterize the properties of dedoped and n-doped PEDOT and reveal its doping and dedoping mechanism.

References

[1] J. Kim, J. Lee, C. W. Han, N. Y. Lee, and I. Chung, *Appl. Phys. Lett.* **82** (2003), 4238

[2] C. Kvarnstrom, H. Neugebauer, A. Ivaska, and N.S. Sariciftci, *J. Mol. Struc.* **521** (2000), 271

[3] H. J. Ahonen, J. Lukkari, and J. Kankare, *Macromolecules*, **33** (2000), 6787

[4] Y. Fu, H. Cheng, and R. L. Elsenbaumer, *Chem. Mater.* , **9** (1997), 1720

[5] H. Huang, and P. Pickup, *Chem. Mater.* , **10** (1998), 2212

[6] Q. Pei, G. Zuccarello, M. Ahlskog, and Ol Inganas, Polymer, **35** (1994), 1347

Chapter 4

Electronic Structure of Doped and Dedoped PEDOT:PSS Systems

4.1 Introduction

Doping in polymeric materials that involves addition or removal of electrons from polymer chains is the central key to achieving conductivity in conducting polymers. By chemical or electrochemical method, the doping level can be controlled. For example, poly(3, 4-thelenedioxythiophene), or PEDOT [1, 2], is an electro-chemically stable conjugated polymer which can be oxidized (p-doped) to a state of high electrical conductivity [3], while maintaining moderate transparency [4-7]. Oxidized PEDOT (p-doped with poly(4-styrenesulfonate), or called as PEDOT:PSS, is used as anti-static coatings on Agfa photographic film [8]. It is also used as a hole transport layer in proto-type polymer-based light-emitting devices (p-PLEDs) [7, 9]. PEDOT:PSS is now one of the most commercially successful organic conductors for its excellent characteristic properties. [8]

Up to now, much work has been done to study the doping and dedoping effect of PEDOT:PSS. Heeger et al. found that the conductivity of PEDOT: PSS at room temperature is dependent on the pH of solutions from which the film is cast. [10] Aasmundtveit, et at found that electrochemical doping and dedoping of PEDOT/tosylate takes place with no significant changes in the arrangement of polymer chains and tosylate ions in the unit cell, and the doped material has a more

well-defined structural order than the dedoped material. [11] Froberg et al. found that the crystallinity and the surface morphology of PEDOT films on platinum surface could be easily controlled in electrochemical synthesis by tuning the polymerization potential, which corresponds to the doping level of PEDOT. At low switching potential, a dense amorphous PEDOT film on the platinum surface is obtained, and at higher potential (which means a high doping level), a porous crystalline film is formed. [12] In our previous work, it was found that diffused/dissoluted indium dedopes PEDOT in a system of PEDOT: PSS/ITO, and this leads to a degradation of the corresponding PLED devices. In addition, the Fermi level of PEDOT:PSS shifts upwards through pH dedoping method. [13] In the work described this chapter, XPS and Kelvin probe measurements were used to reveal the doping and dedoping mechanisms associated with electrochemical treatments.

4.2 Sample Preparations

The first step of sample preparations is to prepare samples for electrochemical reactions. This step is the same as sample preparations for CV, as have been described in Chapter 3.1. Samples were electrochemically dedoped at room temperature in a homemade setup as has been illustrated in Fig. 2.5. The supporting electrolyte was tetrabutylammoniumhexaflurophophate ($TBAPF_6$) 98% (Aldrich) in acetonitrile anhydrous (Aldrich) at a concentration of 0.2 M. The working electrode was PEDOT:PSS/Au/glass while the counter electrode was Au. Then PEDOT:PSS film was electrochemically dedoped at certain potential for enough time (commonly 10 min to 15 min) until the current did not decrease and reached a saturated value. The potentials selected for dedoping were -0.2 V, -0.4 V, -0.6 V, -1.0 V, -1.2 V, -1.4V, -1.6 V, and -1.7 V, respectively. The electrochemical process is illustrated in Fig.

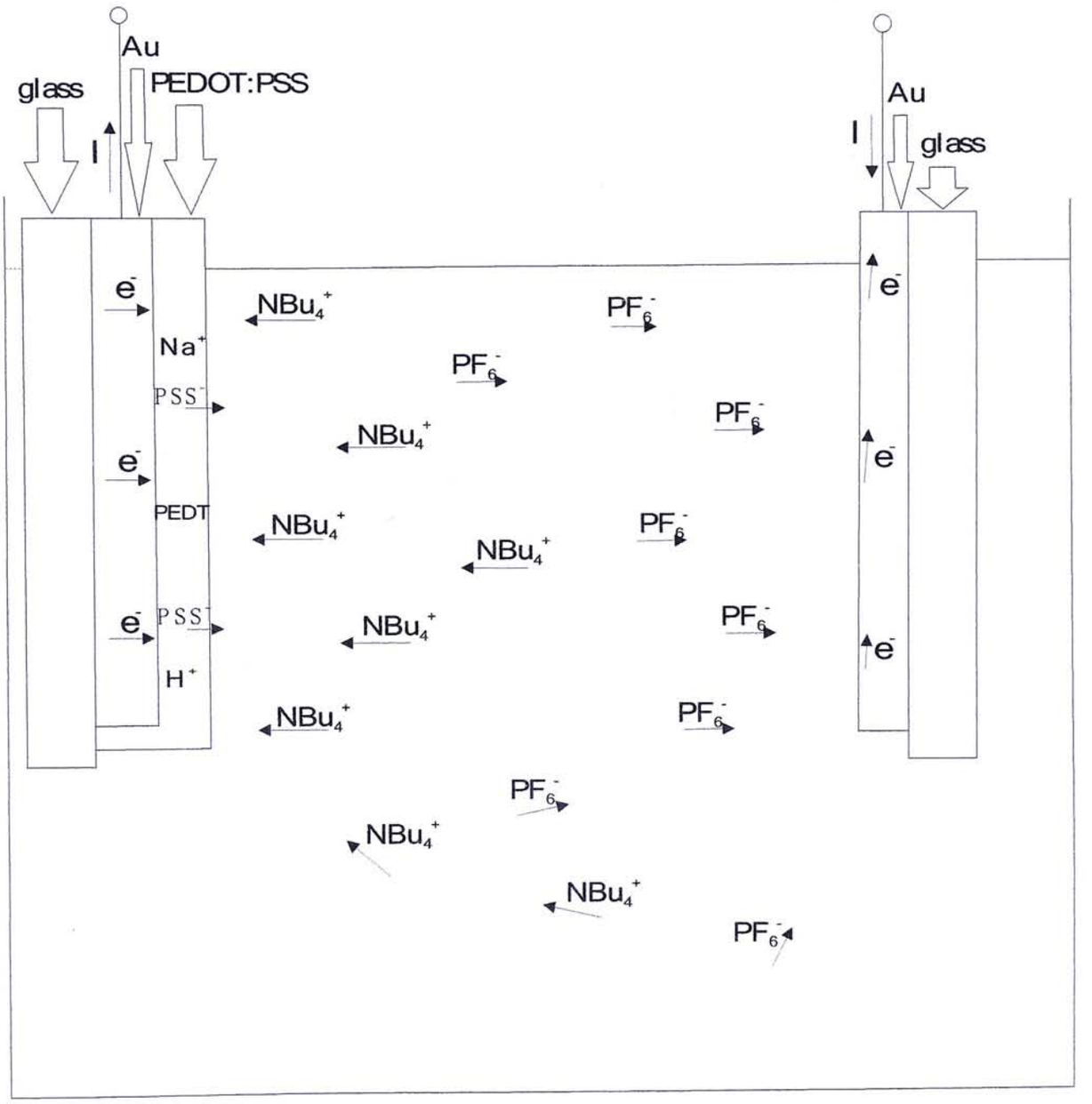

Fig. 4.1 Picture illustrating the electrochemical reaction in the solution

4.1. During dedoping, the positive ions, NBu_4^+, were attracted towards the working electrode, PEDOT:PSS/Au, which was maintained at a negative potential. The negative ions, PF_6^-, were attracted to the counter electrode with a positive potential. The negative ions, PSS^- which were originally coupled to $PEDOT^+$, H^+, and Na^+, decoupled from them and part of the PSS^- might even move out from the film and dissolute to the electrolyte. After the electrochemical reaction, the PEDOT:PSS/Au/glass was taken out and carefully dried under a dry N_2 flow. Finally it was loaded into the analysis chamber for XPS or Kelvin probe measurements.

4.3 Results and Discussion

The chemical structure of as prepared PEDOT: PSS film under investigation is shown in Fig1.10. The constituent elements in PEDOT are C, O and S with an atomic ratio of 6:2:1 respectively. For PSS, it is actually a polymeric anion that can couple to three different counter ions: $PEDOT^+$, H^+ and Na^+ in the present sample system. The atomic ratio of C, O and S in PSS is 8:3:1 for all three possible couplings. Since PEDOT:PSS is composed of different chemical species, the constituent elements may exist in various chemical states. Thus we must take extra care to interpret the XPS analysis results. Pure PSSH and PSSNa films were, therefore, used to provide standard and reference information for analysis. [13] Compositional analysis, together with spectral analysis on C 1s, S 2p, O 1s core levels, and the valence band of PEDOT:PSS in different doping states (as prepared and electrochemically dedoped and doped) will be described and interpreted in following sections.

4.3.1 XPS of C 1s Core Level of PEDOT:PSS

Since carbon exists in different chemical states, the convoluted C 1s peak is quite broad. Consequently, it is difficult to interpret C 1s spectrum in terms of contributions from different types of carbons among which, the chemical shift difference of some of them may be beyond the limit of XPS. The energy resolution is 0.05 eV~ 0.1 eV for the pass energy of 23.5 eV used in the present series of experiments. Here we used a simplified method and consider that there are only two components in the C 1s peak. The peak at a lower binding energy, labeled as "Peak 1", corresponds to C atoms in the PSS and the C atoms in the PEDOT which are not bonded to the oxygen atoms (for dedoped PEDOT:PSS, it also correspond to C atoms in NBu_4^+ ions). The peak at a higher binding energy, labeled as "Peak 2", corresponds to those C atoms in the PEDOT which are bonded to oxygen atoms. [14] This assignment is based on the fact that the binding energy of C 1s in C=O should be much higher than the averaged energy of C=C-C=C and C-C-S, and that the binding energies of **C**-C-S and C-**C**-S should be quite similar as the carbon chain is a conjugated system.

Figure 4.2 shows the C 1s spectra of PEDOT:PSS electrochemically dedoped at –0.2V, -0.3V, -0.4V, and –0.6V. The peak position of Peak 1 and Peak 2 of all these four species were almost identical with Peak 1 at 284.7 eV and Peak 2 at 286.1 eV. Figure 4.3 shows the C 1s spectra of PEDOT:PSS electrochemically dedoped at –1.0V, -1.2V, and –1.4V. It can be seen that the peak positions of Peak 1 and Peak 2 for all the three species slightly shifted to 284.8 eV for Peak 1 and 286.2 eV for Peak 2. Figure 4.4 shows the C 1s spectra of PEDOT:PSS electrochemically dedoped at –1.6V and –1.7V. Peak 1 and Peak 2 shifted to 285.3 eV and 286.7 eV respectively. For clarity, PEDOT:PSS as prepared, and PEDOT:PSS dedoped at the range of (-0.2V

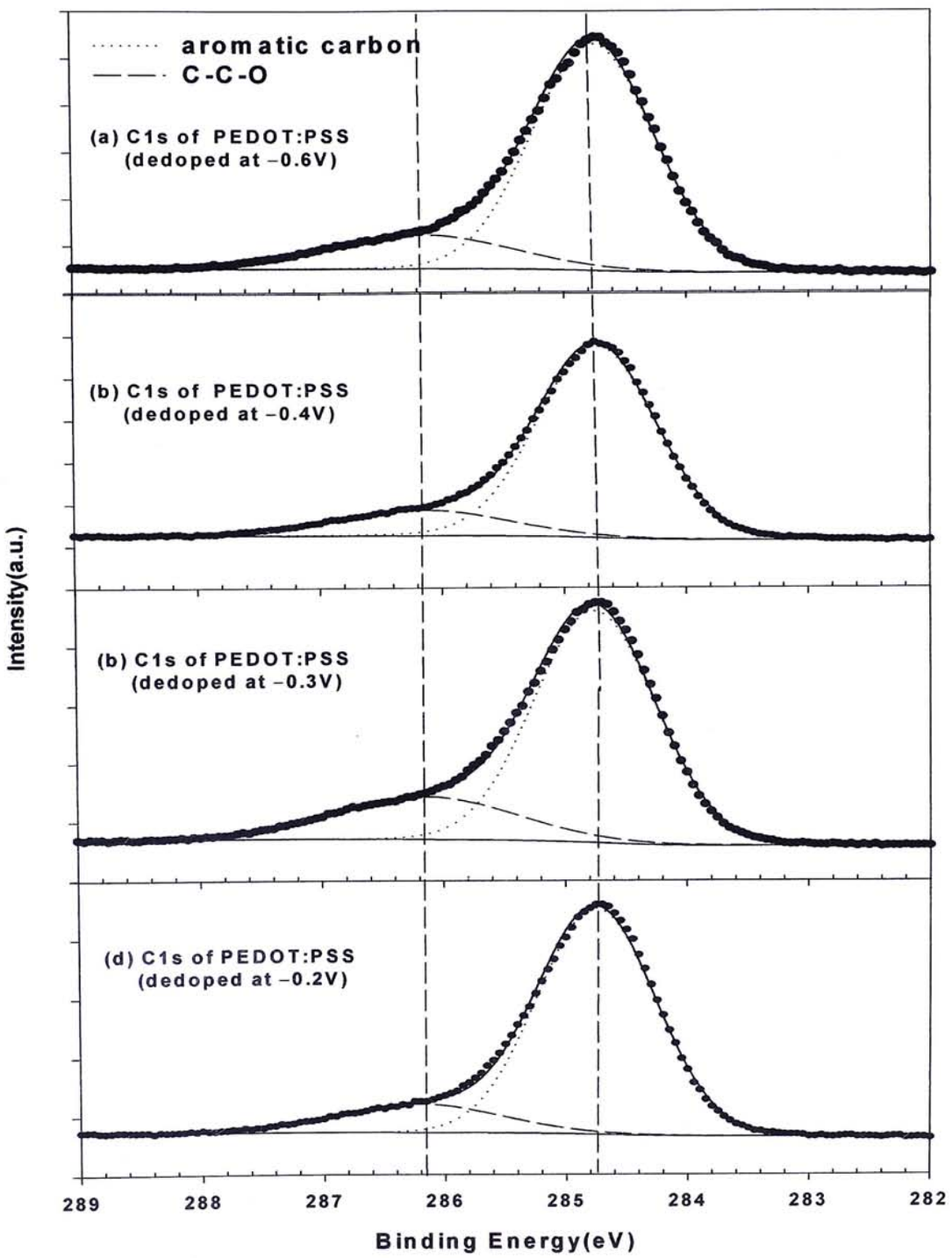

Fig. 4.2 C1s spectrum of PEDOT:PSS dedoped at –0.2V, –0.3V, –0.4V, and –0.6V

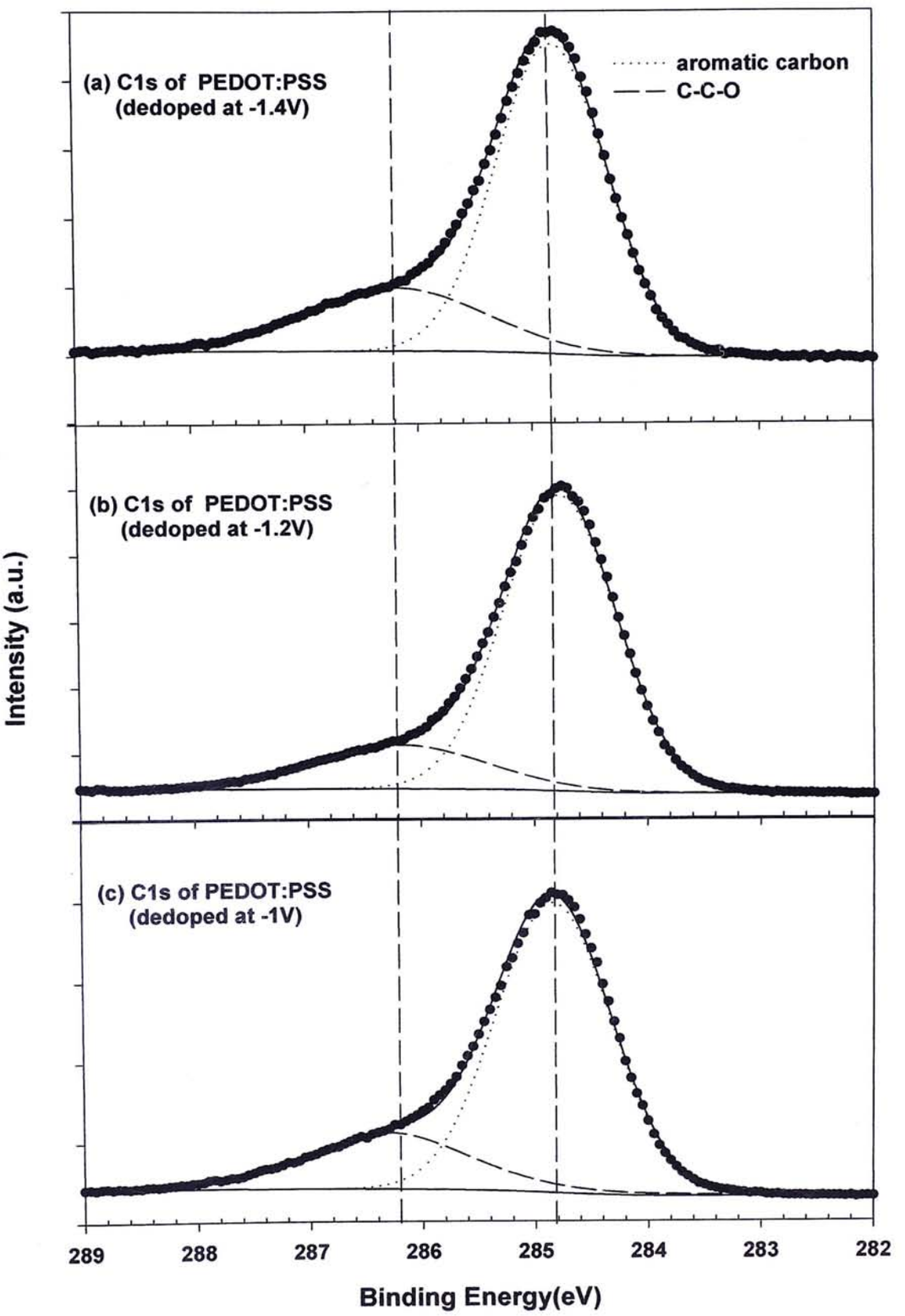

Fig. 4.3 C1s spectrum of PEDOT:PSS deoped at –1V, –1.2V, and –1.4V

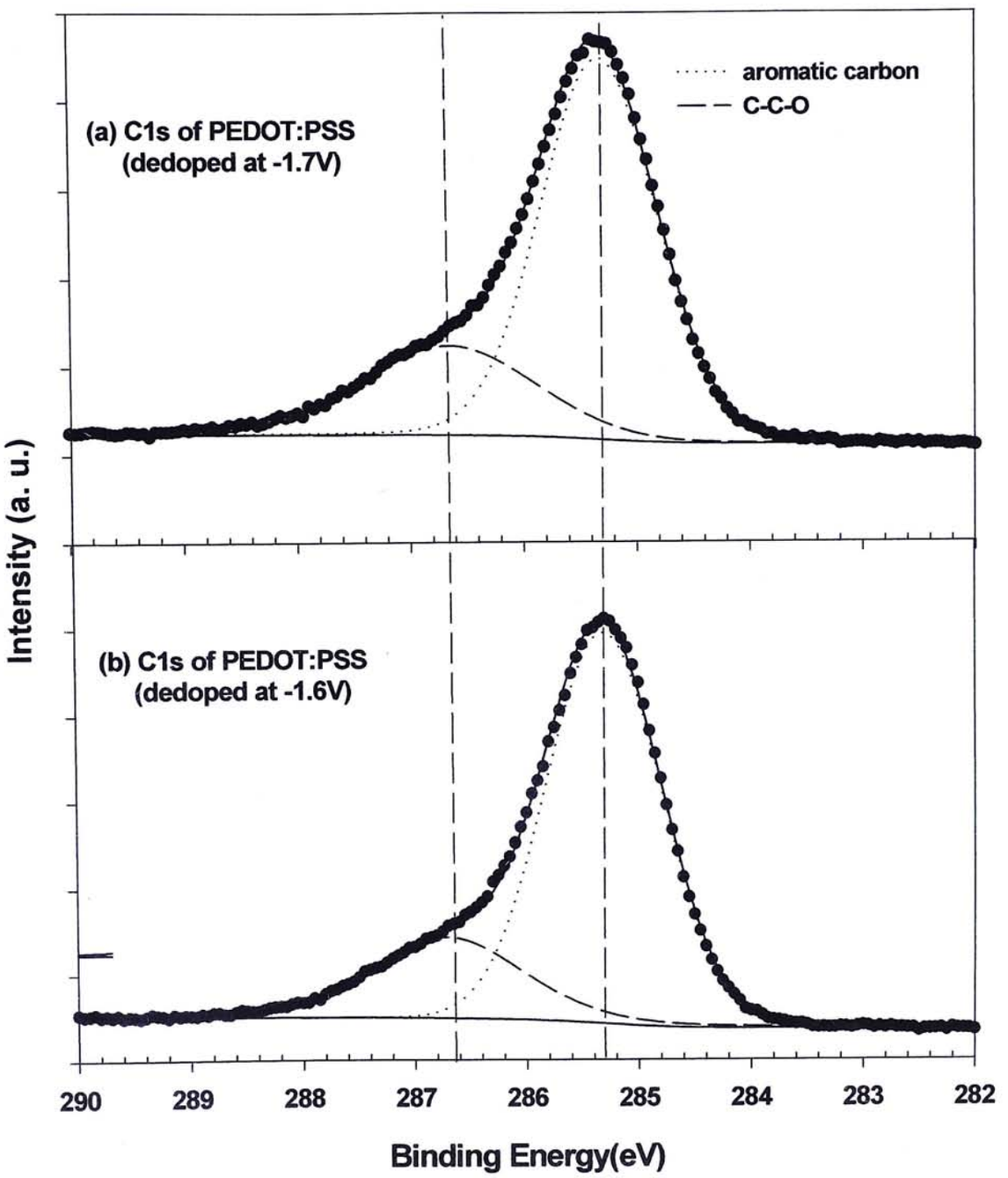

Fig. 4.4 C1s spectrum of PEDOT:PSS dedoped at –1.6V and –1.7V

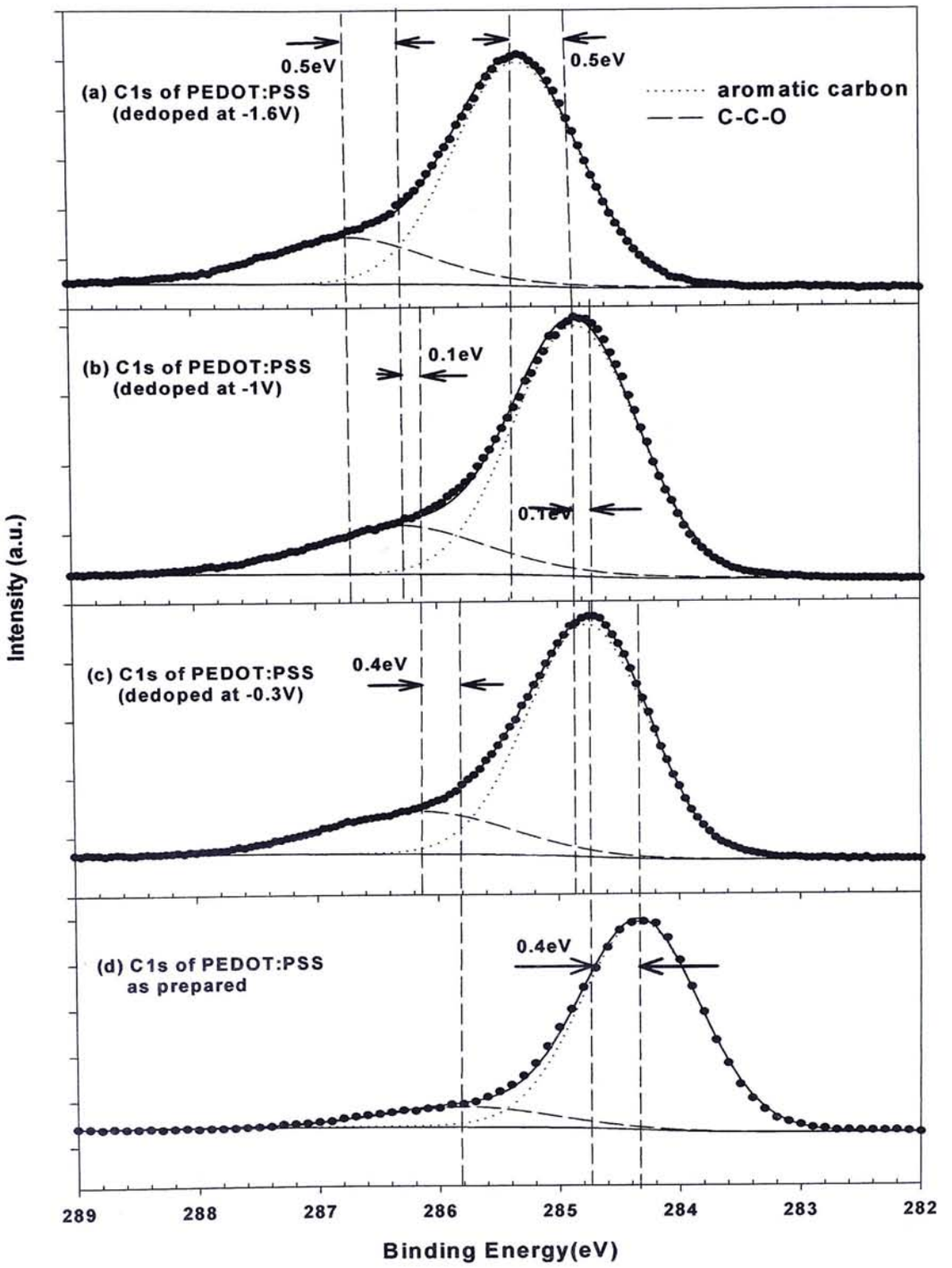

Fig. 4.5 C1s spectrum of the PEDOT:PSS as prepared, dedoped at –0.3V, –1V, and –1.6V

~ -0.6V), (-1.0V ~ -1.4V), and (-1.6V ~ -1.7V) are named as PEDOT:PSS at State I, State II, State III, and State IV, respectively. Figure 4.5 shows the C 1s spectra of PEDOT:PSS at all four states. Explanations and further discussion will be described later in following sections.

4.3.2 XPS of S 2p Core Level of PEDOT:PSS

The S 2p signal is a spin-split doublet, S $2p_{1/2}$ and S $2p_{3/2}$, of an energy splitting of 1.18 eV, and a relative intensity ratio of 1:2. [16] From the chemical formula of PEDOT:PSS as shown in Fig. 1.10, it is expected that the S 2p core level should be a convoluted peak from sulfur in different chemical states and that a dominant signal comes from PEDOT sites, PSSNa, and PSSH. Figure 4.6 shows the S 2p spectra of PEDOT:PSS as prepared, dedoped at -0.3V, -1.0V, and -1.6V. Although the deconvolution is not straightforward, the peak at lower binding energy range of 162 eV to 166 eV can be assigned to those sulfur within the PEDOT chain according to the earlier photoelectron spectroscopic work and results of quantum chemical calculations. [15, 16] On the other hand, the feature at a higher binding energy of ~169 eV can be assigned to the sulfur atoms in PSS. Generally it is assumed that in the PEDOT:PSS as prepared film, the PSSH and PSSNa dominate the intensity of the spectral feature at ~169 eV. [16] The results in photoemission spectroscopy show a 0.4 eV relative energy difference between S in PSSH and PSSNa. [13, 16] These references enable a more accurate deconvolution of the feature at ~169 eV into two spin-split doublets, corresponding to sulfur atoms in PSSH and PSSNa which are separated by 0.4 eV in an as prepared PEDOT:PSS sample. The intensity ratio of S in

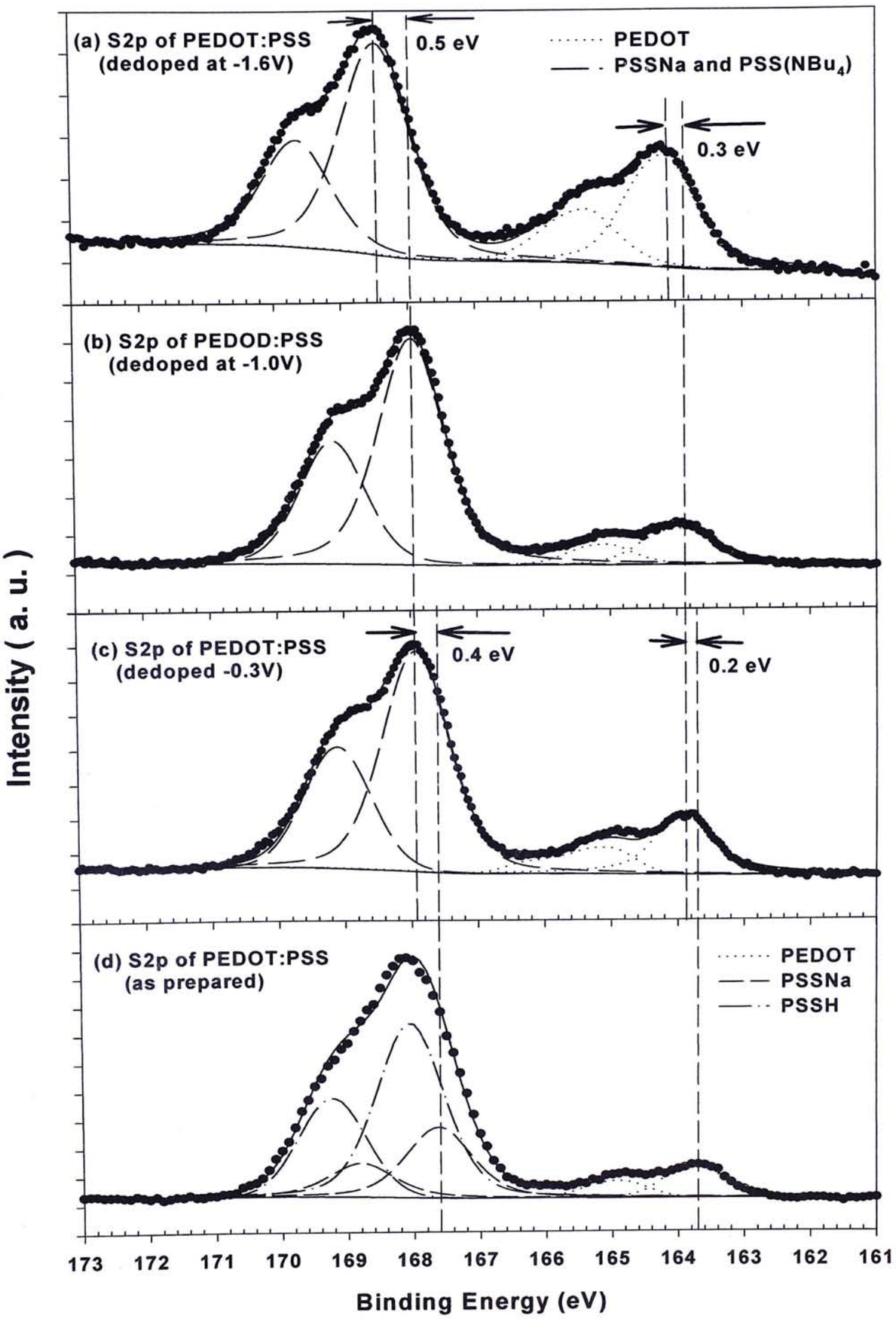

Fig. 4.6 S2p spectrum of PEDOT as prepared, dedoped at –0.3V, -1.0V,and -1.6V

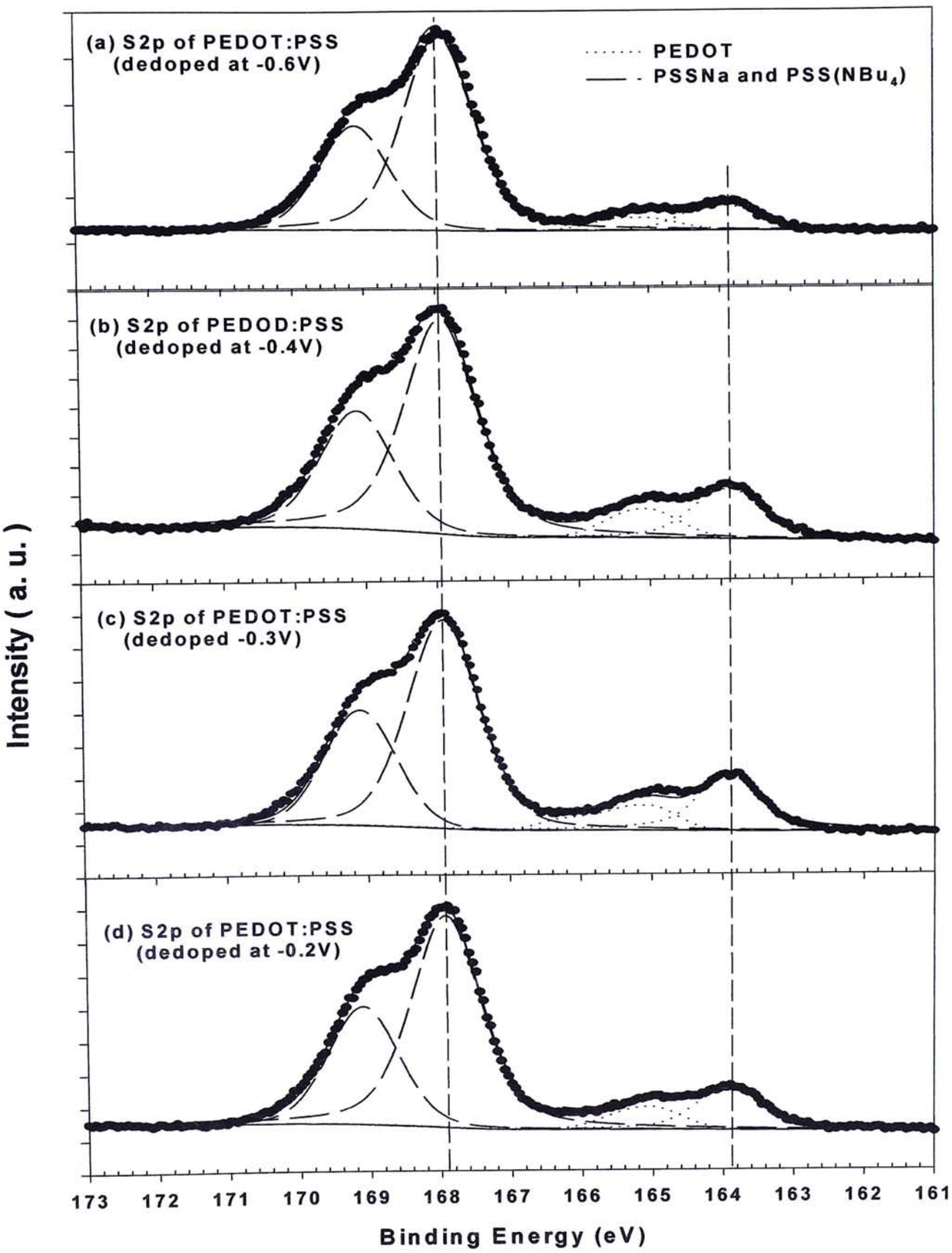

Fig. 4.7 S2p spectrum of PEDOT:PSS dedoped at –0.2V, -0.3V, -0.4V, and -0.6V

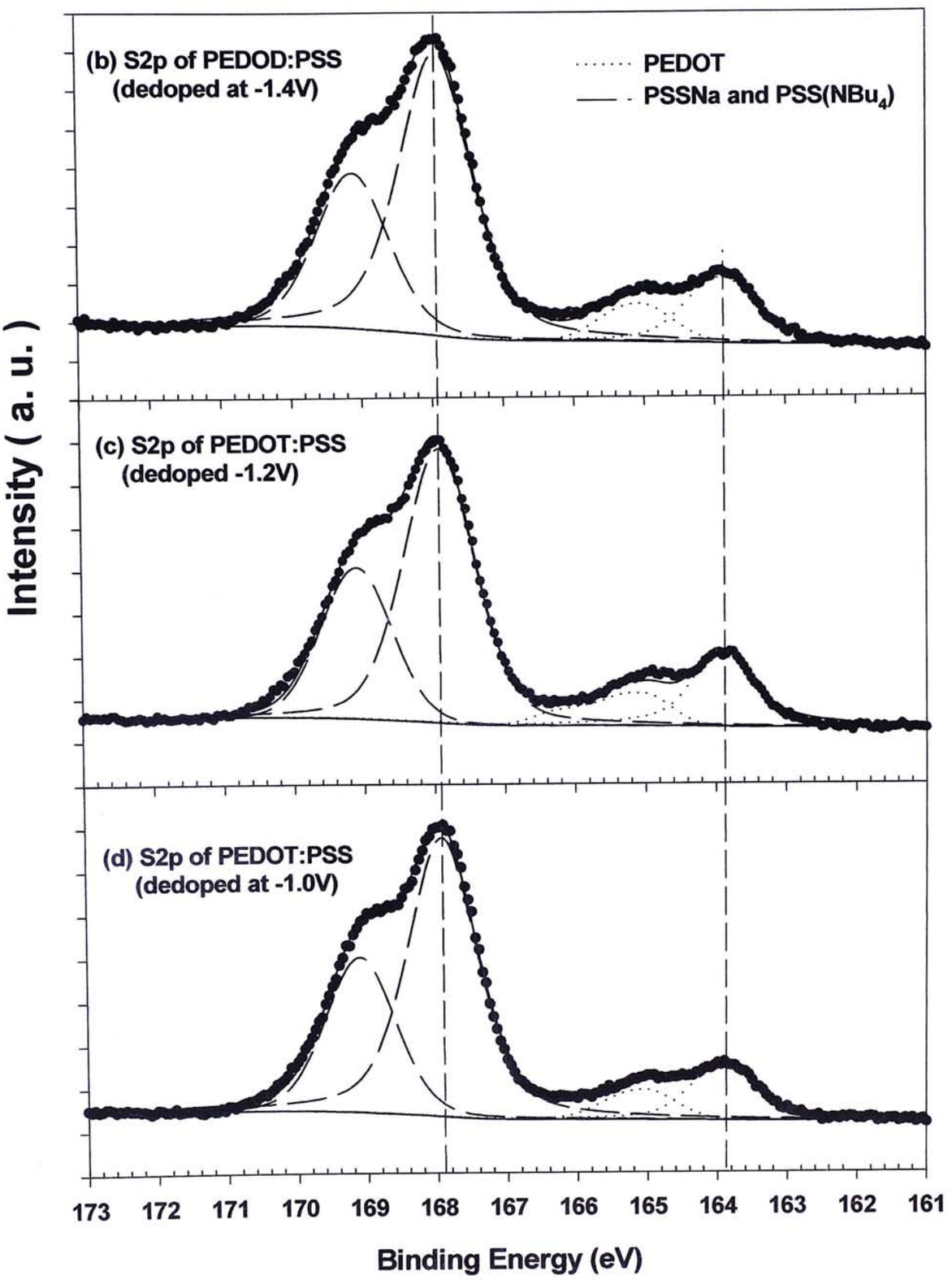

Fig. 4.8 S2p spectrum of PEDOT:PSS dedoped at –1.0V, -1.2V, and -1.4V

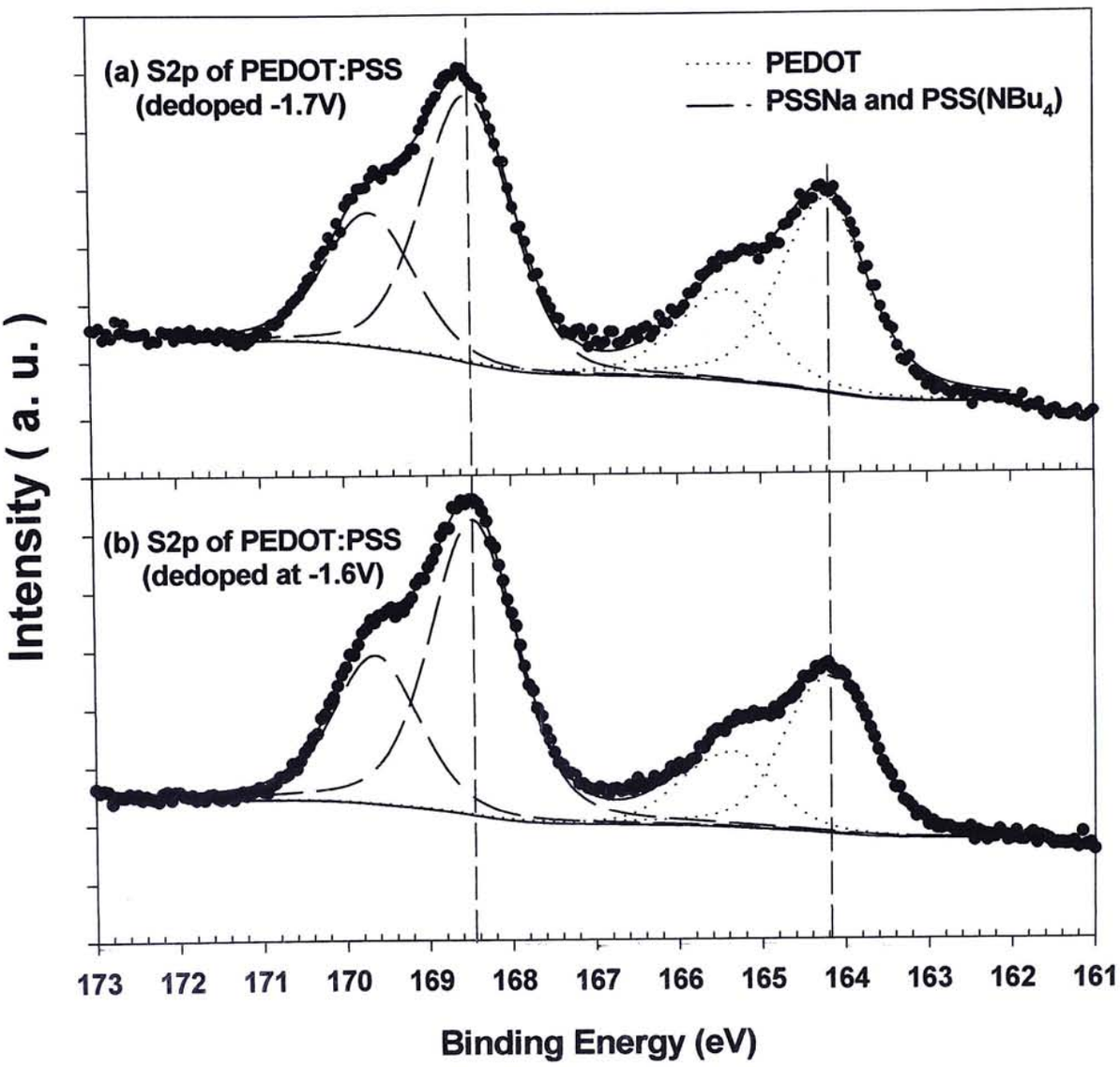

Fig. 4.9 S2p spectrum of PEDOT:PSS dedoped at –1.6V and –1.7V

PSS to S in PEDOT is ~ 10 to 1, which does not agree to the given bulk molar ratio of 1 to 0.8 in the as received solution. This can be attributed to the surface segregation of PSS in the PEDOT:PSS as prepared films as reported by Salaneck et al. [16]. It was also found that PSSNa overwhelms the PSS feature at 169 eV for a pH-dedoped PEDOT:PSS (pH > 5). [13] For PEDOT:PSS electrochemically dedoped at a particular potential, the FWHM of the peak was almost equal to that of the peak of PSSH and PSSNa in the PEDOT:PSS as prepared sample. Therefore, it is reasonable to assume that S in $PSSNBu_4$ and S in PSSNa should be in a similar chemical state with a similar binding energy of ~169 eV.

Figure 4.7 shows the S 2p spectra of PEDOT:PSS electrochemically dedoped at –0.2V, -0.3V, -0.4V, and –0.6V. Peak positions of S $2p_{3/2}$ of PEDOT were all located at 163.9 eV for the four species, while peak positions of S $2p_{3/2}$ of $PSSNBu_4$ were all located at 167.9 eV. Figure 4.8 shows the S 2p spectra of PEDOT:PSS electrochemically dedoped at –1.0V, -1.2V, and –1.4V. Peak positions of S $2p_{3/2}$ of PEDOT were at 163.9 eV for the three species, while peak positions of S $2p_{3/2}$ of $PSSNBu_4$ and PSSNa were at 167.9 eV, without change when compared with previous set. Fig. 4.9 shows the S 2p spectra of PEDOT:PSS electrochemically dedoped at –1.6V, and –1.7V. Peak positions of S $2p_{3/2}$ of PEDOT were shifted to 164.2 eV. Peak positions of S $2p_{3/2}$ of $PSSNBu_4$ and PSSNa were shifted to168.5 eV. The S 2p3/2 spectra of PEDOT:PSS at State I, State II, State III and State IV are illustrated in Fig. 4.6. In this figure, the peak shifts of S 2p of PEDOT:PSS at different states can also be clearly seen, which are significantly smaller than those of C(1s).

4.3.3 XPS of O 1s Core Level of PEDOT:PSS

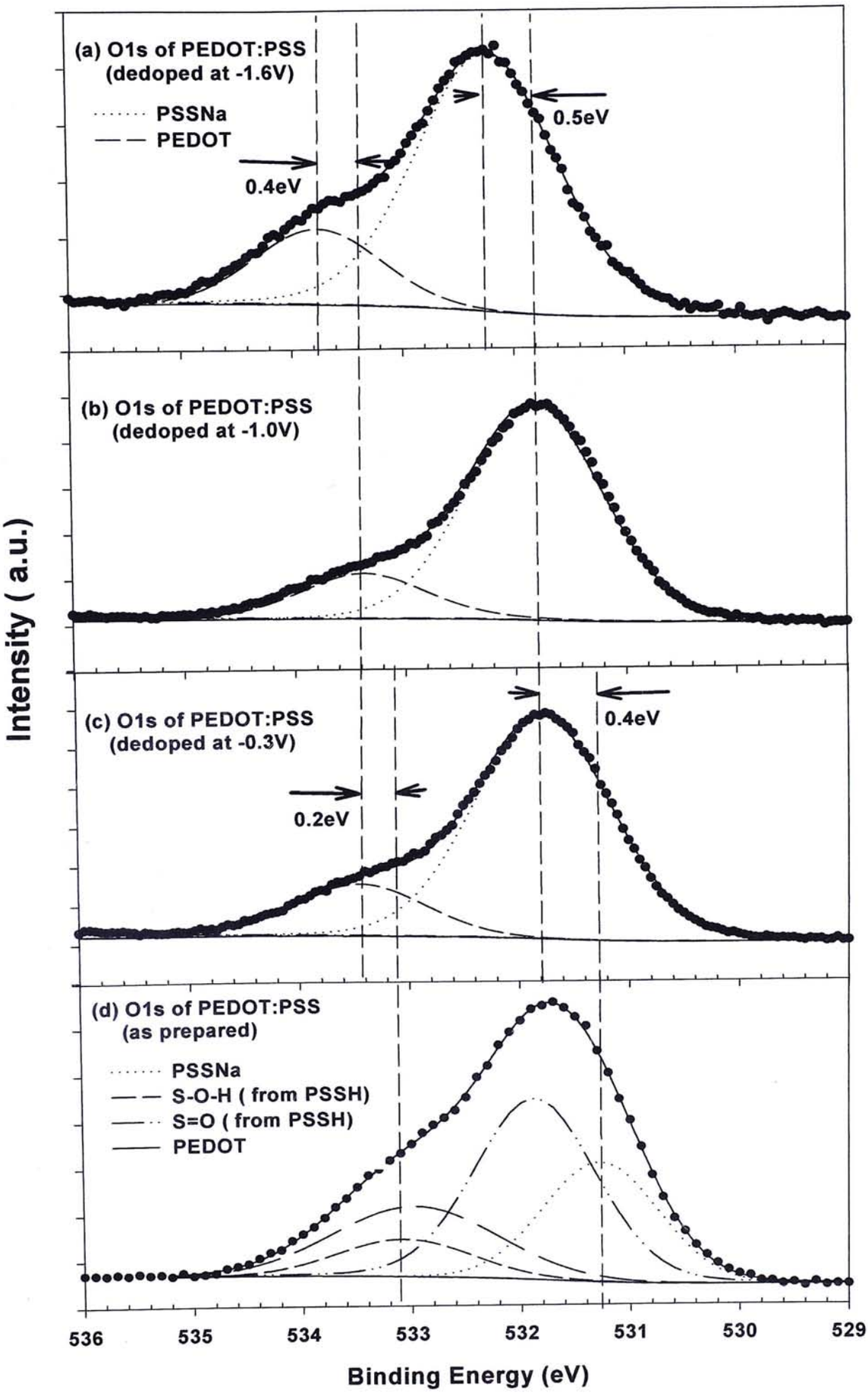

Fig. 4.10 O1s spectrum of PEDOT as prepared, dedoped at –0.2V, -1.0V, and -1.6V

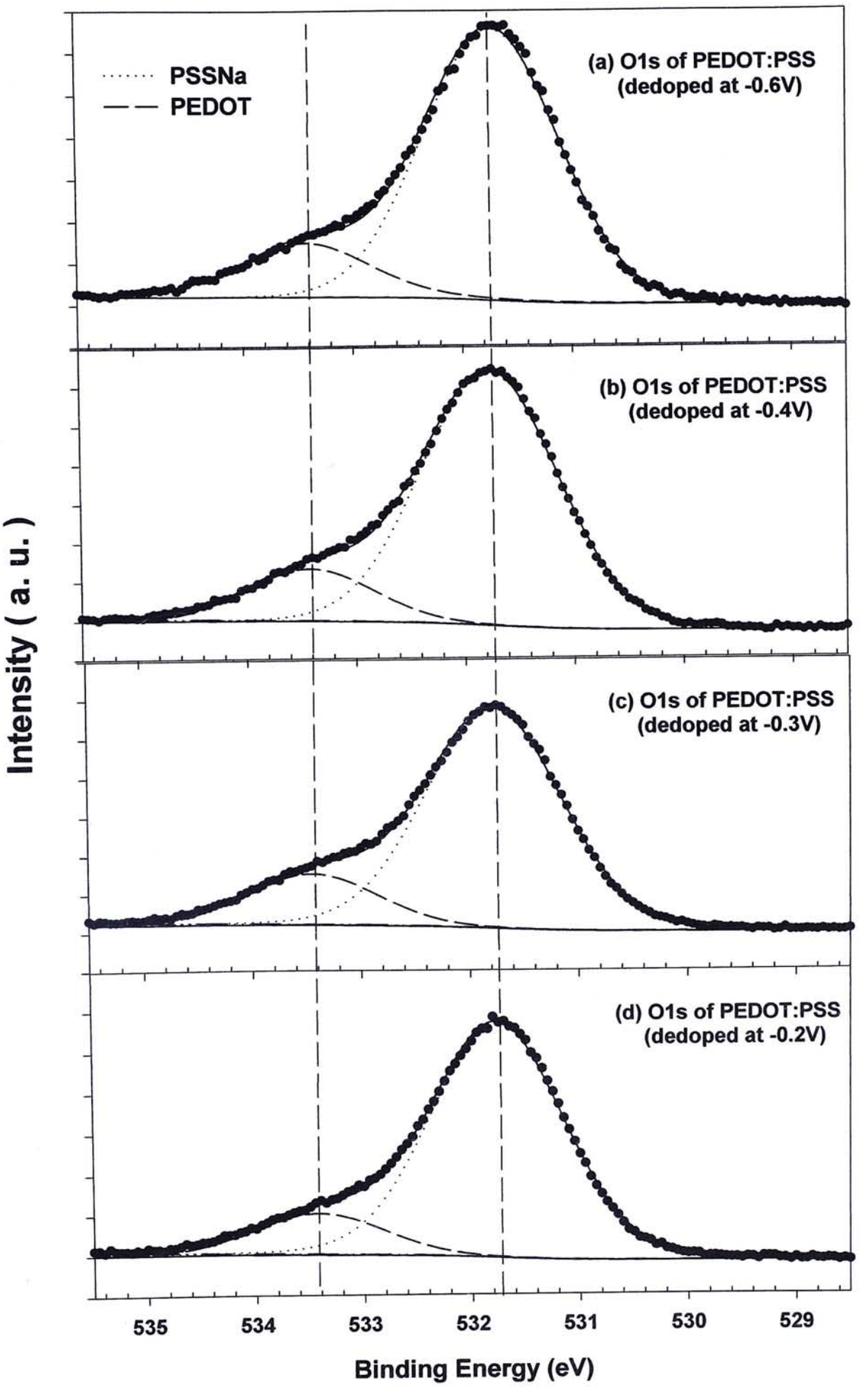

Fig. 4.11 O1s spectrum of PEDOT dedoped at –0.2V, -0.3V, -0.4V, and -0.6V

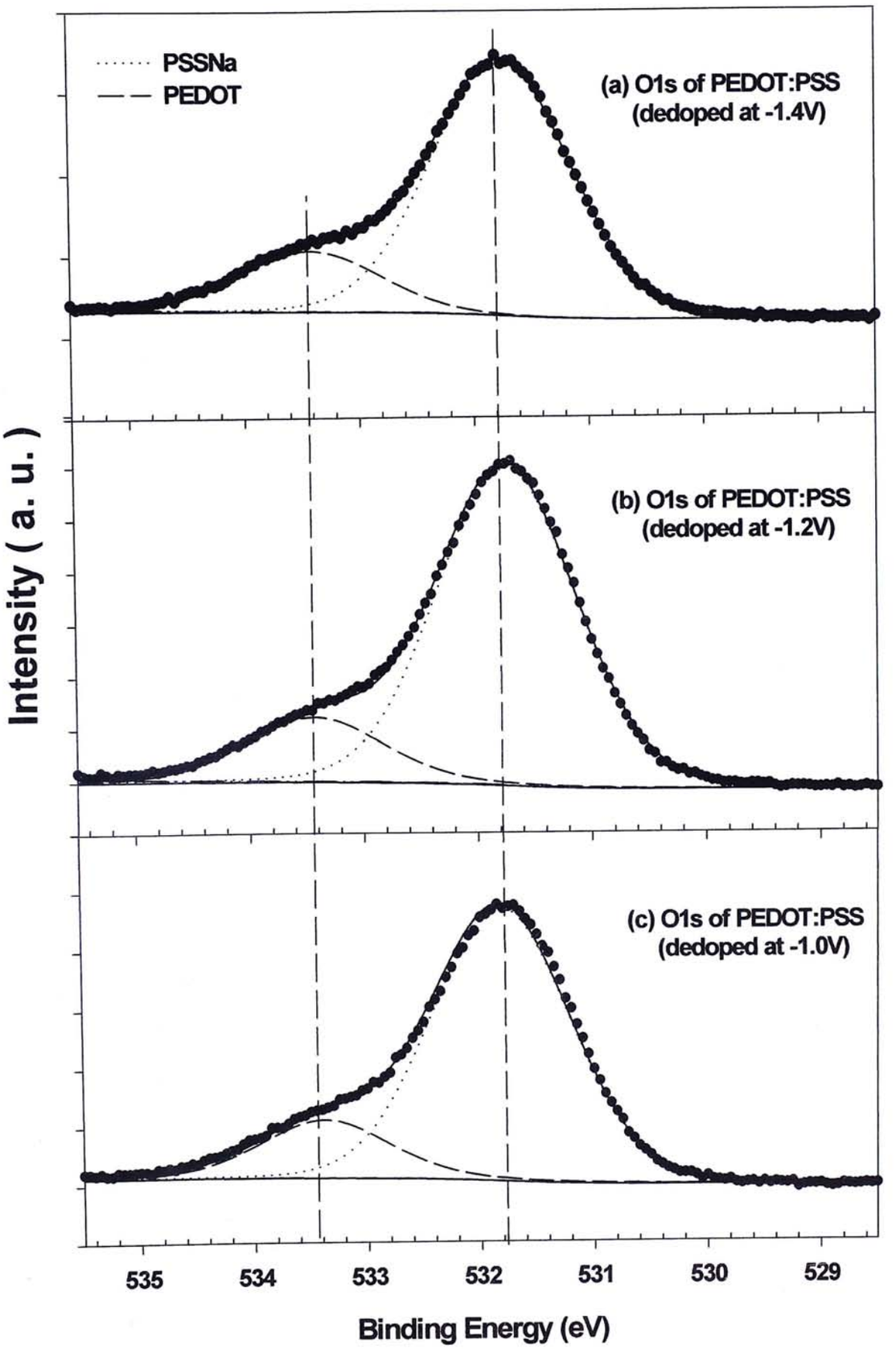

Fig. 4.12 O1s spectrums of PEDOT dedoped at –1.0V, –1.2V, and –1.4V

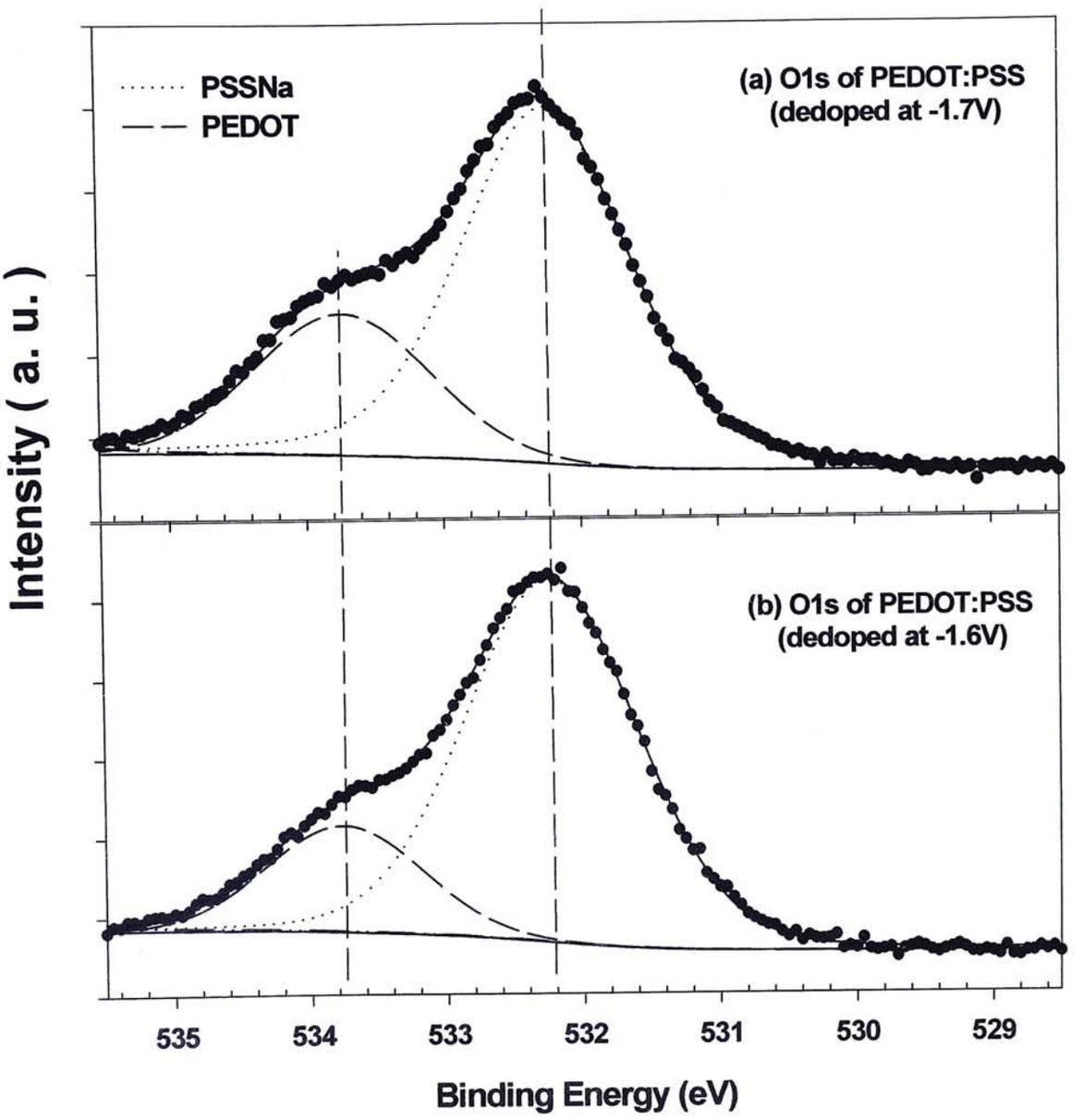

Fig. 4.13 O1s spectrums of PEDOT:PSS dedoped at –1.6V and –1.7V

The O 1s spectrum of the as prepared PEDOT:PSS film is shown in Fig. 4.10 (d). As in the case of sulfur, different chemical species are expected. In analogy to the S 2p spectrum, priori knowledge on the chemical composition and the results from reference compounds were used to deconvolute the O 1s spectrum. It has been reported that the O 1s spectrum of PSSH contains two peak components, separated by 1.1 eV [16]. Of these two peaks, the peak at lower binding energy comes from PSSH in which the oxygen atoms bound to a sulfur atom in the sulfonic acid groups of PSSH; the feature at higher binding energy corresponds to the oxygen atoms in hydroxyl groups. The spectra of O 1s for PSSNa and PSSH show a 0.5 eV relative energy difference with the binding energy of PSSNa part lower than that of the other part. With this additional information, the deconvolution of O 1s spectrum of the PEDOT:PSS as prepared film was performed. For O 1s spectra of electrochemically dedoped PEDOT:PSS, there were only two components, one from O=S in the acid group of PSSH, and the other from C-O-C in PEDOT. Figure 4.11 shows the O 1s spectra of PEDOT:PSS electrochemically dedoped at –0.2V, -0.3V, -0.4V, and –0.6V. Peak positions of O 1s from $PSSNBu_4$ were located at 531.7 eV for the four species, while peak positions of O 1s from PEDOT were located at 533.2 eV. Figure 4.12 shows the S 2p spectra of PEDOT:PSS electrochemically dedoped at –1.0V, -1.2V, and –1.4V, respectively. Peak positions of O 1s from $PSSNBu_4$ were located at 531. eV for the three species, while peak positions of O 1s from PEDOT were located at 533.4 eV. Figure 4.13 shows the O 1s spectra of PEDOT:PSS electrochemically dedoped at –1.6V,and –1.7V. Peak positions of O 1s from $PSSNBu_4$ for the two species were located at 532.2 eV, while peak positions of O1s from PEDOT were located at 533.7 eV. The O 1s spectra of PEDOT:PSS State I, State II, State III, and State IV are illustrated in Fig. 4.10.

4.3.4 XPS of Valence Band of PEDOT:PSS

Information about the density of states of the sample around the Fermi level can be drawn from Valence band spectra. Figure 4.14 and 4.15 show a comparison of valence band (VB) photoemission threshold of as prepared PEDOT:PSS, dedoped PEDOT:PSS at –0.3 V, -1.2V, and –1.6V with reference to sputtered clean Au. For the as prepared PEDOT:PSS film, the VB edge was at –0.5 eV, which was ~0.1 eV above the edge of Au. If the VB edge of Au is taken as the exact Fermi level position, this means that the Fermi level of the PEDOT:PSS film, E_F was ~ 0.1eV above its valence band maximum. This is consistent with the highly p-type characteristic of PEDOT:PSS film. This result is also consistent with the results from Salaneck, et al. [16] For PEDOT:PSS dedoped at -0.3 V, -1.2V, and –1.6V, the E_F data were ~0.5 eV, ~0.6 eV, and ~1.1 eV respectively. Approximately, the electrochemical treatments at –0.2V to -1.4V, caused dedoping by reduction. When the reduction potential increased to –1.6V to –1.7V, the E_F values increased above ~1.1 eV and the samples became n-doped (bandgap ~1.5 eV [5,15]).

4.3.5 Further Explanations and Discussion

Upon investigations on the peak shifts of core levels C 1s, O 1s and S 2p, and the valence band threshold of PEDOT:PSS, the subtle changes to the electronic structure of PEDOT:PSS dedoped at different electrochemical potentials can be revealed. Figure 4.16 shows the core level shift and valence band threshold with the increasing dedoping potential, using the PEDOT:PSS as prepared film as a reference. The result clearly confirms the presence of four distinct states of PEDOT:PSS, each of which corresponds to a particular doped/dedoped state.

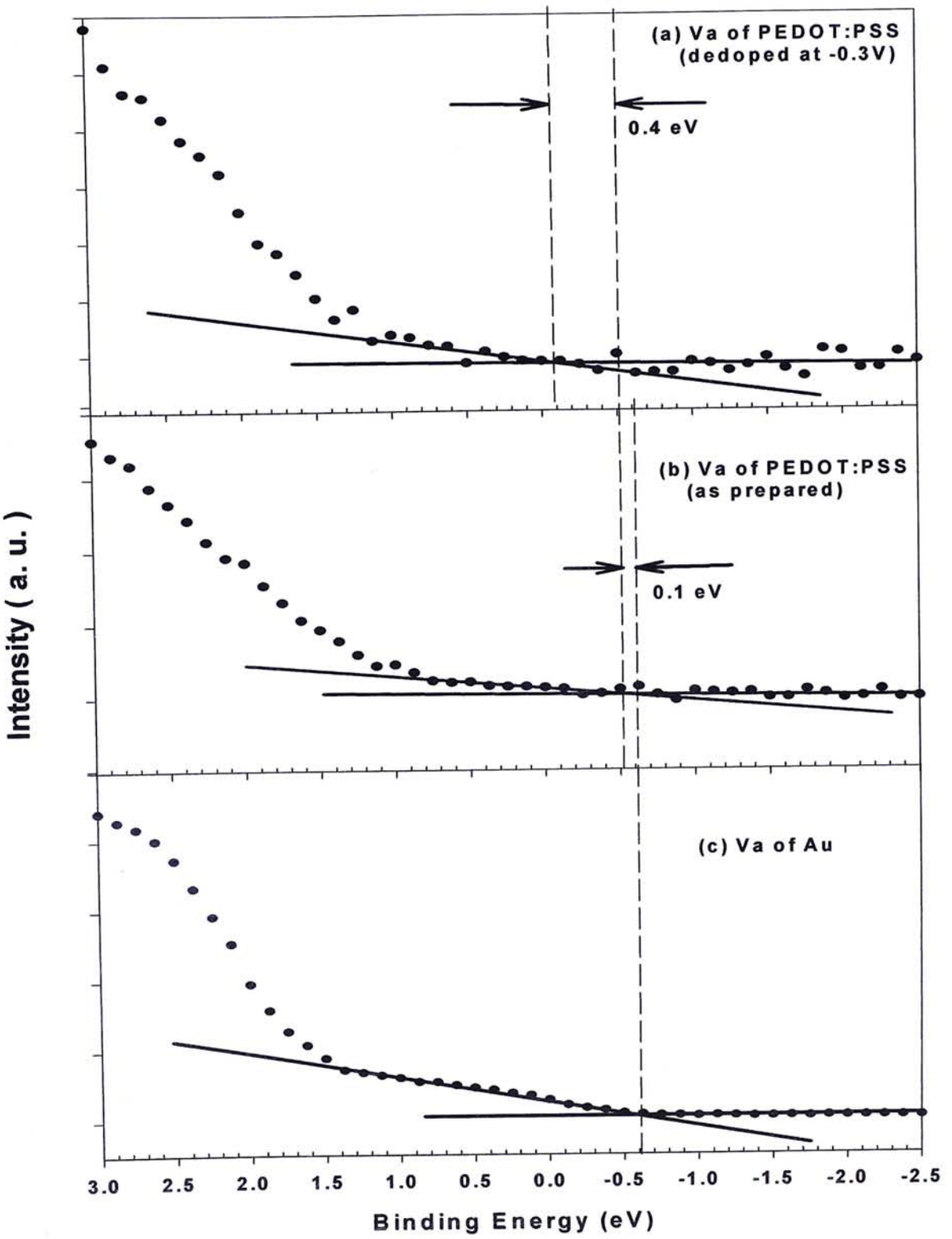

Fig. 4.14 Valence band spectrums of Au, PEDOT:PSS as prepared, and dedoped at –0.2V

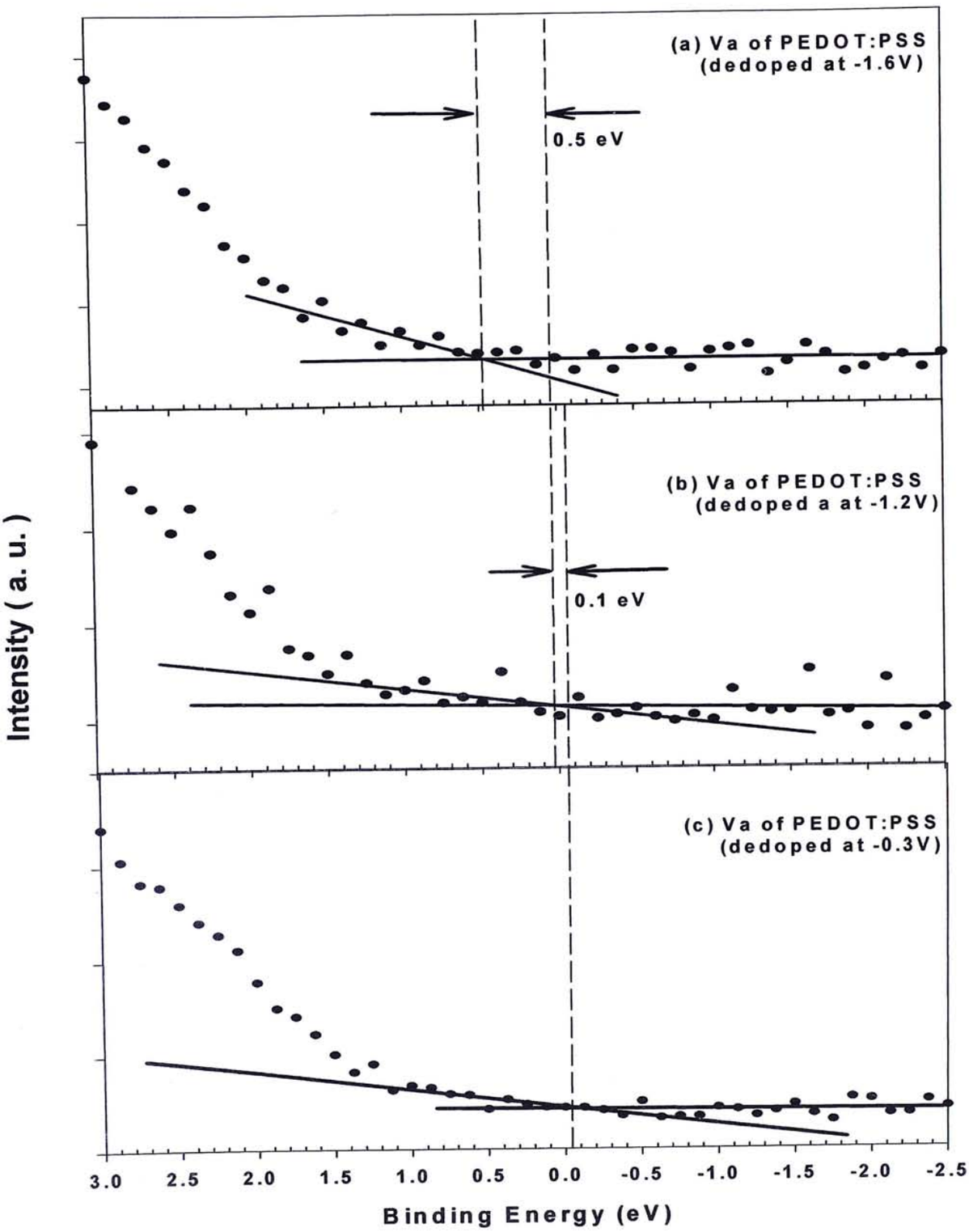

Fig. 4.15 Valence band spectrums of PEDOT:PSS dedoped at −0.3V, −1.2V, and −1.6V

In the electrochemical dedoping potential of -0.2V to -0.6V, the shifts of C 1s in PEDOT, C 1s in aromatic carbon, O 1s in PSSNa and PSSNBu4, and S 2p in PSSNa and PSSNBu4, are consistent with the shifts of the valence band threshold of ~0.4 eV. It indicates that the E_F of PEDOT:PSS moved up from ~0.1 eV to ~0.5 eV. It agrees well with the behaviour of common inorganic semiconductors that the Fermi level will adjust itself to preserve charge neutrality when impurity atoms are introduced or removed [17]. Thus, the E_F of PEDOT at State II was 0.5 eV higher than its HOMO energy level, which is quite close to the mid-gap, assuming a band gap of ~1.5 eV for PEDOT:PSS as reported in the literature [5,15].

The binding energy shift of S 2p in PSS from PSSNa and $PSSNBu_4$ was ~0.3 eV, which is a bit less than the expected value of 0.4 eV. This is probably due to the decreased electric potential energy by excess NBu_4^+ ions coupled to PSS^- in the surface as is shown by the fact that the ratio of positive ions (Na^+ and NBu_4^+) to negative ions (PSS^- ions) was around 1.3 . The binding energy of O(1s) of PEDOT was also a bit smaller than the Fermi level shift. One possible reason is that the chemical state of oxygen atoms in PEDOT changed during electrochemical dedoping, and oxygen atoms in PEDOT got some negative charge in this process. In addition, the water attached in the film surface further complicates this matter, as it is hard to deconvolute this component in O(1s) spectra because the binding energy of this component is almost the same as that of PEDOT.

The binding energy changes of S(2p) of PEDOT were ~0.2 eV less than the Fermi level shifts for State II . As doping of conjugated polymers [16,19,24,25 of Chapter1] is essentially a charge transfer reaction that results in a partially oxidized or reduced polymer, it is reasonable to conclude that the charge transfer mainly occurs in sulfur atoms in PEDOT during electrochemical dedoping.

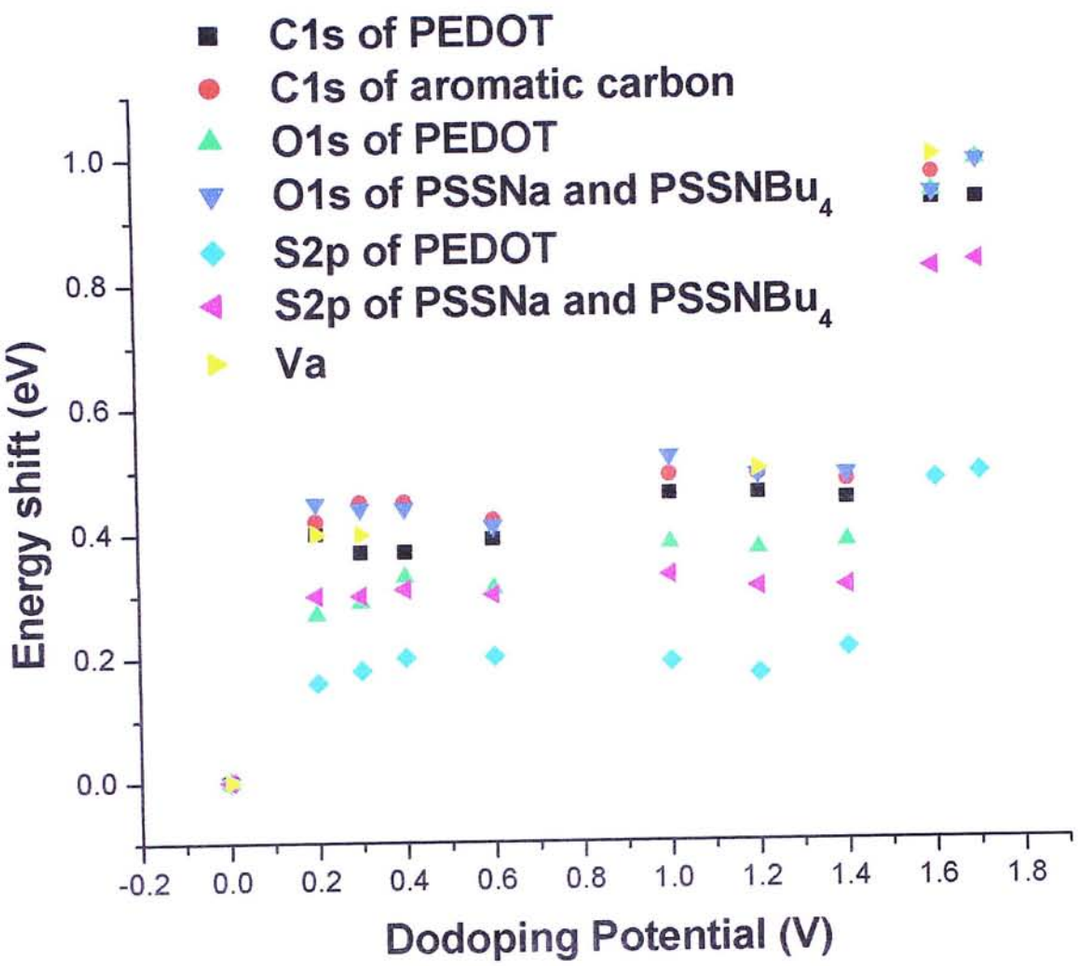

Fig. 4.16 Energy shift of different elements in PEDOT dedoped at different potentials using PEDOT as prepared as reference

In the dedoping potential range of (-1.0V~-1.4V), the Fermi level shift was about 0.1 eV larger than that for State II, indicating that PEDOT was dedoped to close to its neutral state in this potential range. The binding energy shift of S 2p from PEDOT remained at 0.2 eV for State III, the same as that from the PEDOT State II. This means that the inconsistency between the shift of S 2p from PEDOT and the shift of Fermi level for State III was 0.1 eV larger than that for State II. Thus it indicates that sulfur atoms in PEDOT State III were got further reduced than those in the PEDOT State II.

In the dedoping potential range of (-1.6V~-1.7V), E_F value increased to around 1.1 eV, ~0.4 eV lower than the LUMO energy level and ~0.3 eV higher than the mid of the band gap, indicating that PEDOT at State IV was already n-doped. However, the conductivity of this n-doped PEDOT:PSS was still very low because of the wide separation of the Fermi level to the LUMO energy level, which was also found by Ahonen et al [18]. This is also consistent with the conducting AFM results described in the subsequent chapter. The binding energy shifts of S 2p from PEDOT were ~0.5 eV less than the shift of Fermi level, while for State III the binding energy shift of S 2p from PEDOT was ~0.3 eV less than the shift of Fermi level. This indicates that the sulfur atoms were further reduced in this potential range. As PEDOT at State IV was n-doped, there should be excess negative charging in sulfur atoms in PEDOT and $PEDOT^-$ ions were formed. Like p-doped PEDOT, the negative charge of $PEDOT^-$ is not localized on one monomer unit, but is delocalized over several adjacent rings [16].

The energy resolution was 0.05 eV ~ 0.1 eV in these series of XPS experiments, comparable to the energy shift from State II to State III. However, such

energy resolution was much less than the energy shift caused by the change from State I to State II, and from State II to State IV. Therefore, the conclusions about the changes of the state from p-doped to neutral, then to n-doped state, are still reliable.

4.4 Kevin probe measurement

The work function (W_F) measurements of as prepared PEDOT:PSS, electrochemically dedoped PEDOT:PSS at –0.2V, -0.6V, -1.2V, -1.4V, and –1.6V, are shown in Fig. 4.17. The results show that W_F of PEDOT:PSS moved down for ~0.4 eV after dedoping in the potential range of -0.2 V to -1.4 V, and moved down for ~1 eV after dedoping and n-doping at –1.6 V. (In Kevin probe measurement, the error of the data is less than 0.05 eV, which means that the data from Kevin probe is convincible.) These are consistent with the valence band measurements from XPS, and the consistency further supports that PEDOT in PEDOT:PSS was changed from a p-doped state to a neutral state, then to an n-doped state with the increasing dedoping potential.

4.5 Conclusions

As a summary, during electrochemical dedoping, with increasing dedoping potential, the Fermi level of PEDOT:PSS moved up from near the HOMO energy level, first to the mid of the band gap of PEDOT, then close to the LUMO energy level. The PEDOT:PSS films was changed from a p-doped state, first to a neutral state, then to an n-doped state by gradually increasing the dedoping potential, with sulfur atoms in PEDOT acting as the main reduced center.

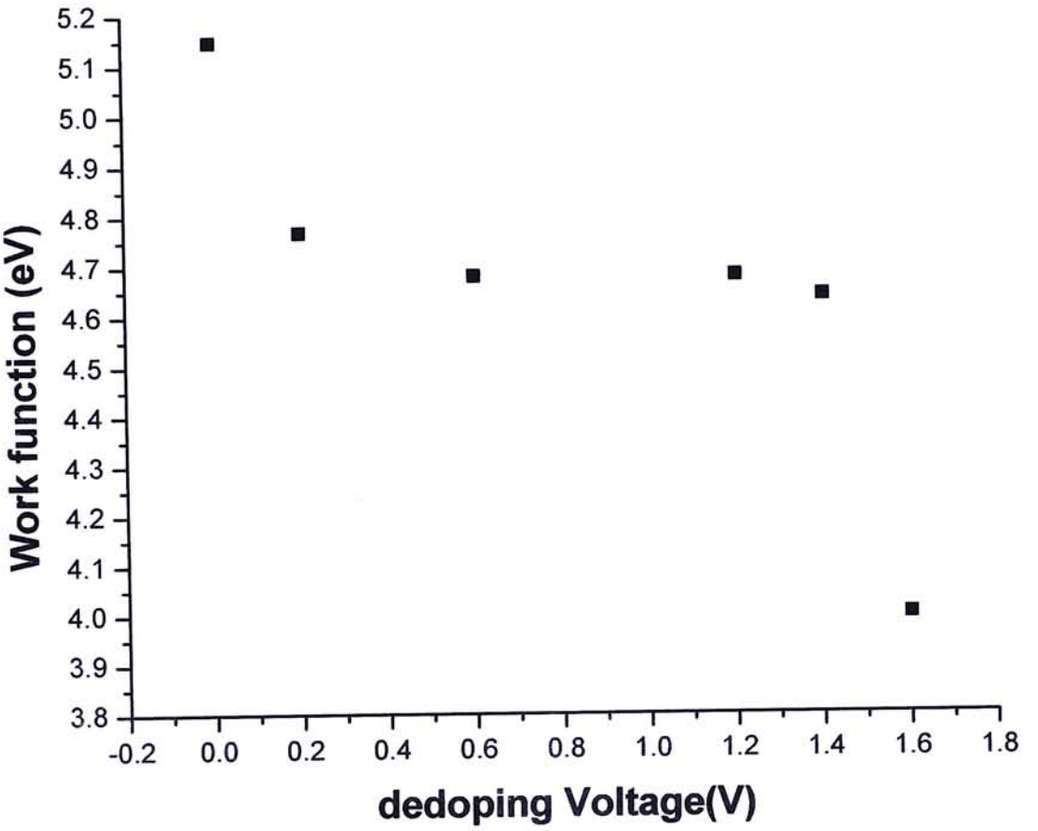

Fig. 4.17 Work function of PEDOT:PSS as prepared and electrochemically dedoped vs. the dedoping voltage

References

[1] F. Jonas, L. Schrader, *Synth. Met.* **41-43** (1991), 831

[2] G. Hermang, F. Jonas, *Adv. Mater.* **4** (1992), 116

[3] A.N. Aleshin, S.R. Williams, A.J. Heeger, *Synth. Met.* **94** (1998), 173

[4] M. Dietrich, J. Heinze, G. Heywang, F. Jonas, *J. Electroanal. Chem.* **369** (1994), 87

[5] Q. Pei, G. Zuccarello, M. Ahlskog, O. Inganas, *Polymer* **35** (1994), 1347

[6] C.M.J. Mutsaers, D.M.d. Leeuw, M.M.J. Siemenon, *Eur. Patent Application* No. PHN 14 385 EP, 1993

[7] Y. Cao, G. Yu, C. Zhang, R. Menon, A.J. Heeger, *Synth. Met.*, **85** (1997), 1197

[8] L. Groenendaal, F. Jonas, D. Freitag, H. Pielartzik, J.R. Reynolds, *Adv. Mater.* **12** (2000), 481

[9] J.C. Scott, S.A. Carter, S. Karg, M. Angelopoulos, *Synth. Met.* **85** (1997), 1197

[10] A.N. Aleshin, S.R. Williams, A.J. Heeger, *Synth. Met.* **94** 173 (1998)

[11] K.E. Aasmundtveit, E.J. Samuelsen, O. Inganas, L.A.A. Pettersson, T. Johansson, S. Ferrer, *Synth. Met.* **113** (2000), 93

[12] Li Niu, Carita Kvarnstrom, K. Froberg, Ari Ivaska, *Synth. Met.* **122** (2001), 425

[13] H.L. Yip, *Mphil thesis* (CUHK) (2003)

[14] A.W. Denier Van der Gon, J. Birgerson, M. Fahlman, W.R. Salaneck, *Organic Electronics* **3** (2002), 111

[15] K.Z. Xing, M. Fahlman, X.W. Chen, O. Inganas, W.R. Salaneck, *Synth. Met.* **89** (1997), 161

[16] G. Greczynski, Th. Kugler, M. Keil, W. Osikowicz, M. Fahlman, W.R. Salaneck, *J. Electron Spectrosc* **121** (2001), 1

[17] S. M. Sze, *Physics of Semiconductor Devices*, 2nd edition, Wiley, New York, 1981

[18] Harri J. Ahonen, Jukka Lukkari, and Jouko Kankare, *Macromolecules*, **33** (2000), 6787

Chapter 5

Morphology and Nano-scale Electrical Properties of PEDOT:PSS Thin Film

5.1 Introduction

By means of conducting atomic force microscopy (CAFM), one can measure electrical properties on insulating, semiconducting, and metallic surfaces. Of equal importance, one can also obtain simultaneously the surface morphology as the tip-sample distance can be controlled independently of the measured current. Therefore, it is an ideal technique to reveal the detailed relationship between surface structure and localized electrical properties of PEDOT:PSS thin film. In this chapter, a series of PEDOT samples was studied to reveal the nano-structure and the electrical characteristics of a typical PEDOT/PSS system. The samples included were as prepared, pH dedoped, neutral and n-doped PEDOT by electrochemical dedoping and doping.

5.2 Sample Preparations

Au/mica was used as substrate for the PEDOT:PSS thin film. Each substrate was UV/O_3 treated for 20 min at an oxygen flow of 500 sccm. Then the as-received PEDOT:PSS solution was dropped onto Au/mica, and spin-cast at 2000 rpm using a spin-coater (CHEMAT TECHNOLOGY, KW-4A). The resulting thin film had an estimated film thickness of ~50nm. The PEDOT:PSS/Au/mica sample was put into vacuum at about 5 Torr for more than 10 hours so as to get a dry PEDOT: PSS film.

The film prepared was named as as-prepared PEDOT:PSS. For electrochemically dedoped PEDOT:PSS, the preparation method is similar to that described in Chap. 3. The prepared samples were loaded into the chamber for conducting AFM analysis.

5.3 Results and Discussions

5.3.1 CAFM on as prepared PEDOT:PSS and Ar^+ sputtered thin film

Figure 5.1 shows simultaneously acquired current image (a) and topography image (b) of PEDOT:PSS/Au/mica surface with a tip bias of +1V. In the current image, it can be seen that there were many small high conducting regions surrounded by very low conducting region of much larger total area. The histogram for the current histogram is shown in Fig. 5.2. As the current of the first column in the histogram was quite small, near to the current limit of the instrument (several pA), the region giving the smallest current should be an insulating phase, while the region giving larger current is the conducting phase. The area ratio of the conducting phase to the insulating phase was ~1:5, which is larger than the ratio of PEDOT to PSS from XPS measurements described in Chapter 4. When a lower bias was applied, the relative conductive area decreased. This is because the higher the bias, the thicker the insulating film-PSS film can the electrons tunnel through, and thus more conducting phase can be revealed. This is consistent with the works by Salaneck et al., that the ratio of PEDOT to PSS increased with the increasing x-ray photon energy, which corresponds to a higher probing depth [1]. The topography had a root-mean-square (rms) roughness of 0.86 nm. The average current was 0.30 nA.

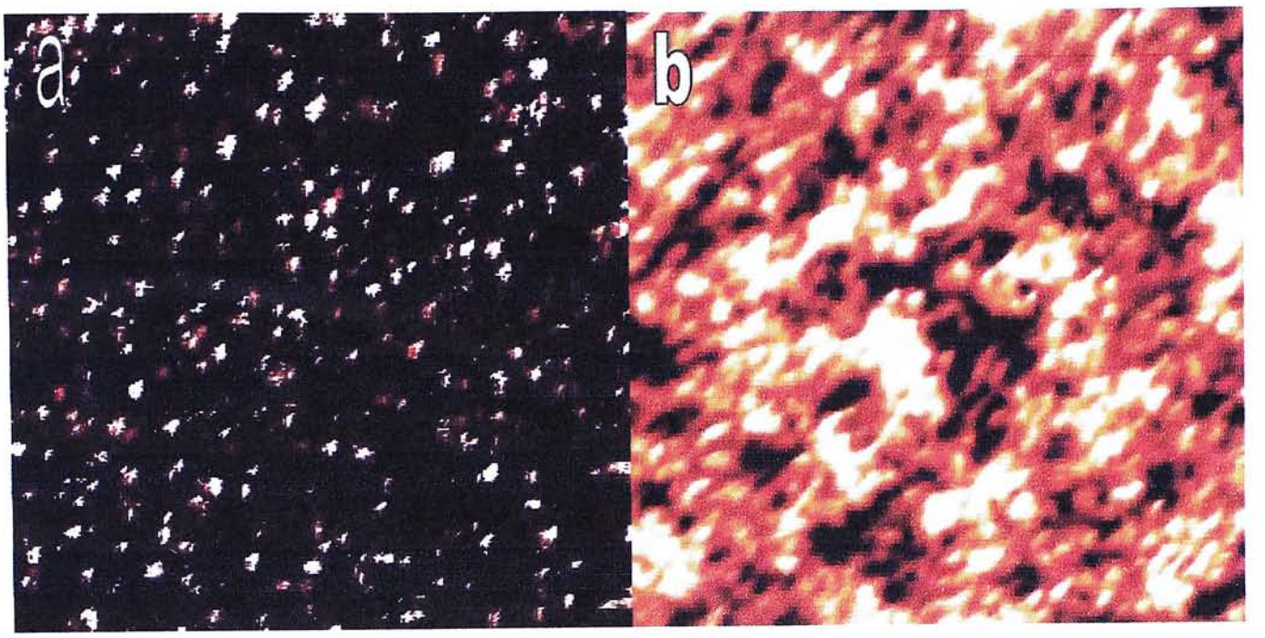

Fig. 5.1 Current (a) and topography (b) images on PEDOT:PSS/ Au/mica with tip bias of 1V and scan size of 1μm×1μm. The brightest scales are 2.5~25.5 nA for current image, and 2.0~3.6 nm for topography image.

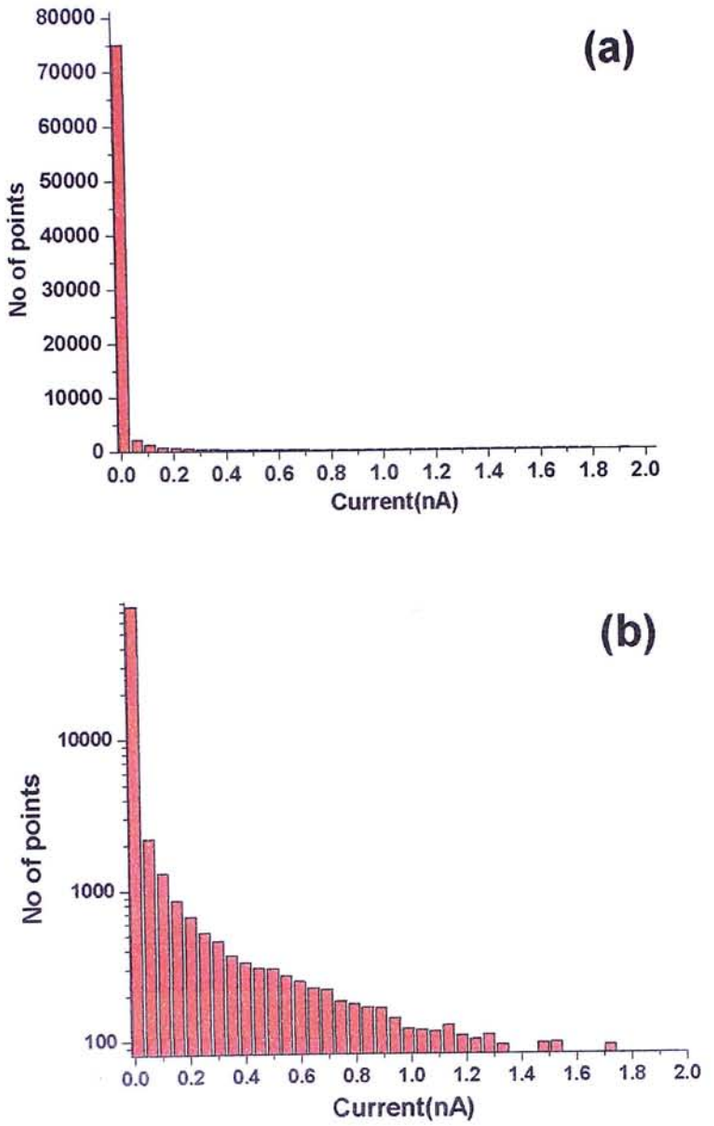

Fig. 5.2 Histogram of the current image in Fig. 5.1 for normal y-scale of (a) and lg y-scale of (b)

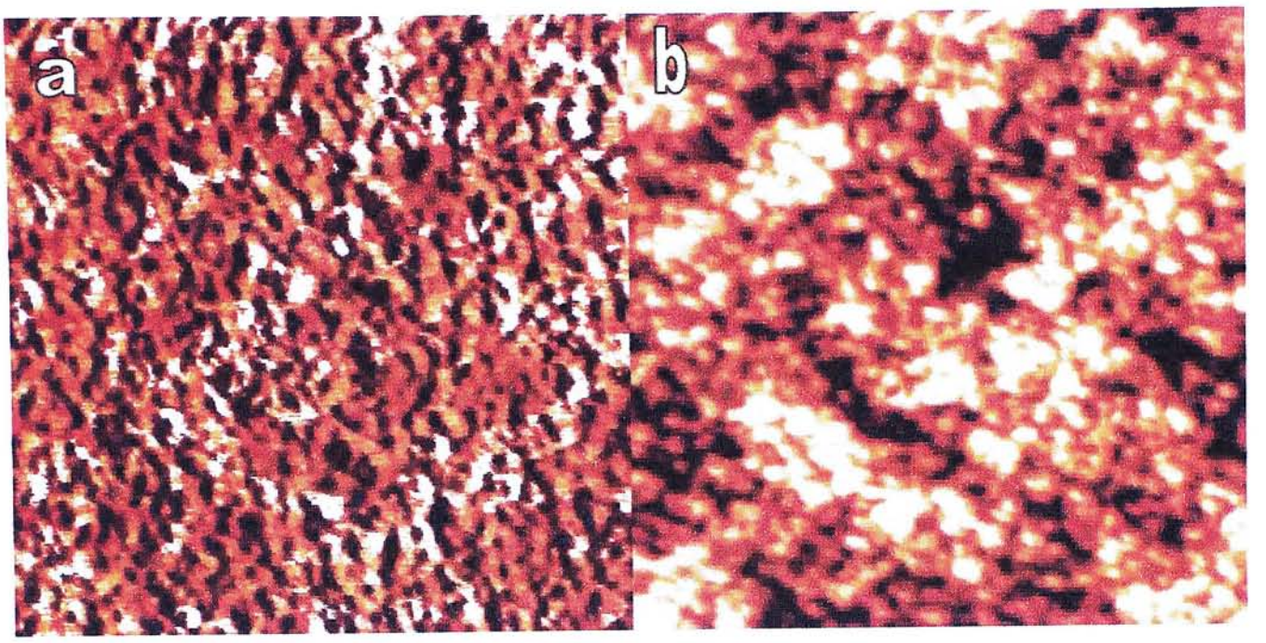

Fig. 5.3 Current image (a) and topography image (b) on PEDOT:PSS/Au/mica sputtered by 500 eV Ar^+ with the tip bias of 1V. The brightest scales are 0.1~0.5 nA for (a), 2.5~4.5nm for (b). The scan size is 1 μm×1μm.

Figure 5.3 shows the simultaneous current and topography images of PEDOT:PSS after sputtering by 500 eV Ar^+ for 40 min. The XPS S 2p spectrum on the film (not shown here) proved that the ratio of PEDOT to PSS decreased to ~1:1, implying that the PSS-rich surface had been sputtered away. The topography had an rms roughness of 0.93 nm, which is quite similar to the one without sputtering. The average current was 0.03 nA, which is much lower than that of as prepared PEDOT:PSS. This is because Ar^+ sputtering produced a destructed layer, which is insulating.

The current image of PEDOT:PSS after Ar^+ sputtering shows that the conducting regions connected to each other and formed a network structure, indicating that PEDOT under the PSS-rich surface had a network structure. The difference in current in the conducting region is attributed to the presence of insulating PSS, which covers PEDOT with different thickness.

Figure 5.4 shows the simultaneous topography and current images of PEDOT:PSS sputtered by 100 eV Ar^+ for 5 hours. The XPS S 2p spectra was obtained and the ratio of PEDOT to PSS is ~1:1, implying that the PSS-rich layer had been sputtered. The average current in current image was 0.24 nA, which is larger than that of PEDOT:PSS sputtered by 500 eV Ar^+, but smaller than that of as prepared PEDOT:PSS. It can be explained by the fact that the destruction layer (an insulating layer) is much thinner than that caused by 500 eV Ar^+. The current image also shows that there was a network structured PEDOT beneath the PSS-rich layer.

Based on the current images as prepared PEDOT:PSS and Ar^+ sputtered PEDOT:PSS, a structure as shown in Fig. 5.5 is proposed. The surface of the

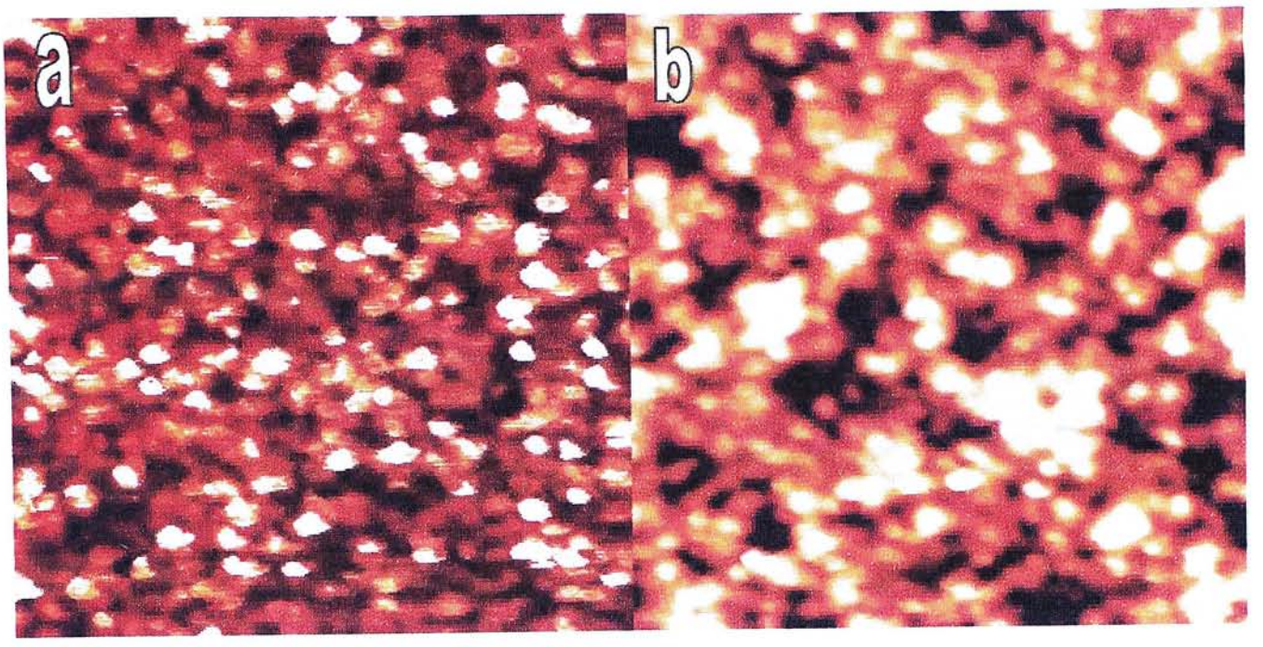

Fig. 5.4 Current image (a) and topography image (b) on PEDOT:PSS/Au/mica after 100 eV Ar^+ ions sputtering with the tip bias of 1V. The brightest scales are 0.6~3.5 nA for (a), and 1.7~3.5 nm for (b). The scan size is 1μm×1μm for both (a) and (b).

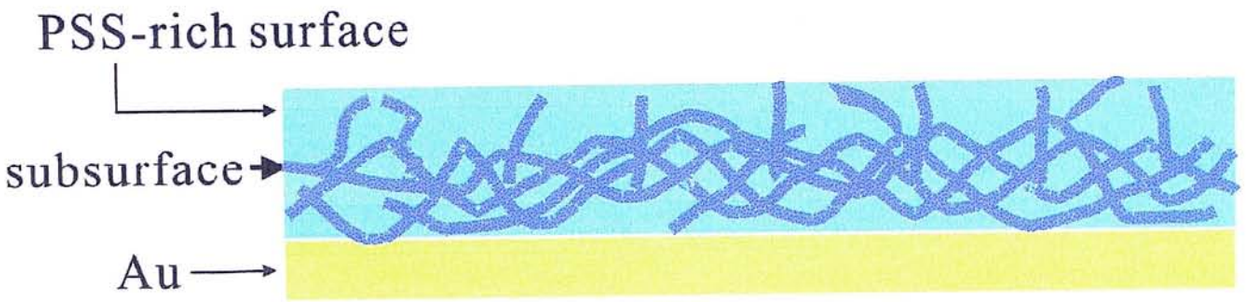

Fig. 5.5 A possible model for the structure of the PEDOT:PSS/Au film

PEDOT:PSS thin film is a PSS-rich layer, within which the conducting phase were covered by PSS with different thickness. Under this surface, there was a network structure.

5.3.2 CAFM on pH Dedoped PEDOT:PSS (pH=6.6)

Figure 5.6 shows the simultaneous current image (a) and topography image (b) on pH dedoped PEDOT:PSS (pH=6.6) with a tip bias of +1V. The current image shows a structure similar to that of the as prepared PEDOT:PSS film. Several conducting zones distributed randomly and were surrounded by insulating zones. The topography image shows a non-uniform and amorphous structure. The rms roughness of the topography image was 0.66 nm, which is similar to that of as prepared PEDOT:PSS. The average current was 0.11 nA, which is smaller than that of the as prepared PEDOT:PSS (0.3 nA). This is consistent with the findings by A.J. Heeger, et al [2] and by H.L. Yip [3] that the conductivity decreased when PEDOT:PSS was pH dedoped. However, the decrease is smaller here. The average current in the current image can only give a qualitative analysis, because the actual current injection area is unknown and often larger than the area of a single pixel in the current image, which is equal to the ratio of the current image area to the total scanning points.

Local I-V measurements on the most conducting region give more direct data to compare the transport characteristics of PEDOT. Figure 5.7 shows the local I-V plots on the as-prepared-PEDOT:PSS/Au and on the pH(6.6)-PEDOT:PSS/Au. The characteristics of the I-V plots are mainly caused by two factors, the space-charge-limited process and the tunneling process, which are expressed by Eq. (1) and Eq. (2), respectively,

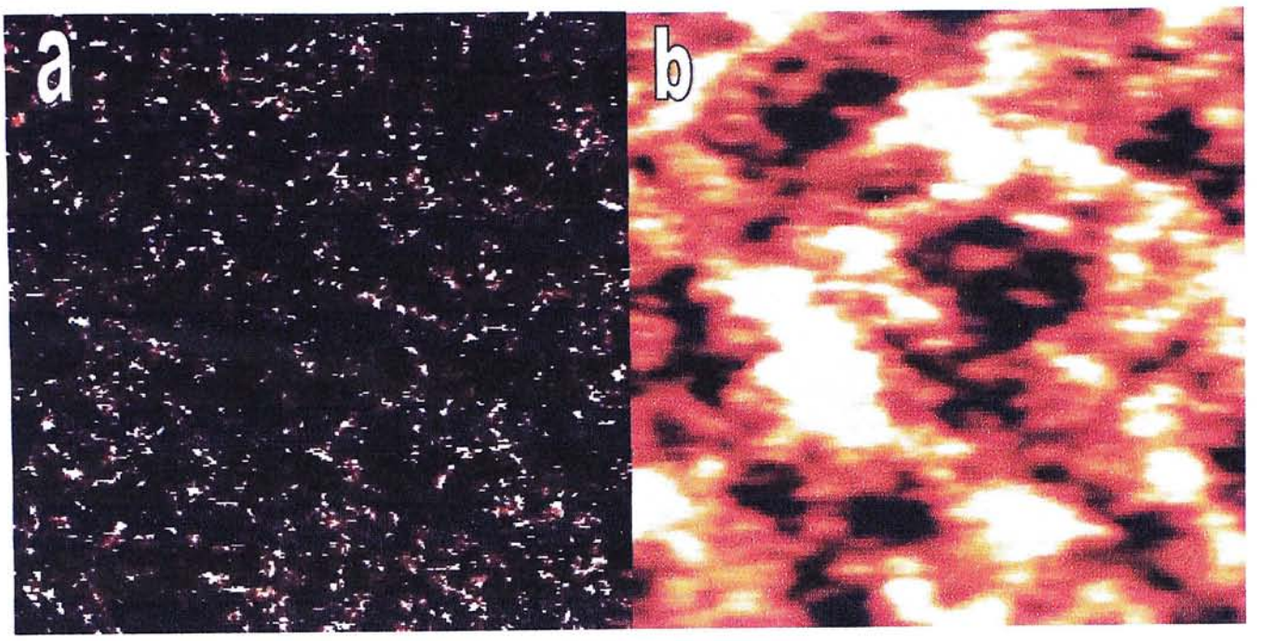

Fig. 5.6 Current image (a) and topography image (b) on pH6.6–PEDOT:PSS/Au/mica with the tip bias of 1V. The brightest scales are 1~17 nA for (a), and 1.7~2.8 nm for (b). The scan size is 1μm×1μm for both (a) and (b).

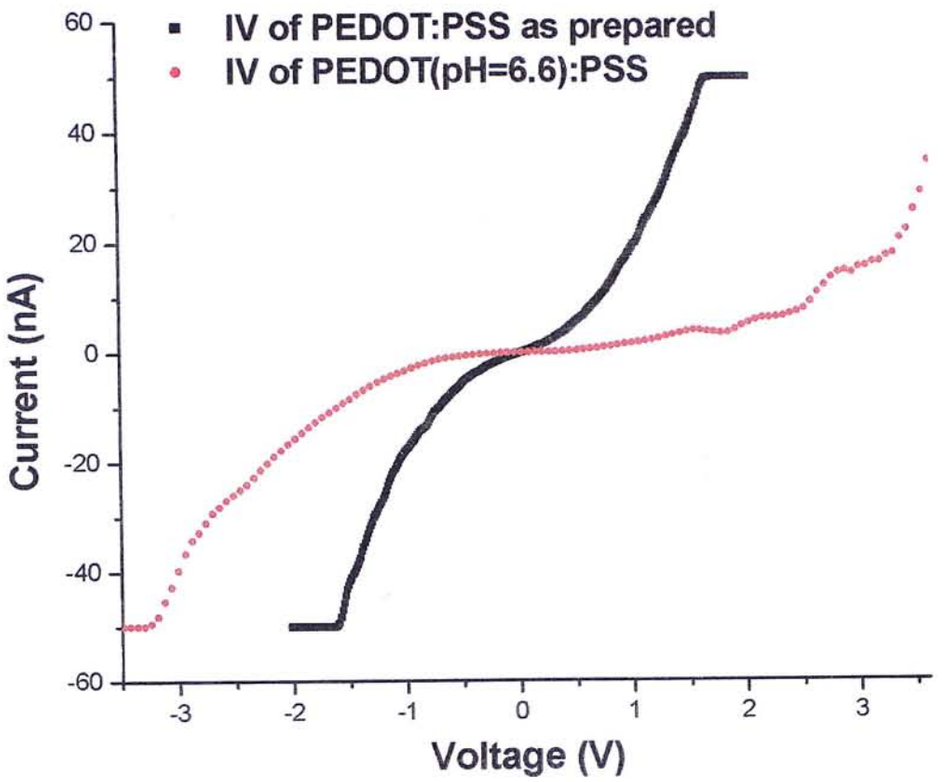

Fig. 5.7 Illustration of the local I-V measurements on as-prepared-PEDOT:PSS/Au and pH(6.6)-PEDOT:PSS/Au

$$I = \frac{9}{8}\frac{1}{A_{eff}}\varepsilon_r\varepsilon_0\mu\frac{V^2}{d^3}, \quad (1)$$

$$I = A_{eff}\frac{e^3 m_0}{8\pi h m_{eff}}\frac{1}{t(E)^2}\frac{\beta^2 V^2}{\Phi d^2}\times\exp\left(-\frac{8\pi\sqrt{2m_{eff}}}{3he}\nu(E)\frac{d\Phi^{3/2}}{\beta V}\right), \quad (2)$$

where I is the current, A_{eff} is the tip-sample contact area, ε_r is the dielectric constant, ε_0 is the vacuum permittivity, μ is the mobility, V is the applied voltage, d is the film thickness, e is the electronic charge, m_{eff}/m_0=0.5, $\nu(E)$=0.93, $t(E)$=1, and h is the Plank's constant. The injected current first tunneled through the thin insulating PSS layer, then passed through conducting PEDOT:PSS via a space-charge-limited process. It is difficult to perform a very accurate curve fitting, as there are too many unknown parameters in the fitting equation. Therefore, the I-V plots can only show the relative difference in conductivity and cannot give further quantitative information. The current ratio of the as prepared PEDOT and the pH dedoped PEDOT at the same bias can be considered as the rough ratio of conductivity. It is 3 ~ 6 throughout the bias range, which is 2 orders smaller than the macroscopic results given by Heeger et al [2]. In their works, the conductivity decreased through pH dedoping is ~3 orders smaller than theoretical calculated result [4]. Therefore, the most conductive region in pH dedoped PEDOT:PSS is probably the slightly dedoped phase. Such a small amount of slightly dedoped PEDOT made a conductivity decrease smaller than that revealed by macroscopic measurements and theoretical calculations [2,4]. It is consistent with the results reported by Johansson, et al., that it is hard to dedope PEDOT to a completely neutral form, and that some residual doping cannot be excluded proved by their spectroscopic ellipsometry measurements [5].

5.3.3 CAFM on Electrochemically Dedoped PEDOT:PSS

Besides pH dedoping, PEDOT can also be electrochemically dedoped. As mentioned in the last chapter, PEDOT:PSS can be electrochemically dedoped to a neutral state, then to an n-doped state by increasing the dedoping potential. In this section, PEDOT:PSS films which were dedoped at –1.2V (neutral) and –1.6V (n-type) were studied using conducting AFM.

Figure 5.7 shows the topography image on the PEDOT:PSS/Au/mica electrochemically dedoped at –1.2V and current images corresponding to a tip bias of 1V, 2V, 2.5V, 3V, and 3.5V respectively. The scan size was 1μm ×1μm for all images. The topography image shows an amorphous structure, similar to the previous two of the PEDOT:PSS as prepared sample, and the pH dedoped PEDOT:PSS sample. The rms roughness was 0.94 nm. It is evident from Fig. 5.7(b) that the number of the conducting zones was much less than that of as prepared PEDOT:PSS with the same tip bias. The area of individual conducting inland was aslo smaller. The current in the most conductive region, ~7nA, was also smaller than that of as prepared PEDOT:PSS (~25 nA). Similarly, the most conducting region in the current image should probably be the least dedoped region. The total area of conducting region was much less than that of the pH dedoped PEDOT:PSS, indicating that electrochemical dedoping was a more effective dedoping method than pH dedoping. The amount of the conducting zones gradually increased when the tip-sample bias was increased, as can be seen in Fig. 5.7 (c), (d), (e), and (f). The newly emerged conducting areas should probably be the dedoped phase, which cannot be revealed under a low bias.

Figure 5.9 shows the local I-V plots on the partly dedoped region and the fully dedoped region of PEDOT:PSS electrochemically dedoped at –1.2V. The

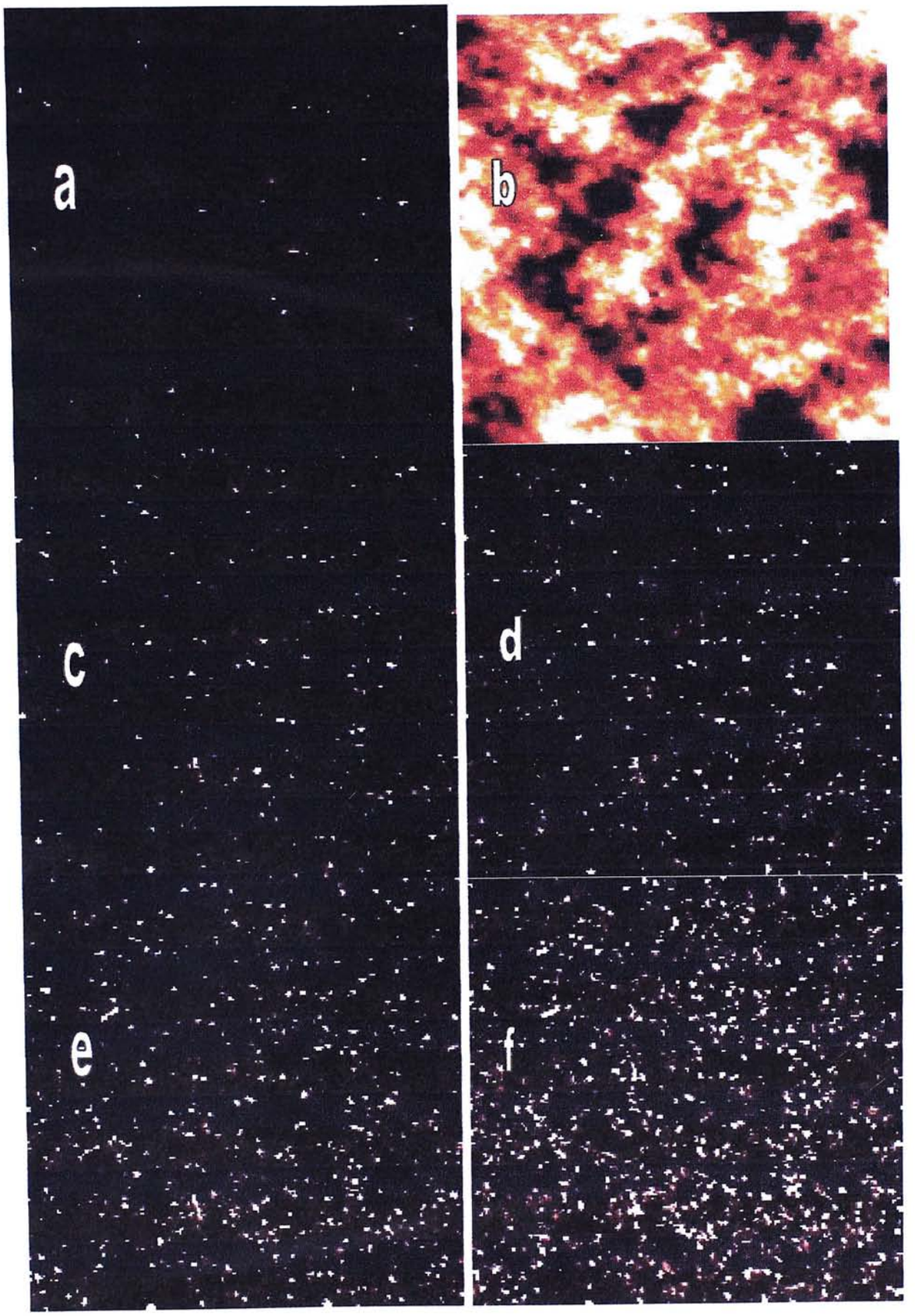

Fig. 5.8 Topography image (b), and Current image (a), (c), (d), (e), and (f) on PEDOT:PSS/Au/mica electrochemically dedoped at –1.2V with the tip bias of 1V, 2V, 2.5V, 3V, and 3.5V respectively . The brightest scales are 1~7 nA for (a), 3~5 nm for (b), 1~25 nA for (c), 1~49 nA for (d), 1~50 nA for (e) and for (f). The scan size is 1μm×1μm for all the six images.

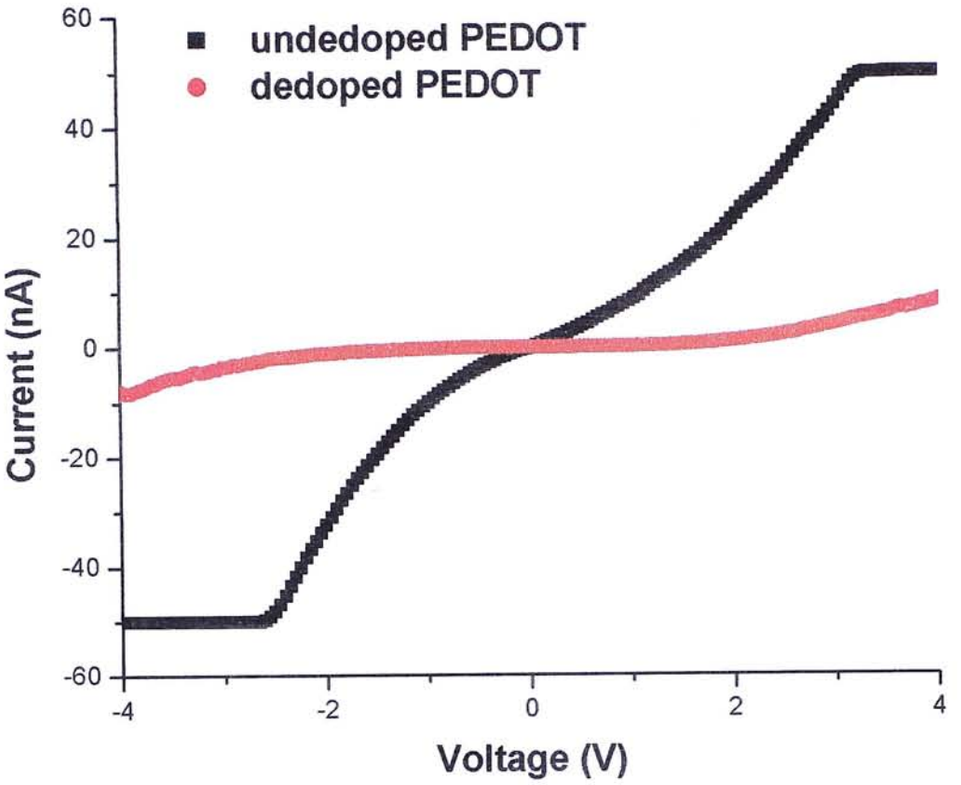

Fig. 5.9 Local I-V plots on the partly dedoped PEDOT and the fully dedoped PEDOT of PEDOT:PSS electrochemically dedoped at –1.2V

conductivity of the conducting region was lower than that of the as prepared PEDOT:PSS film. Even the most conducting region from the electrochemically dedoped PEDOT:PSS (dedoped at –1.2V) sample was also a partly dedoped region. Moreover, this partly dedoped region had a much better conductivity than those completely dedoped region.

Figure 5.10 shows the current image (a) and topography image of the PEDOT:PSS which was electrochemically dedoped at –1.6V. The topography image shows a similar amorphous structure as the n-doped PEDOT:PSS film. The rms roughness was 1.8 nm which is larger than three of the PEDOT:PSS as prepared sample, the pH dedoped PEDOT:PSS sample, and the PEDOT:PSS electrochemically dedoped at –1.2V sample. It is proposed that PSS^- might decouple from their counter parts, and part of PSS^- might even move to the electrolyte during dedoping under such a high bias. As a result, the surface roughness increased. This proposal is also supported by the XPS results that the ratio of PEDOT to PSS significantly increased for PEDOT:PSS electrochemically dedoped at –1.6V as discussed in Chapter 4. The current image shows that there were much more conducting zones than in the as prepared PEODT:PSS sample. It implies that there were much more PEDOT in the surface as what is concluded based on the results of XPS analysis.

Figure 5.11 shows the local I-V measurement on the conducting region of PEDOT:PSS which was electrochemically dedoped at –1.6V. The current was higher than that on the neutral PEDOT sample by 2 orders of magnitude, and was close to that on the most conducting region of the as prepared PEDOT:PSS sample, implying a strong n-doping effect.

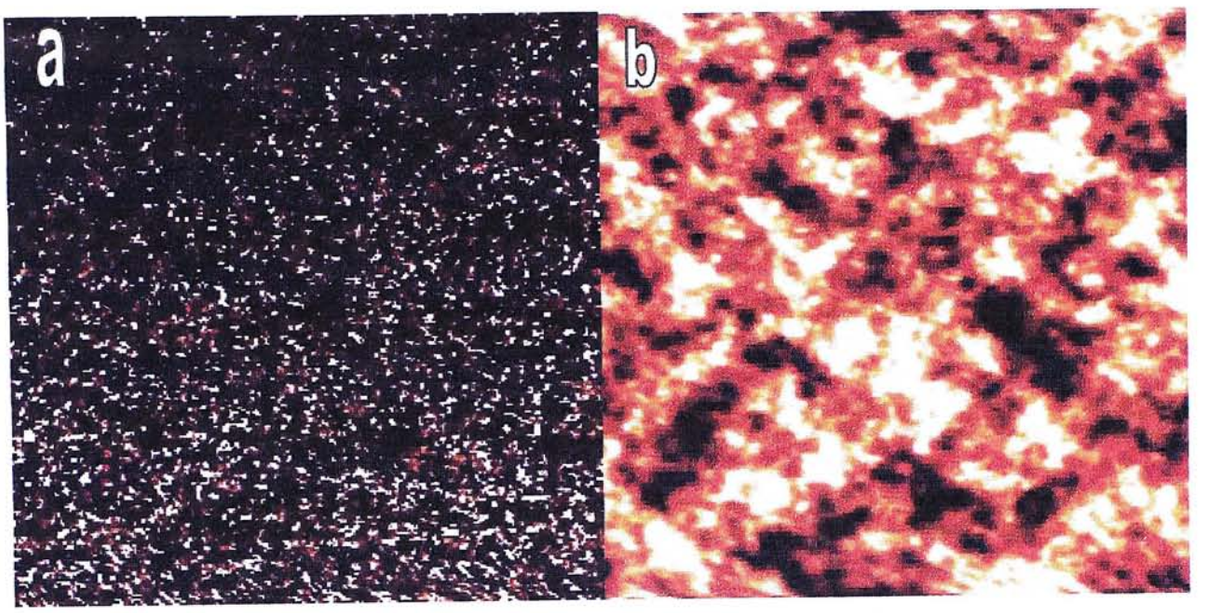

Fig. 5.10 Current image (a) and topography image (b) on PEDOT:PSS/Au/mica electrochemically dedoped at –1.6V with the tip bias of 1V. The brightest scales are 15~50 nA for (a), and 8~13 nm for (b). The scan size is 1μm×1μm for both (a) and (b).

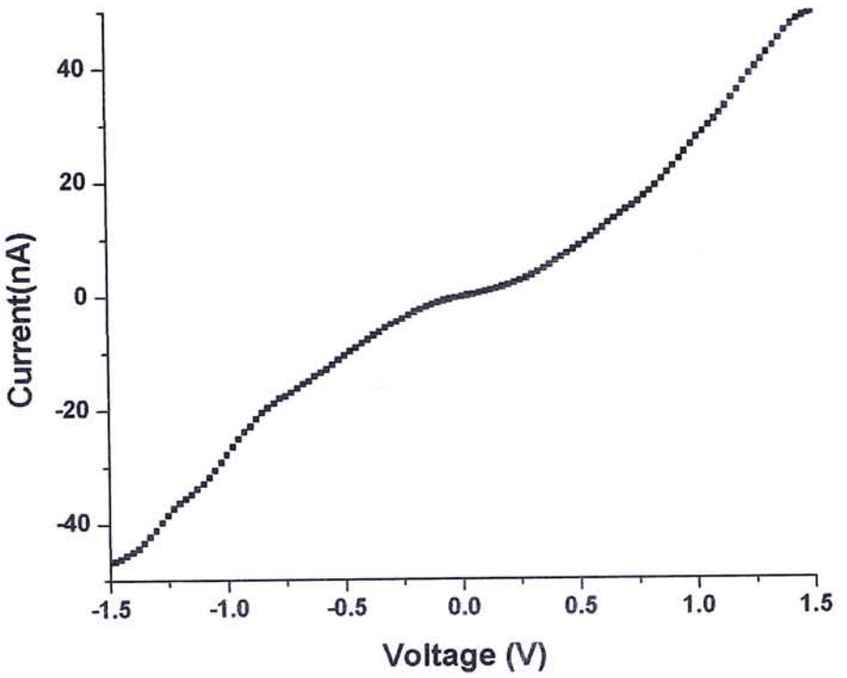

Fig. 5.11 Local I-V measurement on the conductive region of PEDOT:PSS electrochemically dedoped at –1.6V

5.4 Conclusions

The film of the as prepared PEDOT:PSS is proposed to have a structure as illustrated in Fig. 5.5. The surface was dominated by PSS with a few PEDOT chains covered by PSS at different thicknesses. Beneath the surface had a network structure. By either pH dedoping or electrochemically dedoping, one could not completely dedope the original PSS-doped PEDOT to its neutral state. However, compared to pH dedoping electrochemical dedoping was more effective in dedoping. N-doped PEDOT had conductivity between neutral PEDOT and p-doped PEDOT.

Reference

[1] G. Greczynski, Th. Kugler, M. Keil, W. Osikowicz, M. Fahlman, W.R. Salaneck, *J. Electron Spectrosc* **121** (2001), 1

[2] A.N. Aleshin, S.R. Williams, A.J. Heeger, *Synth. Met.* **94** (1998), 173

[3] H.L. Yip, *Mphil thesis* (CUHK) (2003)

[4] L. Zhang, unpublished results

[5] Thomas Johansson, Leif A.A. Pettersson, Olle Inganas, *Synth. Met.* **129** (2002), 269

[6] Harri J. Ahonen, Jukka Lukkari, and Jouko Kankare, *Macromolecules*, **33** (2000), 6787

Chapter 6

Concluding Remarks and Future Work

6.1 Concluding Remarks

PEDOT:PSS, a p-type polymer with PEDOT doped by PSS, can be electrochemically dedoped to a neutral state and further doped to an n-doped state. X-ray photoemission spectroscopic study on such systems was used to disclose some information on the doping and dedoping mechanisms of PEDOT. It proves that during electrochemical dedoping with increasing dedoping potential, the Fermi level of PEDOT:PSS moved up from near the HOMO energy level, first to the mid of the band gap of PEDOT, then to the LUMO energy level. The corresponding PEDOT:PSS film was changed from a p-doped state, first to a neutral state, then to an n-doped state, with sulfur atoms in PEDOT acting as the main reduced center (or charge transfer center).

Conducting atomic force microscopic study gives the morphology and the structure of PEDOT:PSS film. PEDOT:PSS film is amorphous for p-doped, neutral, and n-doped state. The film of the as prepared PEDOT:PSS is proposed to have a structure as illustrated in Fig. 5.5. In addition, this technique can further characterize the doping and dedoping states of PEDOT. Either pH dedoping or electrochemically dedoping cannot completely dedope PSS-doped PEDOT to a neutral state. However, electrochemical dedoping was shown to be more effective, as electrochemical dedoping gave much less conducting PEDOT:PSS after dedoping. The dedoped PEDOT:PSS in neutral state was much less conducting than p-doped PEDOT:PSS. It is consistent with the results from XPS that the Fermi level moved from near HOMO

to the midgap. N-doped PEDOT had a higher conductivity than neutral PEDOT, but a lower conductivity than p-doped PEDOT. It is also consistent with the results from XPS that the Fermi level of n-doped PEDOT lied near LUMO.

6.2 Future Work

Based on the findings described in previous chapters, the following future works are proposed to further study the doping mechanism of conducting polymer, in particular PEDOT:PSS:

1. Conducting atomic force microscopy (cAFM) study can be extended to PFO/PEDOT:PSS/Au and PFO/Au. Such study can provide information on the effect induced by phase segregation of PEDOT:PSS within the near surface region.
2. Conducting atomic force microscopy studies on ITO, PEDOT:PSS/ITO, PEDOT:PSS/SAM/ITO are proposed. These works can unveil the effects of SAM modification to PEDOT:PSS/ITO interface in nanoscale.
3. Conducting atomic force microscopy studies on ITO, PEDOT:PSS/ITO, PFO/PEDOT:PSS/ITO, and PFO/modified PEDOT:PSS/ITO (The phase segregation in PEDOT:PSS can be partly prevented by some organic solution modification.) are also proposed. These studies can lead to better understanding on the charge transport within different layers and across different interfaces in PLED structure in nanoscale.